Dielectric Response of Glass-Forming Liquids in the Nonlinear Regime

by

Subarna Samanta

A Dissertation Presented in Partial Fulfillment
of the Requirements for the Degree
Doctor of Philosophy

Approved March 2016 by the
Graduate Supervisory Committee:

Ranko Richert, Chair
Timothy Steimle
George H. Wolf

ARIZONA STATE UNIVERSITY

May 2016

ABSTRACT

Broadband dielectric spectroscopy is a powerful technique for understanding the dynamics in supercooled liquids. It generates information about the timescale of the orientational motions of molecular dipoles within the liquid. However, dynamics of liquids measured in the non-linear response regime has recently become an area of significant interest, because additional information can be obtained compared with linear response measurements.

The first part of this thesis describes nonlinear dielectric relaxation experiments performed on various molecular glass forming-liquids, with an emphasis on the response at high frequencies (excess wing). A significant nonlinear dielectric effect (NDE) was found to persist in these modes, and the magnitude of this NDE traces the temperature dependence of the activation energy. A time resolved measurement technique monitoring the dielectric loss revealed that for the steady state NDE to develop it would take a very large number of high amplitude alternating current (ac) field cycles. High frequency modes were found to be ‘slaved’ to the average structural relaxation time, contrary to the standard picture of heterogeneity. Nonlinear measurements were also performed on the Johari-Goldstein β-relaxation process. High ac fields were found to modify the amplitudes of these secondary modes. The nonlinear features of this secondary process are reminiscent of those found for the excess wing regime, suggesting that these two contributions to dynamics have common origins.

The second part of this thesis describes the nonlinear effects observed from the application of high direct current (dc) bias fields superposed with a small amplitude

sinusoidal ac field. For several molecular glass formers, the application of a dc field was found to slow down the system via reduction in configurational entropy (Adam-Gibbs relation). Time resolved measurements indicated that the rise of the non-linear effect is slower than its decay, as observed in the electro-optical Kerr effect. A model was discussed which quantitatively captures the observed magnitudes and time dependencies of the NDE. Asymmetry in these rise and decay times was demonstrated as a consequence of the quadratic field dependence of the entropy change. It was demonstrated that the high bias field modifies the polarization response to the field, even including the zero field limit.

ACKNOWLEDGMENTS

It has been a great experience to pursue my graduate studies under the supervision of Professor Ranko Richert who has been an outstanding mentor. I would be forever grateful to him for giving me the opportunity to work in his lab. I would like to thank him for his guidance, patience and continuous support which will make this journey memorable. I would also like to take this opportunity to express my gratitude to my committee members Professor Timothy Steimle and Professor George Wolf for their support and help.

I would like to thank Professor Austen Angell for his insightful comments and help both as a committee member and as a mentor in CHM501 seminars. I was very fortunate to have researcher like Dr. Lokendra P. Singh, Dr. Zhen Chen, Dr. Wei Huang, Dr. Haibin Yu, Dr. Catalin Gainaru and Dr. Alexander Agapov during my stay in Dr. Richert's lab. I would like to acknowledge their expertise and help in gaining a broad perspective of my research area. My thanks also go to all the former members (Soham Roy, Ullas Pathak, Shobeir K. Mazinani) of the Richert group for their immense love and support which I thoroughly enjoyed. I would also like to give special thanks to my current lab mate, Amanda Young-Gonzales. It was fun working with you. Your craziness will surely be missed.

It is also a pleasure to thank all my friends in Tempe who have all given their love, support, and encouragement during this wonderful journey. I would finally like to thank my family for their love, patience, sacrifice and constant support. I dedicate this thesis to my *parents* for always staying by my side.

TABLE OF CONTENTS

Page

CHAPTER Page

LIST OF TABLES

Table Page

LIST OF FIGURES

Figure Page

Figure Page

Figure Page

Figure Page

Figure Page

Figure Page

LIST OF ABBREVIATIONS

AC	Alternating current
AG	Adam-Gibbs
CD	Cole-Davidson
CPDE (or KDE)	Cresolphthalein-dimethylether
CRR	Cooperatively rearranging region
DC	Direct current
EW	Excess wing
GLY	Glycerol
HN	Havriliak-Negami
JG	Johari-Goldstein
KWW	Kohlrausch-Williams-Watt
MTHF	2-methyltetrahydrofuran
mHz	milliHertz
MHz	megaHertz
NDE	Nonlinear dielectric effect
NMEC	N-methyl-ε-caprolactam
NMR	Nuclear magnetic resonance
PC	Propylene carbonate
PG	Propylene glycol
PVAc	Poly(vinylacetate)
VFT	Vogel-Fulcher-Tammann

Chapter 1

Introduction

One of the unsolved problems of condensed matter physics is related to glass transition phenomena, which occurs due to structural arrest of a liquid structure while cooling down a liquid below its melting point (T_m) fast enough so that crystallization can be avoided.[1] Below its melting point, the liquid enters into a metastable supercooled state where its structural relaxation time (τ) or viscosity (η) grows rapidly with lowering temperature. Further cooling results in a relaxation time which becomes experimentally inaccessible. At that point the resulting sample behaves like a solid on an experimental timescale although its structure has not been changed much. Usually this seemingly liquid to solid like transition often termed as glass transition, which for convenience is usually defined as a point where liquids relaxation time reaches 100s or its viscosity achieves a value around 10^{13} Poise. But unlike liquid to crystal transformation (which is a first order phase transition), the glass transition cannot be considered as a true thermodynamic transition[2] as it depends on the cooling rate. Fig. 1.1 illustrates the cooling rate dependence of the glass transition phenomena. Smaller cooling rate provides an opportunity for the molecules to return to the equilibrium. Hence glass transition temperature is lower in that case (glass 2 in Fig. 1.1).

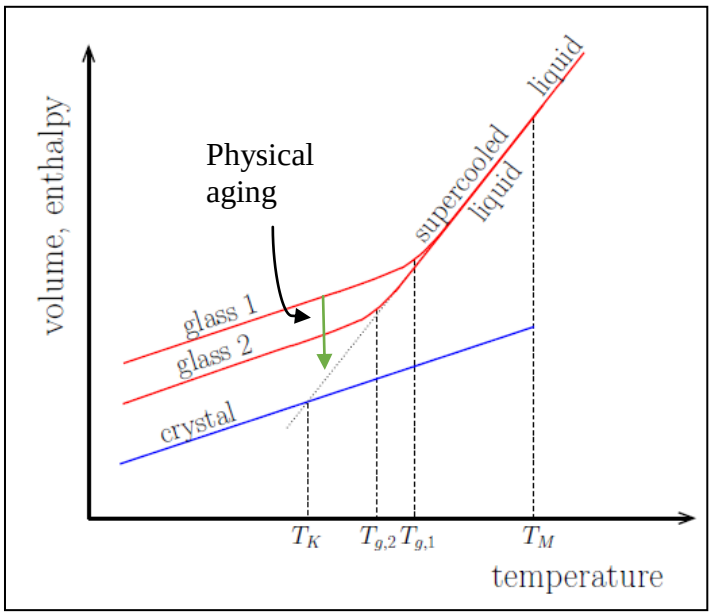

Fig. 1.1: A Volume / Enthalpy vs. Temperature plot showing three distinct regions of a glass-forming liquid while cooling from a liquid state. Depending on the cooling rate the glass transition will occur either at temperatures $T_{g,1}$ or $T_{g,2}$. Equilibrium supercooled liquid line below T_g is shown via dotted line which cuts the crystal line at Kauzmann temperature, T_K. The relaxation of the high enthalpy glassy state towards low energy value with time (physical aging) is indicated by the green arrow. (taken from Hecksher [2011][3])

This 'glass transition' phenomenon is associated with some generic features independent of the chemical bonds involved (metallic, polymeric, molecular glass formers) which make its description challenging from a theoretical perspective. In this chapter focus will be on these facts from a phenomenological point of view.

1.1 Generalized features of glass transition

A. Non-Arrhenius temperature dependence of structural relaxation time

The glass transition is not only remarkable in the sense that structural relaxation time spans over almost 14 decades in the temperature range starting from T_m to close to the glass transition temperature (T_g), it is the temperature dependence of the structural

relaxation time in the supercooled phase that is also puzzling. For example, in Fig. 1.2, the temperature dependence of structural relaxation timescale of Diethyl phthalate (DEP) is shown.

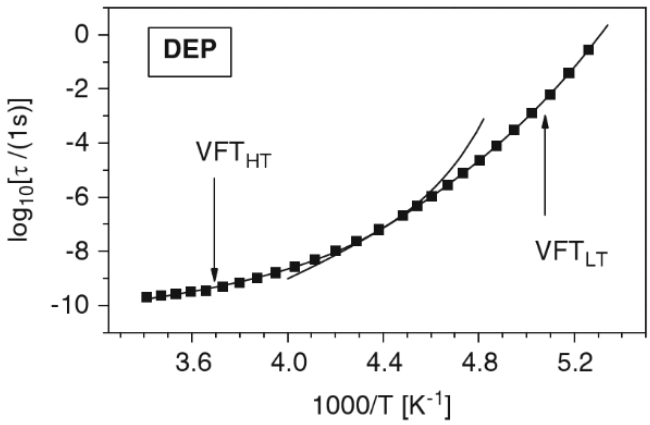

Fig. 1.2: Temperature dependence of structural relaxation timescale for Diethyl phthalate is presented. The solid fit lines are based on Eq. (1.1). While VFT_{LT} describes the experimental data well in low temperature regime, VFT_{HT} captures the high temperature data.

It is quite evident from the figure that structural relaxation grows in super-Arrhenius fashion with decreasing temperature. It indicates that in the supercooled state, the barrier height (or activation energy, E_a) is no longer a temperature independent quantity. The dramatic increase in viscosity can then be thought of as a manifestation of a mechanism which is collective in nature. Most often this temperature dependence of structural relaxation time or viscosity has been fitted with an empirical Vogel-Fulcher-Tammann (VFT) equation[4]:

$$\tau(T) = \tau_\infty \exp\left(\frac{B}{T-T_0}\right) \qquad \text{Eq. (1.1)}$$

where $\tau(T)$ is the relaxation time at temperature T, τ_∞ is the high temperature limit relaxation time, B is a constant and T_o is the Vogel-Fulcher temperature. The above

mentioned VFT equation suggests a divergent time scale at a finite temperature T_0 and therefore indicates some sort of underlying phase transition. When T_0 is zero, the Arrhenius equation is obtained and then B reflects the value equal to E/k_B where E is activation energy, k_B represents Boltzmann constant. Although the VFT equation can describe the temperature dependence of structural relaxation for a wide range of timescales, a single VFT fit usually does not perform that well in the high temperature limit (Fig. 1.2).

Angell classified supercooled liquids based on their rate at which they approach towards glass transition temperature (fragility, m).[5] The kinetic fragility is defined as:

$$m_{kin} = \frac{E_{app}(T_g)}{T_g} \ , \ E_{app}(T) = dlog\eta/d(1/T) \qquad \text{Eq. (1.2)}$$

A liquid is called "strong" if it follows a straight line in the Angell plot (logη vs. T_g/T) which corresponds to Arrhenius temperature dependence. Similarly, a "fragile" liquid will show a curvature in the plot. A larger temperature dependence of E_{app} means a higher value of fragility index of the liquid (Fig. 1.3)[6]. A higher value of the constant B in Eq. (1.1) corresponds to a stronger liquid.

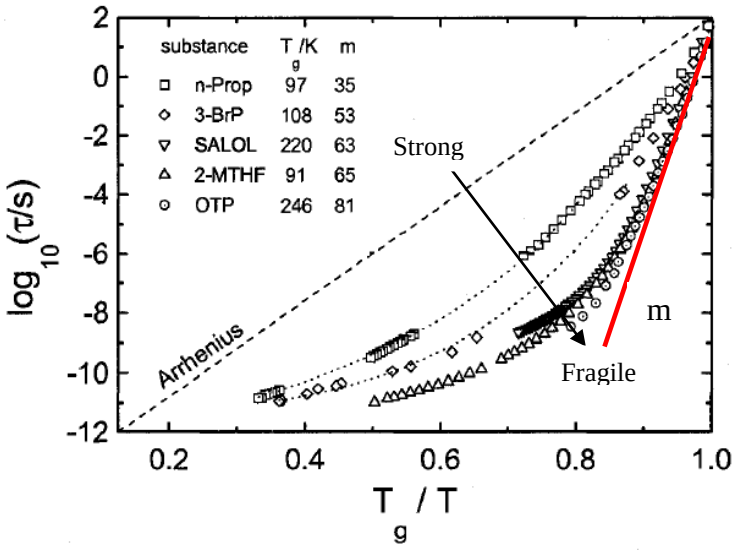

Fig. 1.3: Strong-fragile classification of supercooled liquids is shown by plotting logarithm of structural relaxation timescale against a reduced temperature scale (T_g/T). The dashed line indicates the Arrhenius temperature dependence. The steepness index (m) which can be obtained from the slope of the red line represents the fragility value. [taken from Ref. 6]

B. Non-exponential response of the structural relaxation process

Deviations from exponential response functions for the primary relaxation process are a ubiquitous feature in the dynamics of supercooled liquids. This non-exponential nature of the correlation function has been observed in different experiments and in widely different systems[7]. Although liquid relaxation seems to be exponential above the melting temperature, the relaxation becomes more and more non-exponential as it approaches near the glass transition region. This response has been captured with a single parameter empirical function (stretched exponential), namely the Kohlrausch-Williams-Watts function (KWW)[8]. It can be written in the following form:

$$\varphi(t) \sim \exp\,(-t/\tau)^{\beta_{KWW}} \qquad \text{Eq. (1.3)}$$

Here $\varphi(t)$ describes the relevant normalized correlation function depending on the experiments used and β_{KWW} value in general lies between 0 and 1. The smaller the value of β_{KWW}, larger the deviation from the exponential response (dispersive relaxation). In the frequency domain representation, this stretched exponential relaxation appears as an asymmetric loss peak. Cole-Cole, Cole-Davidson and Havriliak-Negami functions are useful in that case which will be described later. The origin of this non-exponential relaxation in supercooled molecular liquids is believed to be due to the existence of 'dynamical heterogeneity'[9,10]within the sample. 'Dynamic heterogeneity' refers to a situation where different regions (domains) in a liquid sample relax at different rates (spatially varying time scales) at the same time and hence producing a broad distribution of relaxation times **(**Fig. 1.4a**) .** Although each domain relaxes with a different timescale, their ensemble average turns out to be non-exponential which one observes macroscopically **(**Fig. 1.4b**)**. A non-exponential decay function *ϕ(t)* can be thought of as a superposition of exponential functions with a distribution of relaxation times, *g(lnτ*). Mathematically this can be written as follows:

$$\phi(t) = \int_{-\infty}^{\infty} g(ln\tau) \exp\left(-\frac{t}{\tau}\right) dln\tau \;\; ; \qquad \int_{-\infty}^{\infty} g(ln\tau) dln\tau = 1 \qquad \text{Eq. (1.4)}$$

There are many experimental results ranging from NMR[12], dielectric-hole burning[13], solvation dynamics[14], photo-bleaching technique[15], single molecule studies[16] in support of the idea of dynamic heterogeneity.

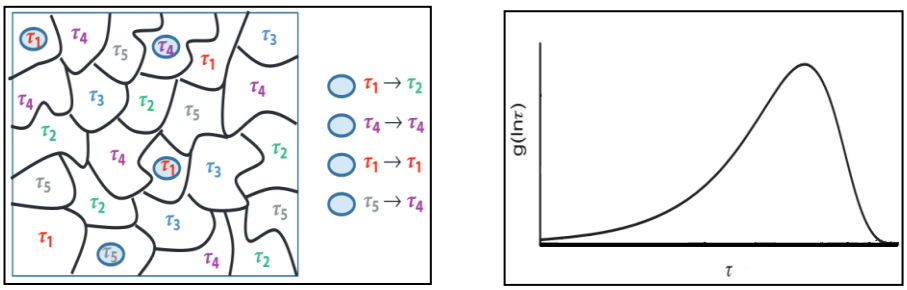

Fig. 1.4a: Schematic representation of a spatio-temporal heterogeneity within a supercooled liquid sample which produce a broad distribution of relaxation times. The τ values represent the dynamics of the host molecules reported by the probe molecules (taken from Kaufmann[11])

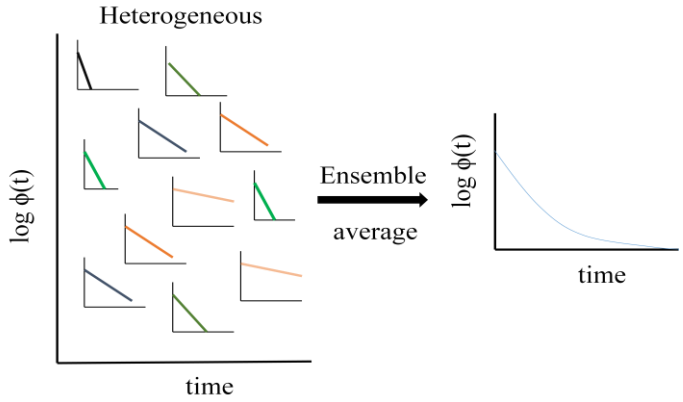

Fig. 1.4b: Extreme picture of spatial heterogeneity in supercooled liquids where each domain relax in an exponential fashion, but the overall observation (ensemble average) of the response function, $\phi(t)$, shows non-exponential behavior.

This heterogeneous distribution of relaxation times is not only responsible for non-exponential response in glass forming liquids, but also believed to be the cause behind the violation of the Stokes-Einstein relation[17,18](Dτ = constant, where D and τ stand for self-diffusion coefficient and structural relaxation time, respectively, at thermal equilibrium) often observed in liquids in their supercooled state (Fig. 1.5a)[19]. Enhancement of translational diffusion by more than two orders of magnitude or higher compared to rotational motions has been observed in low molecular weight glass formers

and polymers. A plethora of research has been carried out to understand the true nature of the dynamically heterogeneous regions (especially its length scale and time evolution).

A most obvious question that comes to mind whether there is any connection between the above mentioned two generalized features (non-exponential relaxation and non-Arrhenius temperature dependence). Böhmer *et al.*[20] tried to find a correlation between the non-exponential parameter β and the fragility parameter m. They looked at existing data of 70 different glass formers obtained from various experimental procedures and found a rough correlation between these two parameters (Fig. 1.5b). In general a higher fragility value corresponds to a larger departure from exponential relaxation (smaller β value). Often β values close to 0.5 have been found for fragile liquids near their T_g.

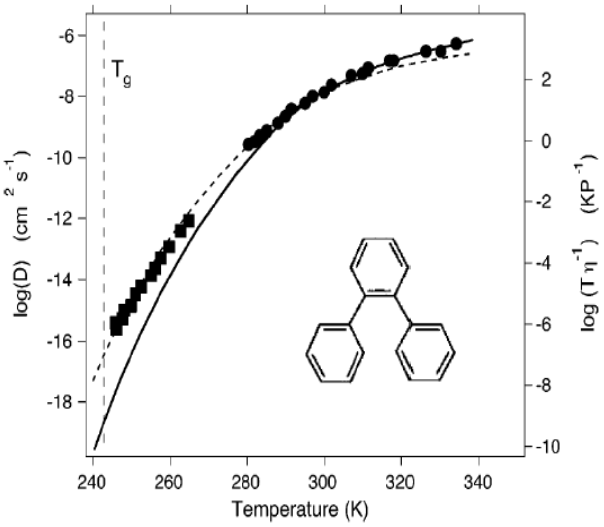

Fig. 1.5a: Decoupling between viscosity (solid line) and self-diffusion coefficient (symbols) in supercooled OTP. The dashed line shows a fit with a ‘‘fractional’’ Stokes-Einstein relation $D_s \sim (T/\eta)^{\zeta}$ with $\zeta = 0.82$ instead of the ‘‘normal’’ value $\zeta = 1$ which holds only at high temperatures.(taken from Ref. 19)

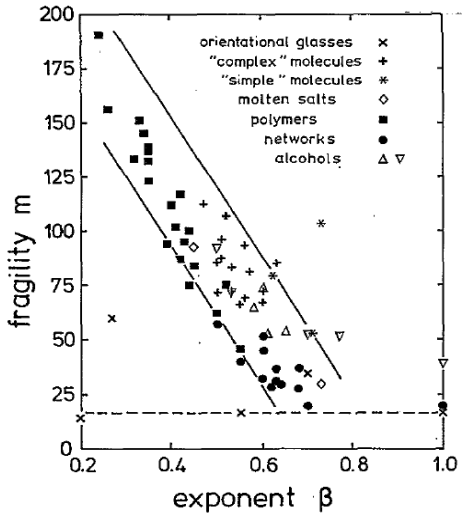

Fig. 1.5b: Correlation of fragility m vs. stretching exponent β for variety of glass-forming liquids. The dashed line indicates the minimum value of fragility. The solid lines are based on Equation 6 in Ref. 20.

C. Thermodynamic signatures of glass transition

Most thermodynamic studies of vitrification deal with evolution of the system's macroscopic properties as a response to heat flow. Isobaric heat capacity is often measured experimentally using Differential Scanning Calorimetry (DSC) techniques, which shows a significant drop in its value near the glass transformation range while cooling. ΔC_p, the heat capacity step, is defined as the difference between C_p of the liquid and that of the glass (Fig. 1.6). This type of discontinuity has been also observed in thermal expansivity and compressibility measurements. This is another way of finding glass transition temperature. Although the transitions looks like a second order phase transition, one has to keep in mind that glass is not in thermal equilibrium. Also, the transition temperature depends on its thermal history[2].

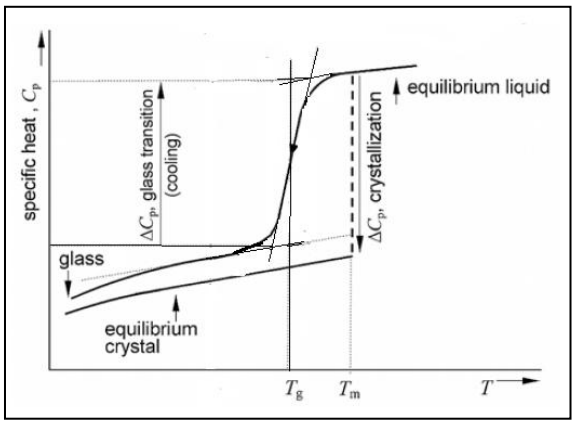

Fig. 1.6: Specific heat (C_p) vs. Temperature at the glass transition temperature. Specific heat drops in a gradual fashion at the dynamical glass transition region and the difference between the heat capacities of liquid and glassy states is usually referred to as ΔC_p at glass transition. ΔC_p of crystallization can be obtained by taking the difference between the heat capacity values of liquid and crystal state at the melting temperature, T_m.

It is interesting to explore the nature of the entropy function. It is because one of the useful approaches to look at the glass transition is based on the energy landscape of the liquid. When such materials are cooled down to near Tg, atomic rearrangements become too slow and the material is thought to be trapped in one of many local energy minima which has an excess of energy and entropy with respect to the equilibrium state. While thermodynamics is mainly concerned with the number of energy minima and the corresponding multiplicity of configurations, a kinetic approach is more interested in the rate of transition between energy minima. How these two behaviors are connected, if there is any connection, is a central question to the glass transition phenomena. It is therefore important to observe how entropy varies with temperature while undergoing the glass transition. Entropy can be derived from heat capacity data (from adiabatic calorimetry measurements) by integrating w.r.t. temperature (Fig. 1.7a) [21].

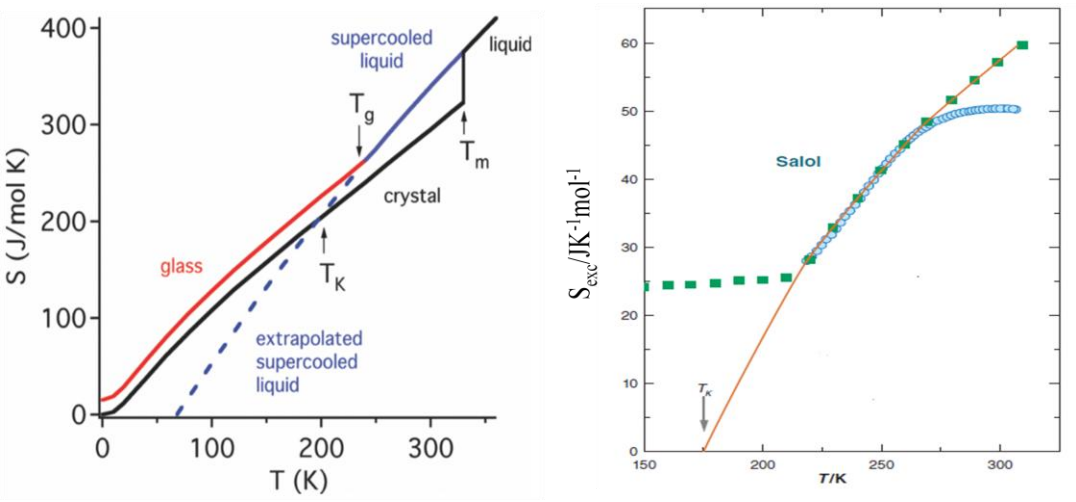

Fig. 1.7: a) Entropy is shown as a function of temperature for o-terphenyl (OTP) in the liquid, supercooled liquid, glass and crystal state. [taken from Ref.21] b) Excess entropy of salol is shown as a function of temperature. [taken from Ref. 22]

The excess entropy can then be defined by taking the difference in entropy between the crystal and the liquid line in the entire temperature range,

$$S_{exc}(T) = \Delta_{fus}S + \int_{T_{fus}}^{T} \frac{C_p^{liquid}(T') - C_p^{crystal}(T')}{T'} dT' \qquad \text{Eq. (1.5)}$$

where $\Delta S_{fus} = \Delta H_{fus}/T_{fus}$ is entropy of fusion or melting. Although this excess entropy usually has been referred to as configurational entropy in the literature (assuming both the glass and the crystal have similar vibrational contribution towards entropy), this nomenclature has been questioned[23]. When the equilibrium excess entropy line is extrapolated to below T_g, it appears to vanish at a finite temperature called 'Kauzmann[24] temperature' (T_K) as shown for a organic molecular glass former salol (Fig. 1.7b)[22]. T_K is sometimes referred as "Ideal glass transition" temperature. The 'Kauzmann temperature' has its own thermodynamic importance. As mentioned earlier, it indicates that S_{exc} will be

zero at a finite temperature, which implies that the entropy of a supercooled liquid will be lower than crystal if one goes below T_K. This is hard to imagine because in general liquid structure poses more disorder than a crystal. More severe problem will arise when one thinks in terms of the Third law of thermodynamics, which states that the absolute entropy can be zero only at zero Kelvin. If equilibrium supercooled liquid line is extrapolated well below T_K, it is quite evident from Fig. 1.7a**,** that entropy will be zero not at zero Kelvin, but at a finite temperature which contradicts Third law of thermodynamics. The glass transition suppresses this impossible scenario. It can be viewed as a kinetically controlled manifestation of avoiding Kauzmann's 'entropy crisis'[25]. Experimentally, it is impossible to reach equilibrium even close to T_K to exploit the proper thermodynamic parameters in that region. Excess entropy has been used to calculate fragility (m), which measures of rate of structural change of glass-forming liquids. It is defined as thermodynamic fragility[26]which depends on the rate at which liquids lose their excess entropy approaching T_g (Eq. (1.6)). The higher the rate the higher the fragility will be (Fig. 1.8).

$$m_T = \left.\frac{d(S_{exc}(T_g)/S_{exc}(T))}{d(T_g/T)}\right|_{T=T_g} \qquad \text{Eq. (1.6)}$$

Wang *et al.*[27] introduced a relation to calculate the dynamic fragility from the measured thermodynamic properties like heat capacity step during glass transition, ΔC_p and melting enthalpy, ΔH_m. This observation also implies the well-known fact that fragility is connected to the amplitude of the heat capacity jump at T_g. A high correlation has been shown between kinetic and thermodynamic fragilities for different types of glass-formers

(molecular, metallic and ionic)[26]. The discrepancy observed in correlation was related to difference in the vibrational heat capacities.

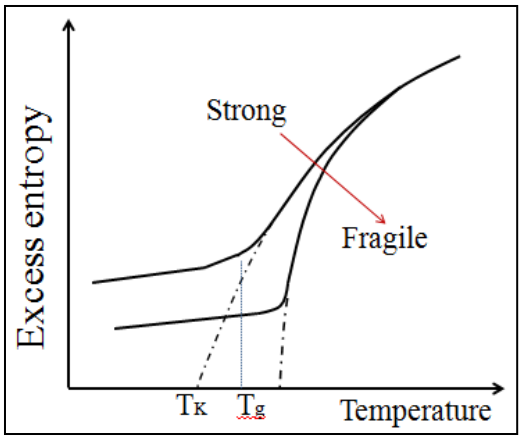

Fig. 1.8: Classification of liquids (strong/fragile) in terms of their rate of losing excess entropy. The higher the rate higher will be the fragility value m_T. Both Kauzmann temperature (T_K) and glass transition temperature (T_g) are indicated.

For molecular glass formers, it was observed that excess heat capacity has a hyperbolic temperature dependence (i.e. varies inversely with absolute temperature)[28]: ΔC_p = constant/T. So excess entropy can take the following form:

$$S_{exc} = \int_{T_K}^{T} \frac{\Delta C_p}{T'} dT' = \int_{T_K}^{T} \frac{C}{T'^2} dT' = \frac{C}{T_K} - \frac{C}{T} = CT_K\left(1 - \frac{T_K}{T}\right) = S_\infty\left(1 - \frac{T_K}{T}\right) \quad \text{Eq. (1.7)}$$

The fit line (red curve) in Fig. 1.7b is generated based on the above equation for the experimental S_{exc} values of the equilibrium supercooled liquid. This kind of agreement has been found for several other glass-forming molecular liquids.[6]

- **<u>Adam-Gibbs Entropy approach:</u>**

(A connection between dynamics and thermodynamics)

One of the most celebrated and successful approaches for explaining non-Arrhenius temperature dependence of transport properties approaching glass transition

temperature is the Adam-Gibbs (AG) entropy theory.[29] It is attractive in the sense that this theory connects the transport properties (dynamic features) to the thermodynamic property, namely configurational entropy. It has been realized that the concomitant increase in viscosity or relaxation time approaching glass transition may be due to the increase in barrier height for thermally activated process i.e. ΔE_a is a temperature dependent quantity. To rationalize this idea Adam-Gibbs introduced the concept of cooperative relaxations. They proposed that a liquid sample can be subdivided into mutually independent cooperatively rearranging regions (CRRs).[29] A CRR can be defined as the minimum region of the liquid which can relax independently of its environment, but the molecules inside a CRR have to move cooperatively. As the temperature decreases, the size of the CRR's grows. The Gibbs free energy involved in the rearrangement of a CRR equals to $\Delta G = Z\Delta\mu$, where Z represents number of molecules involve in the activated transition within a CRR and $\Delta\mu$ is the free energy barrier per molecule of the CRR. So the probability *w* of the cooperative rearrangement at a certain temperature T can be expressed as $w(T) = A \exp\left(\frac{-Z\Delta\mu}{k_B T}\right)$,where A and k_B are pre-exponential factor and Boltzmann's constant respectively. $\Delta\mu$ is assumed to be independent of the temperature and region volume. So the average transition probability can be defined as

$$\overline{w(T)} = \int_{z^*}^{\infty} A \exp\left(\frac{-Z\Delta\mu}{k_B T}\right) = \bar{A} \exp\left(\frac{-z^*\Delta\mu}{k_B T}\right) \qquad \text{Eq. (1.8)}$$

where z^* is the lower limit of the number of cooperatively rearranging molecules for which transition probability is nonzero. If we denote molar configurational entropy to be

S_c, for z^* molecule the contribution towards the configurational entropy would be $s_c^* = \frac{z^* S_c}{N_A}$. The above relation establishes a connection between the minimum size of a cooperatively rearranging region to the system's configurational entropy. So replacing z^*, the average transition probability can be written as, $\overline{w(T)} = \bar{A} \exp\left(-\frac{N_A s_c^* \Delta\mu}{k_B T S_c(T)}\right)$. Since there must have been at least two configurations to be present for rearrangement to occur, critical configurational entropy (s_c^*) can be taken as $k_B \ln 2$. As the molecular relaxation time τ is inversely proportional to the average transition probability,$(\overline{w})$, the relation between relaxation time and configuration entropy turns out be as follows:

$$\tau \propto exp\left[\frac{N_A s_c^* \Delta\mu}{k_B T S_c(T)}\right] \approx \tau'_\infty \exp\left(\frac{C_{AG}}{T S_c(T)}\right) \qquad \text{Eq. (1.9)}$$

In the above expression C_{AG} represents a constant quantity, $C_{AG} = \frac{N_A s_c^* \Delta\mu}{k_B}$. The above expression is called the Adam-Gibbs relation between relaxation time and configurational entropy. As the configurational entropy decreases with temperature, the relaxation time becomes longer. The main purpose of the AG relation was to describe the non-Arrhenius temperature dependence of the structural relaxation time. But the problem of testing the AG relation lies in the fact that experimentally one cannot obtain the configurational entropy itself.[30] As shown in Eq. (1.7), from the heat capacity data only excess entropy can be calculated, which includes configurational entropy along with vibrational and anharmonic force contributions, secondary relaxation contributions if there is any. Studies focusing on testing the AG relation have taken S_{exc} values instead of S_c, which assumes that vibrational contributions in the glassy and crystal state are same. But in general $S_c \neq S_{exc}$, which has been emphasized by both Goldstein and Johari[31,32]. Instead,

proportionality between these two entropies is assumed and the AG relation has been repeatedly tested by looking at the predicted linearity between $log\tau_\alpha$ and $(TS_{exc})^{-1}$.[33,34,35] Despite the above mentioned shortcomings of the AG relation, it gives a way to find a number of correlated molecules and the length scale of cooperativity. Yamamuro[36,37] obtained values for z^* near T_g, from adiabatic calorimetry measurements for several molecular glass formers, which falls in the range $3.5 < z^*(Tg) < 7$. These numbers seem to be very small compared to the observed lengthscale of dynamic heterogeneity (1- 3nm) from NMR measurements.[12,38] So it is quite natural that AG theory has been criticized heavily.[39] Based on the final expression of AG, it can be seen that when S_c goes to zero i.e. at T_K, τ will diverge. VTF expression also predicts that τ will diverge at T_0. VFT type expression can be obtained after some rearrangements of AG relation using Eq. (1.7) for $S_c(T)$ which is shown below:

$$\tau \approx \tau'_\infty \exp\left(\frac{C_{AG}}{TS_c(T)}\right) = \tau'_\infty \exp\left(\frac{C_{AG}}{TS_\infty\left(1-\frac{T_K}{T}\right)}\right) = \tau'_\infty \exp\left(\frac{C_{AG}/S_\infty}{T-T_K}\right) \qquad \text{Eq. (1.10)}$$

So one may expect that these two temperatures (T_0 and T_K) should coincide. Especially $T_K \approx T_0$ is regarded as a strong support towards the belief that thermodynamics and kinetics of glass forming liquids are not independent of each other. The correlation coefficient has been found to be 0.993.[22,40]

D. Physical aging in glassy state

As pointed out earlier, when a liquid is cooled rapidly from an equilibrium supercooled state to a temperature which is below T_g, a glass is formed. The molecules in the liquid do not have enough time to equilibrate at the targeted temperature. So the

structure has been driven out of equilibrium situation. That is why the glass transition is often regarded as a transition from ergodic to nonergodic state. One may expect that below T_g, as the system is not able to relax, the motions of the particles are completely frozen. Instead experiments show otherwise.[41]With time the glassy state will age, i.e., slowly moves towards its desired thermodynamically stable equilibrium state. This relaxation phenomenon in the glassy state is called 'physical aging'[42] or sometimes 'annealing' (Fig. 1.1). A straightforward method to investigate this process is to monitor how thermodynamic or related properties evolve with aging time towards their equilibrium values after a rapid temperature jump below T_g. Examples of properties measured in aging experiments include volume[41], enthalpy[43], dielectric loss[44,45], etc. This structural recovery process was found to be nonlinear[41] in nature with respect to the temperature jump (asymmetry of approach towards equilibrium) as the aging rate is dependent on structure which itself changes with time while approaching equilibrium. As a result, a downward jump is 'auto-retarded' while upward jump founds to be 'auto-catalyzed'.[41]This is what makes aging a complicated phenomenon. To account for above observation, the concept a of fictive temperature and 'reduced time' was introduced by Tool and Moynihan.[46,47] Fictive temperature (T_f) is defined for a non-equilibrium glassy state as a temperature which corresponds to the same structure in the supercooled equilibrium situation as in the glassy state.

1.2 Linear response from dielectric spectroscopy

In our lab, dielectric spectroscopy is used to gain access to the dynamics of supercooled liquids. The attractive feature of the dielectric measurement is that it can

cover a broad range of frequency (10^{-6} Hz to 1THz) which translates into time scales spanning from picoseconds to a year. This is what makes it suitable for studying relaxation in supercooled liquids whose relaxation time increase tremendously when approaching T_g. This technique relies on the idea involving orientational motion of the dipoles within a material which can be polarized by applying an external electric field. This building up of the macroscopic polarization will depend on the material's structure and temperature. The time required to reach to a steady state value of the polarization will indicate the structural relaxation of the material under study. The overall polarization can be divided into two parts: an instantaneous contribution from electronic polarization and polarization originating from orientating the dipoles (orientational polarization).The orientational polarization is defined as $P_o = \frac{N}{V}\langle\mu\rangle_z$, where N is the total number of dipoles in a macroscopic sample of volume V and $\langle\mu\rangle_z$ is the average of all the dipole moments projected on z-axis (direction of the applied field). We are mostly interested in the later contribution. Dielectric measurements can be performed in both time and frequency domain. In our lab, we use the second approach. In the linear response regime, polarization is proportional to the applied field.

$$P^*(\omega) = \varepsilon_0\chi^*(\omega)E^*(\omega) = \varepsilon_0(\varepsilon^*(\omega)-1)E^*(\omega) \qquad \text{Eq. (1.11)}$$

$\chi^*(\omega)$, the proportionality constant connecting polarization and electric field, is called the complex dielectric susceptibility. It is related to the material property called permittivity, $\varepsilon^*(\omega) = \varepsilon'(\omega) - i\varepsilon''(\omega)$. Permittivity is a complex quantity where real part, $\varepsilon'(\omega)$, corresponds to the energy stored in the material from the applied field, while imaginary part (relaxation part), $\varepsilon''(\omega)$, describes the dissipative nature of the material,

usually referred to as ‘dielectric loss’. A schematic representation of the real and imaginary part of the dielectric permittivity is shown in Fig. 1.9.

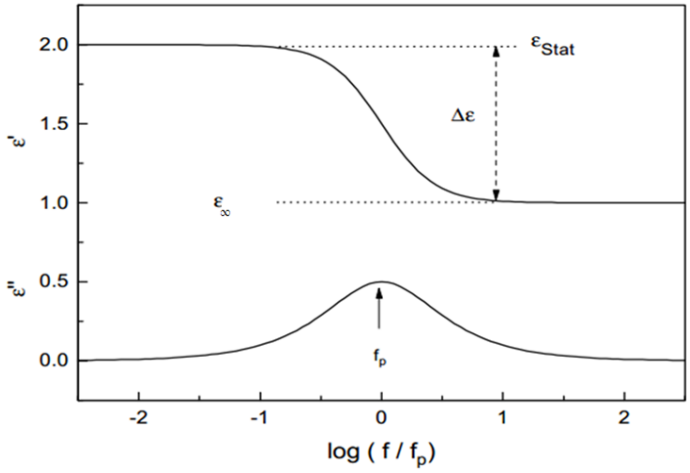

Fig. 1.9: Schematic representation of a relaxation process in terms of the dielectric spectra. Both real and imaginary parts of the permittivity are shown. Relaxation strength ($\Delta\varepsilon$) can be obtained from the difference between low and high frequency limit of the real part permittivity, whereas a relaxation peak in the imaginary part will appear correspond to the steepest change in real part spectrum.

Relaxation peaks are observed in the spectrum when the relaxation rate of the sample matches the frequency of the applied field. The real part of permittivity actually reflects the dipole density that can respond to the alternating field. At higher frequencies compared to the relaxation rate in the sample, dipoles cannot keep up with the rate of change of the applied field, so that the real part has a smaller value. Similarly, when frequency of the field is low, all the dipoles have a chance to orient along the field direction which in turn reflects a higher value in the real part. The difference in these two extreme values for each relaxation process is called relaxation strength ($\Delta\varepsilon$) of the process. The timescale of the relaxation process can be found from the dielectric loss peak, $\tau \sim 1/2\pi f_p$. The very high frequency part of the real part (ε_∞) often found to be close

to n^2, where n represents the refractive index of the material. As both the real and imaginary parts are derived from the same complex function, they are related to each other. This relation is known as 'Kramers-Kronig' relation. One of the important consequences of this relation is that, Δε can be obtained from the integration of the relaxation part of the loss spectrum $\varepsilon''(\omega)$ as follows: $\Delta\varepsilon = \frac{2}{\pi}\int_{-\infty}^{\infty}\varepsilon''(\omega)dln\omega$.

In this section, some of the fitting functions will be introduced which are usually used in the study of supercooled liquids in the frequency domain. The simplest type of response function that one can think of is of exponential in nature: $\varphi(t) = \exp(-t/\tau)$, where τ represents the relaxation time and $\varphi(t)$ is the related correlation function. In frequency domain, this exponential response equivalent is called the Debye relaxation.

$$\varepsilon^*(\omega) = \varepsilon_\infty + \frac{\Delta\varepsilon}{1+i\omega\tau} = \varepsilon_\infty + \Delta\varepsilon\left(\frac{1}{1+\omega^2\tau^2} - i\frac{\omega\tau}{1+\omega^2\tau^2}\right) \qquad \text{Eq. (1.12)}$$

However, this expression is not suitable to describe the response most often observed in glass forming liquids in their supercooled state. Dielectric loss peaks are always most often found to be broad and asymmetric in nature. Havriliak-Negami function has been extensively used to capture this deviation from Debye response, which will be introduced in the next chapter.

1.3 Nonlinear dielectric spectroscopy

Based on the experiments performed in the linear regime it is impossible to distinguish between the two extreme scenarios that can be thought of responsible for the overall observed non-exponentiality in response. In one scenario, one can assume that all the domains in the liquid relax exponentially but with different rates (heterogeneous

distribution). Other possibility lies in the fact that all domains approach equilibrium intrinsically in non-exponential fashion (homogeneous picture).[48] But linear response experiments only look at two time or two point correlation functions, so they are not able to indicate the difference between these scenarios. But there are experiments that go beyond measuring two point correlation functions, like 4D-NMR, dielectric hole burning, photo-bleaching experiments. Nonlinear dielectric spectroscopy[49] also found to be useful in this regard, as it corresponds to a higher order correlation function. In the nonlinear approach, the applied field is very high, so polarization is no longer a linear function of the applied field. As a result, higher order terms will contribute to the overall polarization.

$$\frac{P}{E\varepsilon_0} = \chi + \chi_2 E + \chi_3 E^2 + \chi_4 E^3 + \ldots\ldots\ldots \qquad \text{Eq. (1.13)}$$

Due to symmetry reasons, $\vec{P}(\vec{E}) = -\vec{P}(-\vec{E})$, all the even order susceptibility will vanish. It is usually the χ_3 component whose contribution at higher fields is considered the most.

There are two approaches one can take to drive the sample in nonlinear regime. Either with a high amplitude AC field, or a high amplitude DC field superimposed with a low amplitude AC probing field (Fig. 1.10).

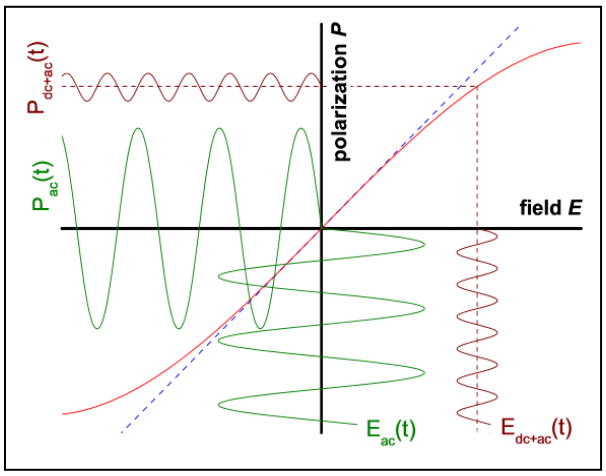

Fig. 1.10: Polarization against field strength is depicted (red curve) indicating the deviation at higher field strength from the linear response (blue dashed line). Two different ways (either a high amplitude ac field or a high amplitude dc bias field superposed with a low amplitude ac field) for achieving nonlinearity are shown.

High amplitude AC field measurements[50-52]have been performed in our group quite extensively over the past decades for looking at heterogeneities in the structural relaxation regime. This has been done by measuring differences in the permittivity values in low and high AC fields. The idea is to transfer energy from the field only to a specific domain whose timescale matches with the frequency of the applied field. This irreversible transfer of energy will raise the configurational temperature of that specific domain. By this technique one can selectively modify a certain mode while other modes will remain unchanged. This idea basically came from the hole-burning technique[13,53] but proved to be useful in explaining the heterogeneity in the simple supercooled liquids like propylene glycol[54], glycerol[55] to ionic liquids like BMIM-PF_6 while combined with its time resolved capabilities[56]. But all these measurements were confined to the frequencies close to structural relaxation peak (α-peak). For almost all these measurements, a common observation was an increase in ε'' in the high frequency side of the α-peak,

while there is almost no change on the low frequency side of the peak. The proposed phenomenological model, called 'box model', is based on heterogeneity[57], worked fairly well for the measurements carried out up to frequencies 10^2 f_{max}, where f_{max} is the frequency correspond to the maximum of the dielectric loss peak. There are various sources of nonlinear dielectric effects other than energy absorption from the field. The most common one is related to 'dielectric saturation' (the Langevin effect)[58], which shows overall negative nonlinear dielectric effect. 'Chemical effects'[59,60] have been reported to be another source of the nonlinear dielectric effect (NDE). In that case, positive changes have been observed. But the amount of NDE observed from the energy absorption is higher than the effects observed in either dielectric saturation or during chemical changes. This source of the NDE can explain why certain reaction kinetics become faster in microwave heating compared to normal heating.[61] The common difference between conventional heating and heating by mode specific energy absorption is that in conventional heating procedure energy being transferred directly to the vibrational modes which can be measured in terms of real temperature difference. But in dielectric heating energy is absorbed by slow degrees of freedom, from there eventually transferred into the phonon bath (vibrational modes). The observed NDE effect has been found to be proportional to E^2. There is another route to measure NDE which determines the higher harmonics of permittivity or susceptibility. Theories have been proposed which link third order susceptibility $\chi_3(\omega)$ to the number of correlated molecules (N_{corr})[49] present in the sample in their supercooled state which are believed to be responsible for the observed increase in viscosity. Experiments have also been performed based on the

above theory for both strong and fragile materials. A significant increase in N_{corr} with decreasing temperature was reported.[62] Dielectric saturation is also observed at low frequencies in the $\chi_3(\omega)$ spectra. But it is important to mention here that these two different approaches, which look at nonlinear dielectric effects, provide distinctly different information.[63] In Chapter 4, I will focus on the very high frequencies ($>10^2$ f_{max}) of the dielectric loss curve using the first approach of measuring NDE. Although the concept of dynamic heterogeneity to explain the overall non-exponential response looks attractive, it poses certain questions which are difficult to answer from an experimental point view. Some of those questions include the length scale of the heterogeneous domains and their lifetimes (Fig. 1.11). Very few experiments were able to predict a value for the length scale which turned out to be around 1-3nm.[64-66] It is important to point out here that although pictures showing heterogeneity in supercooled liquids often indicate a distinct demarcation line between different domains, in reality those separations do not exist. The time that a certain domain remains associated with its own timescale of relaxation is termed as its lifetime or 'exchange time' (τ_{ex}). Most often exchange times are reported in the literature in comparison with τ_α ($Q = \tau_{ex} / \tau_\alpha$). Exchanges times have been measured for different materials ranging from simple molecular liquids to polymers with various techniques involving single molecule studies[67], NMR[68], solvation experiment[69], atomic force microscopy.[70] But there is no consensus regarding the value of exchange times. Q values have been reported ranging from 1 to 10^6. But for the majority of experiments, the exchange time has been found to

be equal to 2-3 times τ_α. We will come back to this problem of rate exchange in Chapter 4 from our observations through nonlinear dielectric experiments.

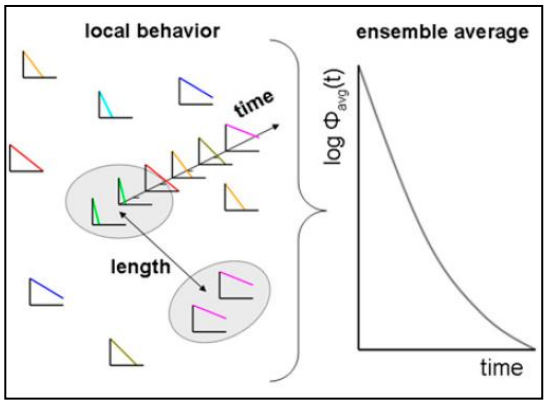

Fig. 1.11: Schematic representation of heterogeneous relaxation dynamics in terms of local exponential decay curves, where each graph represents intrinsically exponential dynamics with different time constants. Length scale and lifetime of a dynamically heterogeneous domain are also shown in the left panel. Overall nonexponential response from the ensemble average is depicted on the right panel. [taken from Ref. 71]

In case of applying a large DC bias field, the inversion symmetry (or isotropic state) will be lost. In this approach nonlinear contributions from the even harmonics may show up. To overcome this problem, measurements need to be carried out using both positive and negative bias field. A small amplitude AC field (used as a probing field) can be superimposed on top of the large DC field. So overall field can be expressed as $E(t) = E_{dc} + E_{ac} \sin(\omega t)$ where $E_{dc} > E_{ac}$. This approach has recently been employed in our group to several molecular liquids. In contrast to the positive permittivity difference obtained in large amplitude AC fields, overall peak shift towards lower frequencies have been observed by the application of large amplitude DC bias. This particular observation has been explained in terms of the change in configurational entropy via application of the field, as derived from a Maxwell relation. For most of the liquids according to

Boltzmann's equation static dielectric constant (ε_s) value would decrease with increasing temperature i.e. $\left(\frac{\partial \varepsilon_s}{\partial T}\right) < 0$. The effect of applying large DC bias field in these type of liquids results in overall reduction of their relaxation times (via Adam-Gibbs relation[29]) in an isothermal condition. We quantified this effect for several molecular glass formers and find a way to calculate the configurational part of the observed heat capacity/entropy. Those experiments will be described in detail in Chapter 5.

Chapter 2
Experimental Setups

In this chapter, experimental setups for different techniques that have been employed in our lab will be described. Setups from linear dielectric measurements to nonlinear dielectric experiments along with their time resolved version will be outlined. Some of the functions used to fit the obtained data will be introduced.

2.1 Linear Dielectric Measurements:

Dielectric measurements are used to quantify the response of the material to a field induced perturbation. It can be performed both in time and frequency domain. When an external electric field is applied to the sample, macroscopic polarization (P) will develop within the sample over a period of time, not instantaneously. By analogy, when the field is removed, the decay function of polarization can be written as φ(t) = P(t)/P(0). Dielectric experiments access this response function. In the linear response regime, this relaxation function φ(t) is independent of the field magnitude and equivalent to the macroscopic dipole correlation function i.e.,$\varphi(t) \approx \frac{\langle \mu(t)\mu(0)\rangle}{\langle \mu(0)\mu(0)\rangle}$, where $\mu(t)$ is the macroscopic dipole moment representing the vector sum of all the molecular dipoles. The dielectric displacement vector, D(t), for the time dependent electric field is related to the polarization vector by the following equation:

$$D(t) = \varepsilon_0 E(t) + P(t) \qquad \text{Eq. (2.1)}$$

where ε_0 is the dielectric permittivity in free space. From the linear response theory, D(t) can be represented as $D(t) = \varepsilon_\infty E(t) + \int_{-\infty}^{t} \frac{d\Phi(t')}{dt'} E(t-t')dt'$, where ε_∞ represent the

high frequency limit of the dielectric permittivity in the frequency domain, $\Phi(t)$is the dielectric step response function: $\Phi(t) = (\varepsilon_s - \varepsilon_\infty)[1 - \varphi(t)]$. ε_s represents the low frequency limit of the dielectric permittivity.

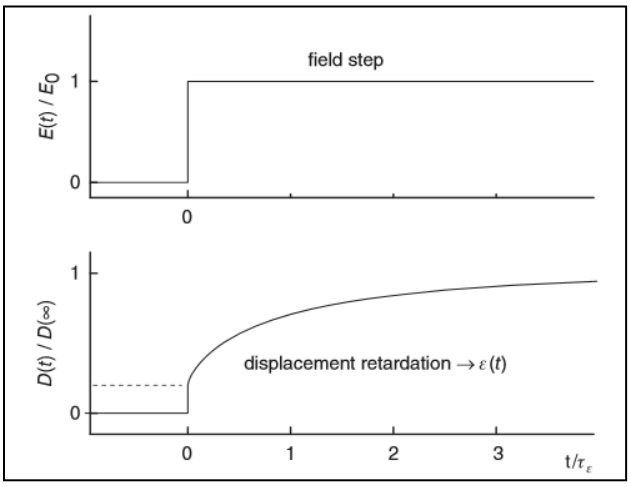

Fig. 2.1: The typical dielectric displacement retardation [D(t)] observed in response to a field step E(t) is shown where the displacement has an instantaneous and a time-dependent contribution. In this "constant field" situation, ε(t) is a retardation function, although most often it is referred to as 'dielectric relaxation'.

In the frequency domain, the complex dielectric permittivity $\varepsilon^*(\omega)$ can be found from its relation with the relaxation function, $\varphi(t)$.

$$\frac{\varepsilon^*(\omega) - \varepsilon_\infty}{\varepsilon_s - \varepsilon_\infty} = \hat{L}[-\frac{d}{dt}\varphi(t)] \qquad \text{Eq. (2.2)}$$

where $\hat{L}$ is the operator for Laplace transform whose general formalism for a time dependent function is given below.

$$\hat{L}[f(t)] = \int_0^\infty e^{-i\omega t} f(t) dt \qquad \text{Eq. (2.3)}$$

Using the above equations, the relations between time and frequency domain quantities of dielectric permittivity in its explicit form can be written as:

$$\varepsilon^*(\omega) = \varepsilon_\infty + \int_0^\infty \frac{d\varepsilon(t)}{dt} e^{-i\omega t} dt = \varepsilon_\infty + i\omega \int_0^\infty (\varepsilon(t) - \varepsilon_\infty)\, e^{-i\omega t} dt$$

$$\varepsilon(t) = \varepsilon_\infty + \frac{1}{2\pi}\int_0^\infty \frac{\varepsilon^*(\omega) - \varepsilon_\infty}{i\omega} e^{i\omega t} d\omega \qquad \text{Eq. (2.4)}$$

As mentioned in the previous chapter, for the simplest type of relaxation function, exponential response [$\varphi(t) = e^{(-t/\tau)}$], where τ is the relaxation time, the frequency domain response turns into a Debye relaxation:

$$\frac{\varepsilon^*(\omega) - \varepsilon_\infty}{\Delta\varepsilon} = \frac{1}{1 + i\omega\tau} \qquad \text{Eq. (2.5)}$$

In our lab all the dielectric measurements are done in frequency domain. To perform a dielectric experiment, usually materials are placed between two electrodes with a separation d and a small amplitude sinusoidal voltage (V) is applied across the material, which acts as perturbation (Fig. 2.2). The reorientation of the dipoles under the influence of the applied field (E = V/d) will give rise to polarization (P) which can be measured via displacement current (I). From Fig. 2.2, ϕ ($= \varphi_V - \varphi_I$) is the phase difference between voltage and current signal. Dielectric loss angle is tanδ where δ = ($\pi/2 - \phi$). Both the applied voltage and the response current are recorded and analyzed to calculate the impedance (Z^*) due to the sample. Comparing the capacitance obtained from the measured impedance against the empty capacitance or geometric capacitance (C_0), the material property called complex dielectric permittivity ($\varepsilon^* = C/C_0$) is obtained via Eq. (2.6). Geometric capacitance is defined by the separation between electrodes and the area (A) covered by the electrodes, where ε_0 is the free space permittivity.

$$C_0 = \frac{\varepsilon_0 A}{d}$$

$$Z^*(\omega) = \frac{V^*(\omega)}{I^*(\omega)}\ ;\ Z^*(\omega) = \frac{1}{i\omega\varepsilon_0 C^*(\omega)};\ \frac{C^*(\omega)}{C_0} = \varepsilon^*(\omega)$$

$$\varepsilon^*(\omega) = \varepsilon'(\omega) - i\varepsilon''(\omega)\ ;\ tan\delta = \frac{\varepsilon''(\omega)}{\varepsilon'(\omega)} \qquad \text{Eq. (2.6)}$$

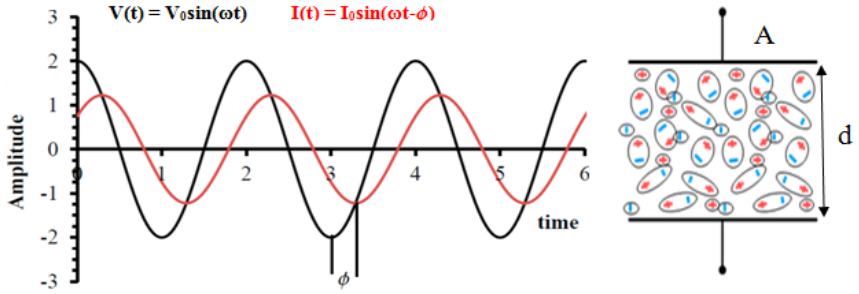

Fig. 2.2: Liquid molecules in between two electrodes having a separation distance d and area A (Right). Schematic representation of the Voltage signal, V(t), applied to the sample, and the corresponding current signal from the sample is represented by I(t). The difference in the phase angle is represented by ϕ (Left).

Samples are generally prepared between two lapped and polished electrodes (stainless steel / titanium / brass) with separations varying from 10μm to 100μm using Teflon ring spacer depending on the liquids or experiments. The Teflon ring covers the circumference of the lower electrode and gives rise to additional stray capacitance. To eliminate the stress changes on the Teflon ring due to variation in temperature, the lower electrode is spring loaded (Fig. 2.3).

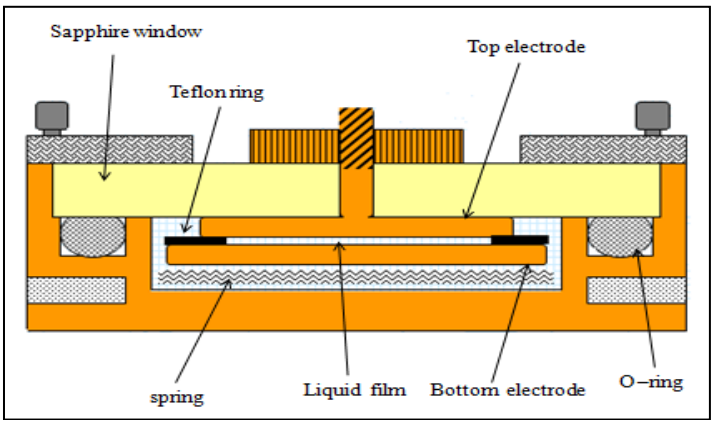

Fig. 2.3: A schematic of a typical dielectric measurement cell used in our lab with its various components

For measurements within the frequency range between 10 mHz and 10 MHz, a gain-phase analyzer, Solartron SI-1260, in combination with home built transimpedance amplifier DM-1360 is used (Fig. 2.4).

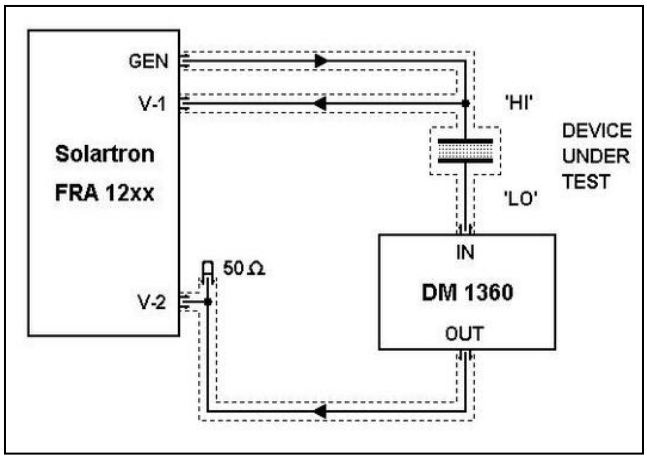

Fig. 2.4: Schematic representation of the linear dielectric response measurement setup. Solartron acts a voltage source while DM 1360, a trans-impedance amplifier, converts the current from the sample to a measurable voltage.

The Solartron SI-1260 produces the desired voltage signal. DM-1360 converts low amplitude currents to measurable voltages over the entire frequency range. The voltage at the sample is recorded via V1 input of SI-1260. The current is recorded via V2 input.

With high accuracy, the amplitude and phase relation of the complex current $I^*(\omega)$ and voltage $V^*(\omega)$ are determined. Then the dielectric function $\varepsilon^*(\omega)$ can be derived directly using the relation described in Eq. (2.6).

As mentioned earlier, most often the obtained spectra of permittivity in supercooled liquids display a broadened and asymmetric relaxation peak (For example, dielectric loss peak for glycerol in its supercooled state T = 201K is shown in Fig. 2.5). As evident from the figure, the Debye response function is not a good descriptor of such behavior. Therefore some modifications had been introduced into the Debye expression to account for the stretching and asymmetry of the loss peak.

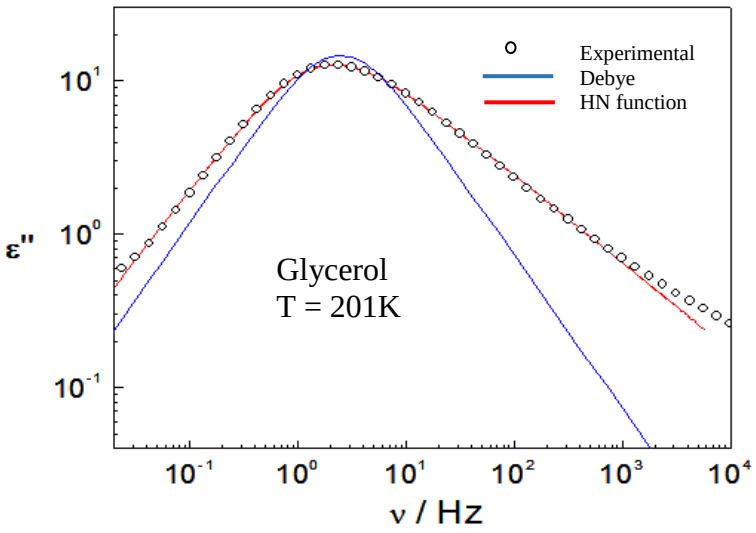

Fig. 2.5: Experimental dielectric loss curve for glycerol (Tg ≈ 190K) in its supercooled state at T= 201K is shown. Experimental data points have been fitted both Debye and Havriliak-Negami fitting functions which are represented as blue and red line respectively.

Cole-Cole[72] and Cole-Davidson approaches were introduced for that purpose. While Cole-Cole expression captures the symmetric broadening, Cole-Davidson

introduced a parameter to account for asymmetric contribution to dielectric relaxation curves.

$$\frac{\varepsilon^*(\omega)-\varepsilon_\infty}{\Delta\varepsilon} = \frac{1}{(1+i\omega\tau)^\beta} \qquad \text{Cole- Davidson}$$

$$\frac{\varepsilon^*(\omega)-\varepsilon_\infty}{\Delta\varepsilon} = \frac{1}{1+(i\omega\tau)^\alpha} \qquad \text{Cole-Cole} \qquad \text{Eq. (2.7)}$$

But when used separately, none of those can describe satisfactorily the broad range of relaxation spectra observed in supercooled liquids. Havriliak and Negami[73] combined these two approaches by introducing two exponents, which are responsible for both the symmetric broadening and asymmetry (See Fig. 2.5). The expression for this Havriliak-Negami (HN) approach is given below:

$$\varepsilon^*(\omega) = \varepsilon_\infty + \frac{\Delta\varepsilon}{[1+(i\omega\tau_{HN})^{\alpha_{HN}}]^{\gamma_{HN}}} \qquad \text{Eq. (2.8)}$$

α_{HN} and γ_{HN} control the symmetric and asymmetric broadening of the loss spectra with the constraint $0 < \alpha_{HN}$, $\alpha_{HN}\gamma_{HN} < 1$. Nonexponentiality captured by these two exponents indicate a distribution of relaxation times. When both α_{HN} and γ_{HN} are equal to 1, the Debye expression is obtained. In the time domain approach, previously mentioned KWW function with only one adjustable parameter (β_{KWW}) captures the deviation from exponential response. The average relaxation time is given by:

$$\langle\tau\rangle = \frac{\tau_{KWW}}{\beta_{KWW}}\Gamma\left(\frac{1}{\beta_{KWW}}\right) \qquad \text{Eq. (2.9)}$$

where Γ represents gamma function. So the interrelations between HN and KWW parameters had also been explored.[74]

2.2 Standard High AC/DC field impedance setup:

For high field measurements, thinner samples and high voltages are required. Typically, a sample thickness of 10μm is used. The impedance for frequencies between 0.1 Hz and 100 kHz is measured by a Solartron SI 1260 gain/phase analyzer, with the generator voltage amplified by a factor of 200 or 100 using either a Trek PZD-700 or Trek PZD 350 high-voltage amplifier which is connected to the high potential side of the sample capacitor (Fig. 2.6a). The voltage at the sample is recorded via input V1 of the SI-1260 using the voltage monitor output of the amplifier which is internally attenuated by a factor of 200 or 100. The low potential side of the capacitor is connected to ground via a shunt of impedance Z_s.

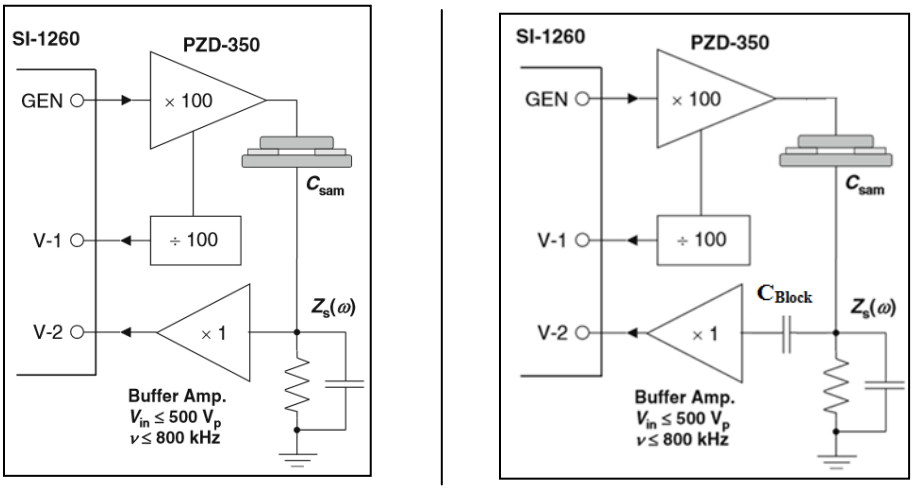

Fig. 2.6: a) Schematic of a high field AC measurement set up (left panel); b) Schematic of a high field DC measurement setup (right panel) with their various components which are described in the text.

The value of $Z_s(\omega)$ is determined by a parallel circuit equipped with a combination of resistors and capacitors, in such a way so that the frequency dependent change in shunt impedance can counteract the reduction of the current towards low frequencies (Fig. 2.7).

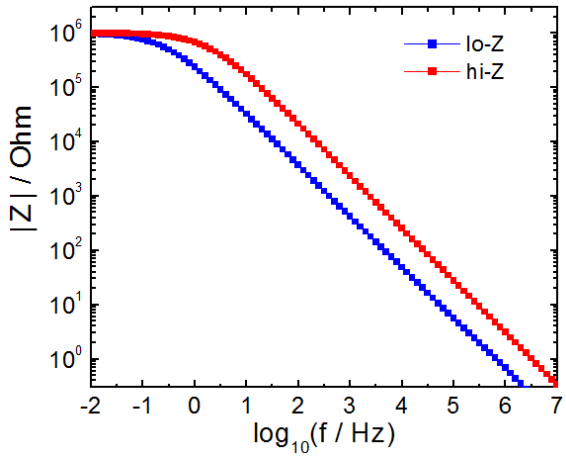

Fig. 2.7: Frequency dependent impedance values for the two different types of shunts used for experiments.

The voltage drop across the shunt is fed to a homebuilt buffer amplifier which protects the SI-1260 against high voltages (up to $500V_p$) in case of a sample failure (dielectric breakdown). The output of the amplifier measures the current through the sample and fed into V2 input. Sinusoidal electric fields, $E(t) = E_0 \sin(\omega t)$, with zero dc offset are applied to the sample while doing high AC field measurements. In standard high field impedance setup, The SI-1260 is programmed to apply the high voltage for first 3 measurements, while last 3 measurements are made with lower voltage (usually 10% of the high voltage). For the high DC field measurements, in addition to the above mentioned components, a blocking capacitor is placed between the shunt and the buffer amplifier (Fig. 2.6b) to prevent any unwanted DC component of the current from the sample. All field induced changes obtained in this manner are entirely reversible. Most of these measurements are performed using either a Novocontrol *l*-N2 cryostat with Quatro controller or with a Leybold Coolpack He cryostat with Lakeshore Model 340 temerature controller.

2.3 Time Resolved Technique (AC field):

In the standard high field impedance technique described above can provide quasi steady state permittivity values after application of the high field. One can also do a time resolved measurement in this technique as will be discussed in chapter 4, but the time resolution is limited to 2s or higher. To obtain a better time resolution in the order of milliseconds, a setup with an oscilloscope is used. For the time resolved measurements, the cryostat used for temperature control of the sample cell is a Leybold RDK 6-320/Coolpak6200 closed-cycle helium refrigerator with Lakeshore Model 340 controller equipped with calibrated DT-470-CU diode sensors (temperature can be stabilized within several mK). The advantage of using a Helium cryostat for time resolved studies is that one can keep the sample at a desired temperature for several months. The applied voltage originates from a programmable function generator (SRS DS-345) instead of SI-1260 and amplified by a PZD 700 or PZD 350. A digitizing oscilloscope (Nicolet Sigma 100) records voltage across and current through the sample (using a shunt of order R = 300Ω/ 1kΩ/ 3kΩ). The frequency range covered in this setup is 100Hz to 8kHz (Fig. 2.8a). This technique allows us to monitor the changes with a period-by-period time resolution subsequent to change in the field amplitude from one period to the next. The amplitude changes by a factor of 5 in case of high AC field measurements under the control of an arbitrary amplitude function that is cycled at a given repetition rate.

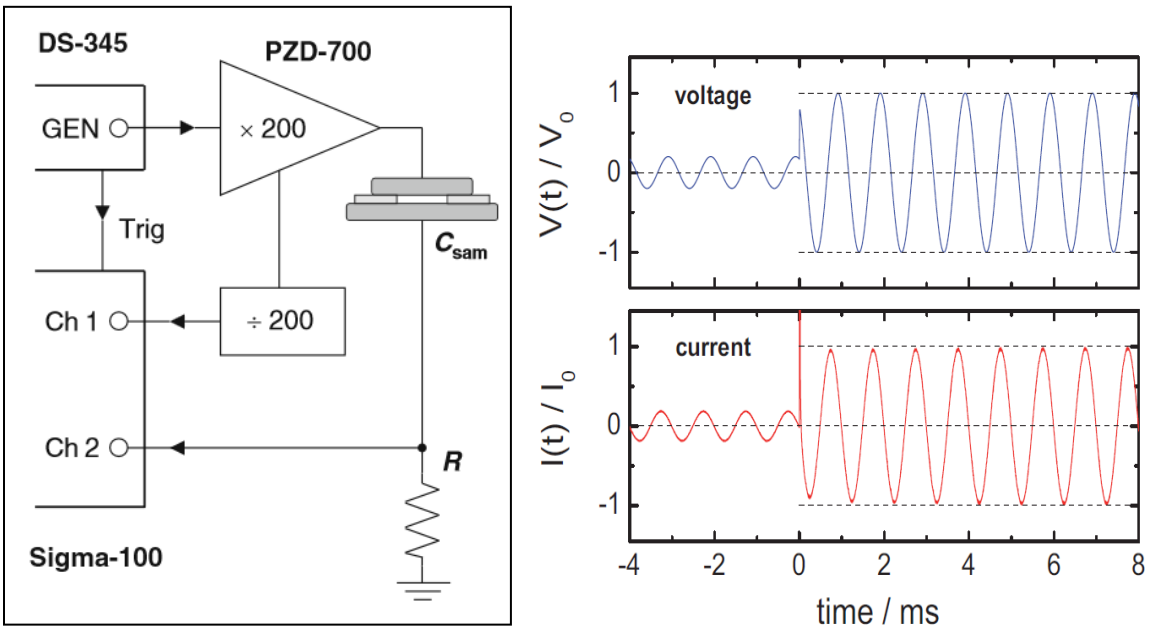

Fig. 2.8: a) Setup for the time-resolved impedance measurements at fields up to 450 kV/cm based on the SRS DS-345 generator and Nicolet Sigma 100 oscilloscope. High voltages are provided by a Trek PZD-700 amplifier with built in voltage monitor signal for a direct return to the Ch-1 input. The current is measured at the Ch-2 input as voltage drop across the resistor. b) A typical example of normalized voltage, $V(t)/V_0$, and current, $I(t)/I_0$,traces recorded using a frequency of ν = 1 kHz. The low and high voltages used correspond to fields which differ by a factor of 5.

In this manner, the transition from low to high voltage and back can be programmed without limitation on the number of cycles associated with high fields, but the amplitude transition does not necessarily coincide with the beginning of a period. Repetition rates of order r = 0.2 Hz are used, implying that the high field duty cycle remains small (0.2) and the sample is given ample time to equilibrate between energy absorption intervals. The oscilloscope can average over up to 5000 repeated signals, so that a resolution of up to $5x10^{-5}$ regarding tanδ for a particular period is achieved. Voltage and current traces are recorded with a Nicolet Sigma 100 four-channel storage scope (resolution 12 bit at 100 MS/s, 14 bit at 10 MS/s, 10^6 points record length). Both

signals are then evaluated via period-by-period Fourier analysis in order to obtain the time resolved change in tanδ or ε after a low-to-high or high-to-low peak amplitude transition. Fig. 2.8b shows a typical example of voltage V(t) and current I(t) traces in the vicinity of increasing the field amplitude by a factor of five. Data are typically recorded with averages over 4000 waveform repetitions. The signals are then subject to period-by-period Fourier analysis to obtain amplitude A and phase angle φ for both voltage and current, S(t)=V(t) or I(t), according to

$$S_{Re} = \frac{\omega}{\pi}\int_0^{\frac{2\pi}{\omega}} \sin(\omega t)S(t)dt = A\cos\varphi, \qquad S_{Im} = \frac{\omega}{\pi}\int_0^{\frac{2\pi}{\omega}} \cos(\omega t)S(t)dt = A\sin\varphi$$

$$A = \sqrt{{S_{Re}}^2 + {S_{Im}}^2},\ \varphi = \arctan\left(\frac{S_{Im}}{S_{Re}}\right) \qquad \text{Eq. (2.10)}$$

where ω is the frequency of the applied field. As each period is evaluated separately, this technique allows us to monitor the time-evolution of the field induced changes after applying the high electric field. From obtained amplitude and phase information of both current and voltage traces, real and imaginary part of the permittivity is calculated based on the following equation:

$$e'(\omega) = \frac{A_I \sin(\varphi_I - \varphi_V)}{A_V \omega C_0}, e''(\omega) = \frac{\mathrm{A_I}\cos(\varphi_\mathrm{I} - \varphi_\mathrm{V})}{\mathrm{A_V}\omega \mathrm{C_0}} \qquad \text{Eq. (2.11)}$$

We prefer to use the above notations for permittivity and loss as the system is generally in non-equilibrium situations during measurements. The code performing the Fourier analysis is also able to evaluate the power transferred irreversibly to the sample.

$$P = VI = \frac{1}{2}V_0 I_0 \cos(\varphi_I - \varphi_V) \qquad \text{Eq. (2.12)}$$

Time resolved technique (DC bias field)

For the high DC bias measurements, the waveform consists of a small amplitude AC voltage with V =V_0 sin(ωt) superimposed with a high DC bias voltage V_B for some of the intermediate periods. The peak voltage of AC field is set to be 25% of the applied DC bias level. The waveform repeats one time per every five seconds. Phase of the harmonic signal is kept unchanged. To eliminate any direct polarization response, both positive and negative bias measurements have been performed. In Fig. 2.9, a typical waveform pattern (6/12/6) is shown with both positive and negative bias applied.[75]Typically, for DC bias field measurements data are recorded for 3000 averages.

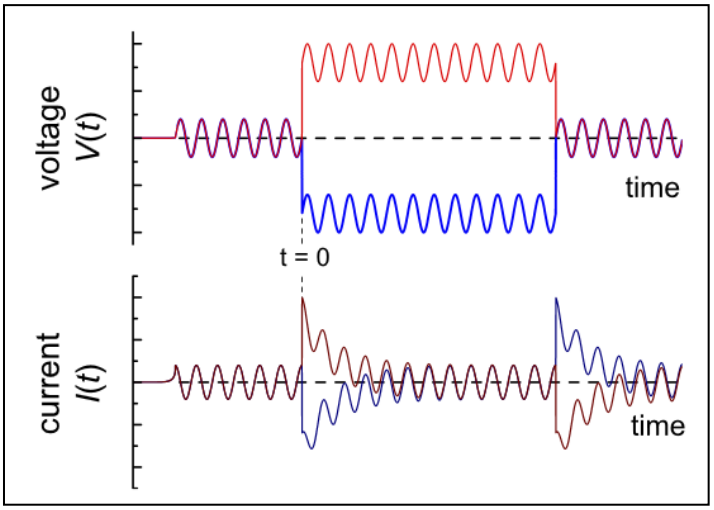

Fig. 2.9: Schematic representation of the voltage protocol used for the time resolved high dc field experiments. The superposition of $V_{ac}(t) = V_0 \sin(\omega t)$ and $V_{dc}(t) = V_B$ for $0<t<2\pi N/\omega$, where the ratio $V_0=V_B/4$ is used.[Figure taken from Ref. 75]

Chapter 3

Box model considerations

In the first chapter, it is mentioned that relaxation behavior in supercooled liquids always found to be non-exponential in nature. This overall non-exponential response is caused by the presence of both fast and slow relaxation domains in supercooled state, i.e., supercooled liquids show dynamically heterogeneous relaxation patterns. Nonlinear dielectric experiments exploiting the idea of dynamic heterogeneity show a frequency dependent nonlinear dielectric effect. This observed nonlinear dielectric effect (NDE) due to the spectrally selective absorption of energy from the external field in different materials has been quantitatively described using the so-called 'Box model'.[13] Here in this chapter, I will revisit the 'Box model' considerations and point out its limitations which have recently been observed. Also, how this concept can be used to correct for the transient heating effect due to the application/removal of a DC bias field will be discussed.

3.1 Introduction of 'Box model':

Box model was introduced to account for the non-resonant dielectric hole-burning experiments in supercooled liquids.[53] In a nutshell; this model calculates the amount of energy irreversibly transferred to the sample from the external electric field depending on the frequency of the applied electric field and dielectric loss of the sample. Due to this energy absorption, there is a change in fictive temperature for the dynamically distinct domains which depends on their respective heat capacity values. Then, the average activation energy translates this increase of the fictive temperature to a change in

relaxation time. This model allows one to quantify the observed nonlinear effects due to the application of high fields. From the model calculation it is possible to determine the configurational component of the excess heat capacities.[76]

3.2 Model assumptions and description:

As stated above, 'box' model considers the supercooled liquid as a composition of different dynamical domains which relax independently of each other i.e. dynamically heterogeneous. The correlation function for each domain is considered to be exponential in nature. In other words, the overall dielectric loss curve of the sample can be thought of as a superposition of Debye type relaxations. The domains pertaining to the same timescale constitute a mode. So each mode *i* can be associated with its own timescale τ_i. Before rate exchange process sets in, each mode can relax independently. Each mode is associated with its own heat capacity step, $\Delta C_{p,i}$ as well. Overall relaxation pattern observed in a linear dielectric experiment can be obtained when contributions of each mode will be taken into account with their own weight factor, g_i, so that $\Sigma_i\, g_i = 1$. In terms of continuous distribution of relaxation times, g_i can be written as a probability density function $g(\tau)d\tau$. This distribution function, $g(ln\tau)$ can be obtained by fitting the frequency dependent loss/susceptibility spectra. This distribution function is assumed to be same for both the overall dielectric loss curve and frequency dependent imaginary part of the dynamic heat capacity curve, as found for glycerol in the α relaxation regime.[77] Every mode can be associated with a fictive temperature, T_f, which can be defined via the relaxation time τ_i of that particular mode as the temperature T, that would lead to the same time constant τ_i if the system were in equilibrium, i.e. if $T=T_f$.

3.3 Model calculation and prediction of nonlinear dielectric effect:

When there is no external field at t ≤ 0, system is in thermal equilibrium with the phonon bath and the fictive temperature is same as the bath temperature (T). Also the sample is not polarized (no displacement). So initial conditions for each mode can be stated as follows:

$$E(t \leq 0) = 0, D_i(t \leq 0) = 0 \; and \; T_f(t \leq 0) = T \qquad \text{Eq. (3.1)}$$

Now, when a material is subjected to a strong sinusoidal field $E(t) = E_0 \sin(\omega_0 t)$, energy will be transferred irreversibly to the sample. Depending on the frequency of the applied field certain modes whose loss profile matches with the power spectrum of the field, will absorb energy from the field. For a sample of volume V, the amount of energy (Q) per period turns out to be $Q = \pi \, \varepsilon_0 \, E_0^2 \varepsilon''(\omega_0) V$. So, for each domain, the energy gain averaged over one cycle will be given by the power $p = Q\omega_0/2\pi$. Due to this energy absorption, there will be an increase in the configurational or fictive temperature for the mode in question. Eventually, the configurational temperature will slowly approach towards the bath temperature (T) with the thermal timescale ($\tau_{T,i}$) of that specific mode. So the energy loss in terms of power for a mode can be written as:

$$p_{loss} = -\frac{\rho \Delta C_{p,i}(\omega) \Delta T(t)}{\tau_{T,i}} \; ; \; \Delta T = T_f - T \qquad \text{Eq. (3.2)}$$

where ρ stands for density. The time dependent change in fictive temperature for a particular mode will depend on the balance between the energy that a mode absorbs from the field and the energy surrendered to the phonon bath.

$$\frac{d\Delta T(t)}{dt} = \frac{p}{\rho \Delta C_{p,i}} - \frac{\Delta T(t)}{\tau_{T,i}}$$

$$= \frac{\varepsilon_0 E_0^2 \Delta\varepsilon}{2\rho\Delta C_{p,i}\tau_i} \frac{\omega^2 {\tau_i}^2}{1+\omega^2\tau_i^2} - \frac{\Delta T(t)}{\tau_{T,i}} \; ; \Delta T(0) = 0 \quad \text{Eq. (3.3)}$$

For the steady state condition (i.e., when $\frac{d\Delta T(t)}{dt} = 0$), the configurational temperature for each mode will eventually settle at

$$T_f = T + \frac{\varepsilon_0 E_0^2 \Delta\varepsilon_i}{2\rho\Delta C_{p,i}} * \frac{\omega^2\tau_i}{1+\omega^2\tau_i^2} * \tau_{T,i} \quad \text{Eq. (3.4)}$$

Assuming thermal ($\tau_{T,i}$) and dielectric relaxation (τ_i) timescale being the same for each mode, the above equation simplified in the following form.

$$T_f = T + \frac{\varepsilon_0 E_0^2 \Delta\varepsilon_i}{2\rho\Delta C_{p,i}} * \frac{\omega^2\tau_i^2}{1+\omega^2\tau_i^2} \quad \text{Eq. (3.5)}$$

We can finally drop the subscript 'i' from both $\Delta\varepsilon$ and ΔC_p, due to the assumption of having similar distribution function $g(\tau_i)$. So the final form can be written in the following expression:

$$T_f = T + \frac{\varepsilon_0 E_0^2 \Delta\varepsilon}{2\rho\Delta C_p} * \frac{\omega^2\tau_i^2}{1+\omega^2\tau_i^2} \quad \text{Eq. (3.6)}$$

Finally, the increase in configurational temperature can be translated into change in the timescale of the modes based on the activation energy equation, $dln\tau_i = E_a d(\frac{1}{k_B T_i})$ for all modes. So assuming isothermal condition, which is maintained during experiments performed in our lab, the field induced modifications in terms of dielectric time scale for a particular mode will follow the equation as shown below:

$$ln\tau_i^* = ln\tau_i - \frac{E_a}{k_B T^2} * \frac{\varepsilon_0 E_0^2 \Delta\varepsilon}{2\rho\Delta C_p} * \frac{\omega^2\tau_i^2}{1+\omega^2\tau_i^2} \quad \text{Eq. (3.7)}$$

At very high frequencies compared to the peak position ($\nu > \nu_{max}$), i.e., when $\omega\tau_\alpha \gg 1$, the overall change will no longer be frequency dependent, thus being a

constant quantity. The usefulness of the above equation has been repeatedly tested for various glass-forming materials in our lab.[55,76,78,79] The deviations from the low field counterpart are most often gauged by taking the difference in either ε''values or in $tan\delta$, denoted as $\Delta ln\varepsilon'' = (\varepsilon''_{hi} - \varepsilon''_{lo})/\varepsilon''_{lo}$ or $\Delta lntan\delta$. One of the examples involving propylene carbonate is shown in Fig. 3.1 where both time dependent (panel a) and steady state predictions (panel b) are shown compare to the experimental results.

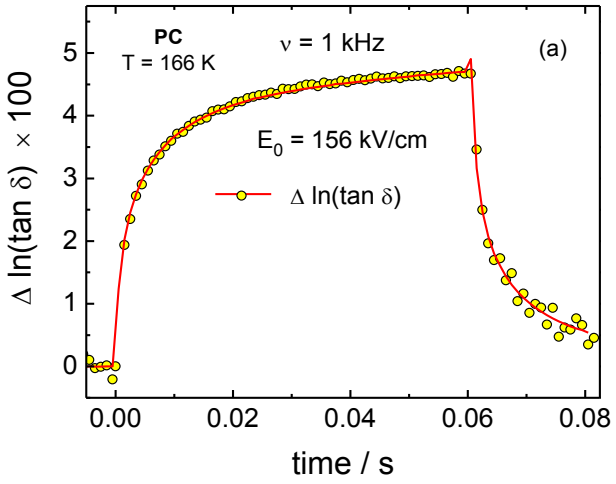

Fig 3.1: Experimental results (yellow circles) for the time-resolved field-induced relative change of tanδ measured at ν = 1 kHz for propylene carbonate at T=166 K (panel a). Red line in that graph corresponds to the model prediction based on Eq. (3.3). (Data taken from Ref. 57)

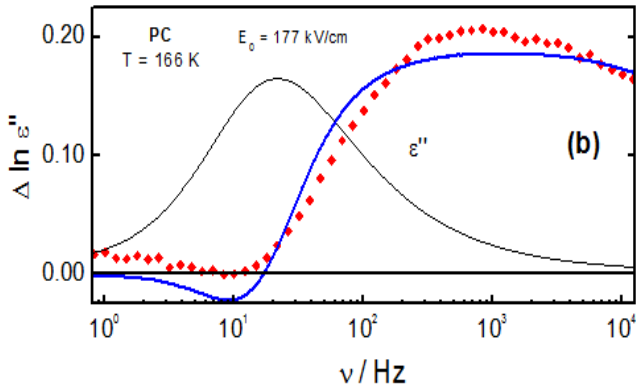

Fig. 3.1: Experimental results for the frequency resolved dielectric loss and its field induced changes for propylene carbonate at T = 166 K. (panel b). The dielectric loss, ε″ (scaled arbitrarily), is shown as black line. The relative field induced change, Δlnε″, is represented by red symbols, derived from high (E_0= 177 kV/cm) and low (E_0= 14 kV/cm) field data. The solid blue line represents the steady state model prediction.(Figure taken from Ref. 51)

It is evident from the above figures that box model predicts the nonlinear dielectric effect quite well in a quantitative manner. The prediction from the 'box' model found to be quite successful for different glass forming liquids studied in our group. From time dependent measurements at various frequencies the heterogeneous picture (different relaxation times at different frequencies) of the supercooled liquids has been confirmed (Fig. 6 in Ref. 57).

In Fig. 3.2 the existence of multiple relaxation times has been shown as a superposition of Debye peaks. It is interesting to note that two modes labeled as "τ_3" and "τ_5", display the same loss ε″ at the applied frequency. So both these modes will absorb the same amount of energy (per volume) from the external field. However, the rate at which they transfer excess energy to the phonon bath depend on their thermal timescale

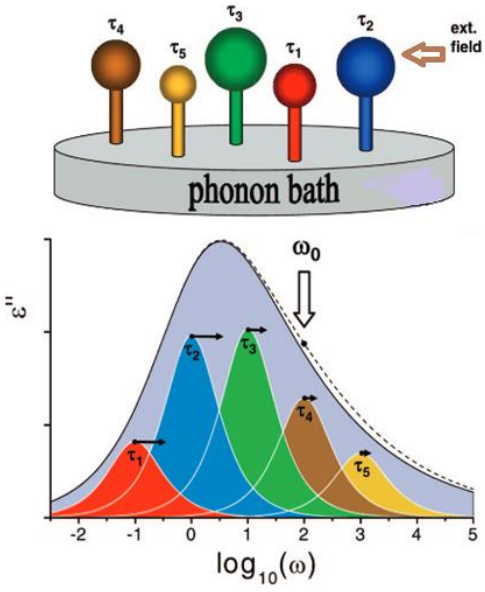

Fig. 3.2: Schematic representation of five independent slow modes with different relaxation times (τi) and how they contribute to heat capacity Cp (top) and to the dielectric loss spectrum ε"(ω) (bottom). The direction of the energy flow resulting from the application of an external field is shown in the top part of the figure (brown arrow). Each mode contributes with a Debye peak to the entire loss spectrum, shown as overall solid line in the ε" versus logω graph. The arrows on top of the individual loss peaks indicate the shift in relaxation time due to increased configurational temperatures after applying a large electric field at frequency ω_0. The net effect of these shifts is an increase of the loss at ω_0, represented by the dot. The dashed line represents ε" at large fields across the entire spectrum. (Picture taken from Ref. 51)

and to be precise the ratio of their timescales(τ_3/τ_5). Therefore, net effective change in temperature will be higher for slower modes, as indicated by the arrows representing $\Delta\ln\tau$ for each mode. The net result regarding $\varepsilon''(\omega_0)$ is an increase, as indicated by the dot in the Fig. 3.2, above the solid envelope representing the low field limit for $\varepsilon''(\omega)$. The dashed line in the figure represents the result of measuring the entire loss spectrum at high fields, consistent with the observation for PC as shown in the Fig. 3.1.

3.4 Limitations of Box model:

Although the simplicity of the box model and its predictive power of nonlinear dielectric effect are quite impressive, the model prediction has been found to fail in some cases in recent years. It started with the work of Huang and Richert,[51] when they observed the time resolved measurements for 2-MTHF. The time evolution of tanδ curves after application of high amplitude AC field show a frequency dependency for frequencies near the peak position ("relaxation regime") which is the hallmark of the heterogeneous nature. But at higher frequencies in the "regime of aging experiments" this structural recovery was found to be frequency invariant. This clearly indicates that in the aging regime the heterogeneity regarding structural recovery is lost, whereas the basis of the box model is the dynamically heterogeneous nature of both, structural relaxation and structural recovery. The box model is also found to be insufficient when nonlinear dielectric effects of monohydroxy alcohols were investigated. The problem associated with these alcohols comes from the fact that they possess a strong Debye peak which dominates the dielectric spectra but this peak is not associated with the characteristic heat capacity step observed in calorimetric measurements.[80] So, clearly the assumption of correlated dielectric and thermal timescale does not apply in the case of mono-hydroxy alcohols.[57] Very recently, NDE measurements from high AC fields have been reported for plastic crystals cyanocyclohexane and a mixture of neopentylglycol in cyclohexanol.[81] These measurements also indicated that the 'box model' predictions do not follow the observed effect even near the peak frequency,$\nu_{max} < \nu < 10^3\nu_{max}$. Here the complicacy is rooted in the intrinsically nonexponential response of the modes of

plastic crystals as confirmed by multidimensional NMR studies.[82] So for the plastic crystals, the assumption of having a Debye type relaxation for each mode in the box model is violated. In the next chapter, the NDE effects in the aging regime will be discussed elaborately both in terms of the steady state prediction and its time resolved variant.

But as box model works well for simple molecular liquids close to the peak frequency, we can still use the prediction for the time evolution for the change in effective temperature at a particular frequency for the application of high amplitude DC bias field. In case of DC bias field application, the overall observed effect will be a combination of field induced change in entropy along with the transient 'heating' contribution from the applied field. So to account for the heating effect in that context, box model will be very useful. Those measurements will be discussed in Chapter 5.

Chapter 4

Nonlinear dielectric measurements in the excess

-wing and β-relaxation regime

4.1 Introduction to excess wing and β-relaxation:

Broadband dielectric spectroscopy is commonly employed in the study of relaxation dynamics due to its high precision and the availability of a wide range of frequencies. In this broad frequency range, dielectric spectra of deeply supercooled liquids usually reveal several relaxation processes. The most prominent process that appears in the dielectric spectrum is the primary or α-relaxation originating from orientational motion of the molecules, which is associated with viscous flow of the sample. Below the glass transition, however secondary relaxations (β-relaxation) persist, which can be followed by dielectric measurements. These type of relaxations can also be observed in the equilibrium liquid at $T > T_g$. All secondary relaxations appear at higher frequencies compared to the α-relaxation. There are different molecular mechanisms that can be responsible for secondary processes in glass-forming liquids. For example, it can originate from intra-molecular motions within a part of the molecule like side chain motion in a polymer.[83] Clearly this type of motion is not connected to structural relaxation, which involves the rotation of the entire molecule. However, Johari and Goldstein found the existence of secondary relaxation in completely rigid molecular glass-formers which lack intra-molecular degrees of freedom.[84] Thus this kind of secondary relaxation definitely originates from the motion of the entire molecule and can be considered as a precursor to the primary relaxation. This second type of secondary

relaxations mentioned above is referred to as JG β-relaxation. NMR investigations have shed light to the correlation between α- and β-relaxation.[85] If the JG secondary relaxation is a fundamental feature of the glassy dynamics, then it must be universally present in all the glass formers, independent of their molecular structures and chemical nature. However, there are many glass formers whose loss spectra show no evidence of any secondary peak, but excess spectral density with respect to the extrapolated high-frequency power law flank of the α-peak.[86] This excess loss contribution is termed as excess wing (EW) in the dielectric spectra and appears as a power law of frequency with exponent smaller than that characterize the high frequency part of the structural peak. Below the glass transition this excess wing persists as slow secondary relaxation process. Kudlik *et al*.[87] proposed a classification of the glass-formers, according to whether their dielectric spectra show a distinct β-peak ('type B') or only an excess wing ('type A').There are two opposing views about the origin of this excess wing feature. Some argued that it is an inherent part of the α-relaxation process. In that notion, Dixon and Nagel[88] proposed a scaling procedure by which dielectric loss curves at different temperatures can be scaled onto a single master curve including the excess wing regime. Nagel scaling works well for many materials. However, there are reports which criticize this scaling procedure. Departures from the scaling law of Nagel and Dixon have also been reported.[89] Also, observations made by Casalini and Roland, that materials having very similar α relaxations can have different EW questions the validity of the idea whether the EW is a component of the α-process or not.[90] The second view considers the excess wing as a submerged JG β-relaxation process under a dominant α-process. Several new

experimental approaches successfully showed that the EW is nothing else but the high frequency tail of a secondary peak. Schneider and co-workers[91]observed via aging experiments below T_g for glycerol and propylene carbonate that EW eventually transform into a shoulder. Their explanation of such behavior is based on different dependences of the structural and secondary relaxations on aging. Another procedure demonstrating the similar observation was achieved by modifying intermolecular interaction within materials from the same family but with slightly modified molecular structures. Dielectric measurements were performed for a family of polyalcohols and polymers with increasing number of repeating units. Broadening of the structural peak along with transformation of EW into a resolved secondary loss peak was observed.[92] The modification of the intermolecular interactions was also achieved by mixing a polar glass former (e.g. picoline) with a high Tg material (e.g. OTP, tri-styrene).[93] In these experiments, the addition of the apolar and lower mobility component produced an increase of the intermolecular interaction experienced by the polar component, as reflected by a broadening of the structural peak, and the appearance of a secondary relaxation peak in the loss spectra instead of the EW of neat polar glass former. Experiments at high pressure have been especially useful in identifying the nature of the EW, since the α- and β-relaxation display different pressure sensitivities. For example, application of very high pressure to glycerol transforms its EW into a partially merged secondary peak.[94] Finally, there are also glass-formers that show in their dielectric spectra both an excess wing and a γ-relaxation peak at higher frequencies. While excess wing has been regarded as a true JG β-relaxation process in that case, γ-relaxation is assumed to be intramolecular in

nature. Pressure dependent measurements support the above idea. The analysis based on the Coupling Model[95] is used to identify JG relaxation, also confirms the validity of the above scenario. Actually, from the above experimental evidences it is very much expected that excess wing and β-process share some common properties. It seems quite appropriate to designate both of them as secondary relaxations of JG type. But the true microscopic nature of EW remains obscure. In this chapter, nonlinear dielectric response in terms of high AC field for both these secondary relaxation modes will be presented with a focus to unveil any correlation in terms of the microscopic origin of these processes.

4.2 Nonlinear dielectric effects in excess wing regime:

I. Motivation

High field impedance spectroscopy has emerged as a novel tool to study structure and dynamics of glass-forming liquids, exploiting the notion that more microscopic insight can be obtained from studying non-linear dielectric effects, relative to the standard linear response experiments. These measurements are often performed with zero bias field with a high amplitude sinusoidal field, $E(t) = E_0\sin(\omega t)$. In case where the detection of non-linear effects focuses on the polarization P at the fundamental frequency ω, the subscript '1' is used to identify the order of the Fourier component of interest. Contributions to P_1 will be dominated by the linear susceptibility, χ_1, and at moderate departures from the linear regime a further contribution arises from a term that is proportional to the third power of the electric field, with susceptibility $\chi_1^{(3)}$. If higher

order terms in the field (n = 5, 7, ...) are disregarded, the relation between P_1 and E_0 can be written as:

$$\frac{\hat{P}_1(\omega)}{\varepsilon_0 E_0} = \hat{\chi}_1(\omega) + \frac{3}{4} E_0^2 \hat{\chi}_1^{(3)}(\omega). \qquad \text{Eq. (4.1)}$$

The present analysis follows common practice in evaluating the data using the standard relations for obtaining permittivity ε in the linear regime, but with different results for the low (linear response) and high field case, identified by the respective indices 'lo' and 'hi', i.e.,

$$\hat{\varepsilon}_{lo}(\omega) = 1 + \hat{\chi}_1(\omega)\ ; \quad \hat{\varepsilon}_{hi}(\omega) = 1 + \hat{\chi}_1(\omega) + \frac{3}{4} E_0^2 \hat{\chi}_1^{(3)}(\omega). \qquad \text{Eq. (4.2)}$$

The energy that a sample absorbs from an external time-dependent field of sufficiently large amplitude has been identified as a source of considerable non-linear dielectric behavior as discussed in Chapter 3. In the extreme case of microwave heating and related experiments, the field induced modification is governed by a change in sample temperature.[96] At lower frequencies and accordingly reduced power levels, changes in permittivity can be detected, even at isothermal conditions. Using the concept of dynamic heterogeneity, these field induced modification can be rationalized on the basis of spectrally selective increases in configurational temperatures (ΔT_{cfg}), which result in a reduction of relaxation time constants, implying that modes shift along the $\ln \nu$ scale with negligible change of their amplitudes. For steady state conditions and for time constants not too far away from the most probable value, $\tau_{\max}$, the difference between $\ln \tau$

values at high (τ_{hi}) and low ($\tau = \tau_{lo}$, linear response value) fields, $E_0\sin(\omega t)$, can be approximated by

$$\ln\tau_{hi} - \ln\tau_{lo} = -\frac{E_A}{k_B T^2} \times \underbrace{\frac{\varepsilon_0 E_0^2 \Delta\varepsilon}{2\rho\Delta C_{cfg}} \times \frac{\omega^2\tau^2}{1+\omega^2\tau^2}}_{\Delta T_{cfg}}, \qquad \text{Eq. (4.3)}$$

where $E_A = d\ln\tau_{max}/d(1/k_B T)$ is the overall apparent activation energy, $\Delta\varepsilon = \varepsilon_s - \varepsilon_\infty$ is the (linear response) dielectric relaxation amplitude, ΔC_{cfg} is the configurational heat capacity step, and ρ is the density. This relation has been found to provide reasonable predictions for the magnitude of the non-linear effects for numerous materials, including D-sorbitol.[76]

Nonlinear dielectric response in glass-forming liquids has gained a renewed interest involving variety of experimental measurements. The interests lie in different directions: determination of the growing correlation length by measuring third order susceptibility, χ_3; characterization of dynamic heterogeneity by looking at the frequency dependent nonlinear contributions to the dielectric permittivity, $\Delta ln\varepsilon''$. But both these approaches are mainly focused in the primary relaxation regime, frequencies near to the peak position. Recently, these type of measurements have been performed at very high frequencies e.g. in the excess wing regime. The very first nonlinear dielectric experiment in excess wing regime was performed by Bauer *et al.*[97] This particular study was motivated by the following facts:

i) origin of the excess wing is controversial; often regarded as an unresolved JG β-relaxation, which itself is believed to be the precursor to primary structural relaxation

process governing the viscous flow in liquids ii) dielectric hole burning experiments found different behaviors of excess wing and α-relaxation regime in terms of the persistence time of the burned holes[98] iii) observations from physical aging experiments in the excess wing region of glycerol can be explained without invoking 'dynamic heterogeneity', which is already a well-established feature of the α-relaxation regime.

In their work,[97] two typical glass forming materials with pronounced excess wing behavior e.g. glycerol and propylene carbonate had been looked at. The chosen nonlinear method is analogous to the one developed by Richert and Weinstein[50] and described in Chapter 2 in the "High AC field" section. The observed field effects are shown below for glycerol at different temperatures (Fig. 4.1). The results for propylene carbonate are found to be very similar in nature.

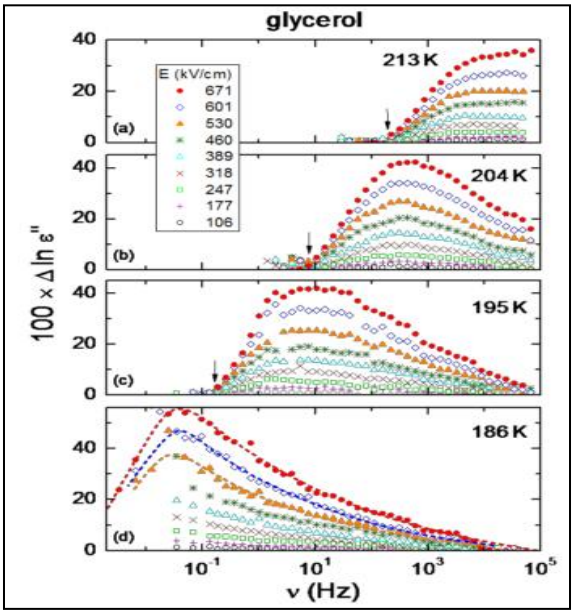

Fig. 4.1: Field induced relative changes in dielectric loss for glycerol at different temperatures. Each curve represents the observed change at different high field value compared with the low field value of 14 kV/cm. Arrows indicate the position of the loss peak frequency at the specified temperature.[Figure taken from Ref. 97]

i) At higher temperatures, above the peak frequency, in the high frequency flank of the α-peak region high field significantly modifies the low field permittivity value. Relative change of about 50% in ε'' was observed with field 671kV/cm for glycerol, which is in accord with the previous result reported for glycerol but at a lower field 282kV/cm. This observed result is quite in agreement with the phenomenological 'box model' prediction which is discussed in Chapter 3.

ii) However, at low temperatures, when the measurements were extended to the very high frequencies near the excess wing regime, even with the highest applied field the relative changes in permittivity dropped back to zero. In other words, low and high field spectra were found to be identical in the high frequency regime. This effect is not in accord with the 'box' model prediction. At very high frequencies ($\omega >> \tau_\alpha$), according to the 'box' model (Eq. 4.3) the nonlinear effect should reach a constant plateau value for $\Delta \ln \tau$.

This unexpected finding of lacking nonlinear behavior in excess wings of glass-formers raises certain concerns about both the validity of the box model and the applicability of the heterogeneous picture of the supercooled liquid in the excess regime:

i) Recent theoretical studies[99,100] have established a connection between a growing correlation length and increasing amount of the nonlinearity. With lowering temperature, observed growth in the overall nonlinear effect indicate that α-relaxation is cooperative in nature and cooperativity increases with decreasing temperature. The observed lack of nonlinearity in the excess wing regime suggests that the microscopic process responsible

for this feature in dielectric spectra is non-cooperative. Secondary relaxation processes below T_g are also non-cooperative in nature as seen by their Arrhenius temperature dependence. So, excess wing can be treated as an unresolved JG β-process. But the experiments presented in the above mentioned paper reports also temperatures which are above T_g. In this temperature range, the evolution of the α-peak and excess wing with temperature follows non-Arrhenius behavior although with different activation energies.

ii) The net observed nonlinear dielectric effect near the α-peak can be quantitatively described by phenomenological 'box' model, which corroborates the idea of dynamic heterogeneity already proven by many different experiments. But the absence of nonlinearity in excess wing regime in marked contrast to the α-peak region indicates that heterogeneity is absent in excess wings, which is very surprising because excess wing spans over few decades at low temperatures. Also, dielectric hole-burning experiment confirms the heterogeneity in the secondary relaxation process.[101]The observed effect is opposite to those observations.

iii) In general, physical aging experiments are carried out mostly in this excess wing regime. In those experiments it has been seen repeatedly that the modes present in the wing region move with a single 'inner clock' after a downward temperature jump i.e., all the modes shift in a concerted fashion mostly with the timescale of the order of τ_α. So one would expect to see NDE effect with field, but it would require almost τ_α timescale to develop. It may be possible that the amount of time these high field cycles were applied is not sufficient to develop any detectable amount of NDE.

To clarify the above mentioned discrepancies, the nonlinear dielectric effects in the excess wing regime up to frequencies $\omega \approx 10^7\ \omega_{max}$ for several molecular glass formers involving glycerol and propylene carbonate (PC) also has been obtained. Both the steady state effects and their time resolved variants will be reported here.

II. Experiment

The glass-forming liquids used for the study are propylene carbonate (PC, 99.7%, anhydrous), 2-methyltetrahydrofuran (MTHF, 99+%, anhydrous), and glycerol (GLY, 99.5+%, spectrophotometric grade), all purchased from Sigma-Aldrich and used as received. High field impedance experiments are performed for frequencies from 0.1 Hz to 100 kHz using a system based upon a Solartron SI-1260 gain/phase analyzer that has been described in Chapter 2. The capacitor consists of two polished stainless steel disks (16 and 20 mm ∅), separated by a 10 μm thick Teflon ring that leaves an inner area of 14 mm ∅ for the sample. For those cases where a time resolution of a few seconds is sufficient, time resolved experiments are performed by programming a sequence of measurements ($1 \le i \le 100$) at the same frequency, with the field amplitude set to a high value of E_0 for the entire time interval for which $10 \le i \le 50$ and with a low (linear response) field otherwise. In this mode, a permittivity value is stored once every few seconds.

III. Results

All NDE features which are shown below, are qualitatively equal for PC, MTHF and GLY, but the best resolved data is obtained for PC. All magnitudes of field induced changes scale with E_0^2, and are thus proportional to the energy associated with that field

amplitude. Linear response dielectric loss spectra are depicted for PC for several temperatures on a reduced frequency scale in Fig. 4.2.

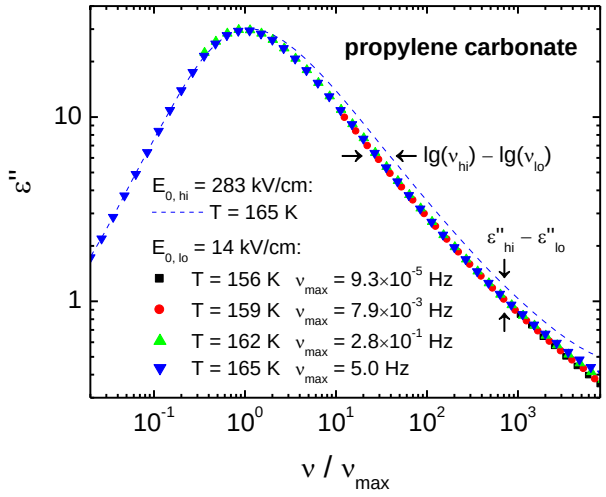

Fig. 4.2: Symbols represent linear response ($E_{0,\ lo}$=14 kV/cm) dielectric loss spectra, $\varepsilon''_{lo}(\nu/\nu_{max})$, for propylene carbonate at the temperatures indicated. The superposition is obtained by normalizing the frequency axis to the respective peak values, ν_{max}, listed in the legend, while the amplitudes are not subject to normalization. The dashed line shows the high field ($E_{0,hi}$=283 kV/cm) loss spectrum, $\varepsilon''_{hi}(\nu/\nu_{max})$, for T=165 K, using the same ν_{max}=5.0 Hz value as for its low field counterpart. Arrows at the high frequency wing indicate the two distinct approaches to report the field effect: the "vertical" difference, $\varepsilon''_{hi}-\varepsilon''_{lo}$, and the "horizontal" difference, $\lg(\nu_{hi})-\lg(\nu_{lo})$.

It is quite evident from Fig. 4.2 that in the investigated temperature range, time-temperature superposition (TTS) is valid and the dielectric constant ε_s as well as the relaxation strength, $\Delta\varepsilon$, is virtually temperature invariant. The graph also includes a loss curve for one temperature (T = 165 K) obtained at a high field of E_0 = 283 kV/cm, and the deviation from its low field counterpart is clearly visible at frequencies exceeding the loss peak position ($\nu > \nu_{max}$). The figure also indicate the two different ways of measuring the field induced changes: in terms of the 'vertical' difference, $\varepsilon''_{hi} - \varepsilon''_{lo}$, or as

the 'horizontal' difference, $\lg(\nu_{hi}) - \lg(\nu_{lo})$ or equivalently $\lg(\tau_{hi}) - \lg(\tau_{lo})$, calculated according to

$$\ln\tau_{hi} - \ln\tau_{lo} = \frac{\left(\varepsilon''_{hi} - \varepsilon''_{lo}\right)/\varepsilon''_{lo}}{d\lg\varepsilon''_{lo}/d\lg\omega}. \qquad \text{Eq. (4.4)}$$

Standard high field measurements (total 6 avg.) are performed for all the above mentioned temperatures. In Fig. 4.3, field induced relative changes (vertical difference) in the dielectric loss ε'' for propylene carbonate at different temperatures are depicted. This relative vertical difference is equal to $\Delta\ln\varepsilon''$ for small values, where Δ refers to the difference between high and low field result. This result is consistent with the previously reported observations from Bauer *et al.*[97] The values of $\Delta\ln\varepsilon''$ approach zero for frequencies exceeding about $10^5\omega_{max}$. The arrows corresponding to each curve indicate the peak position at that temperature.

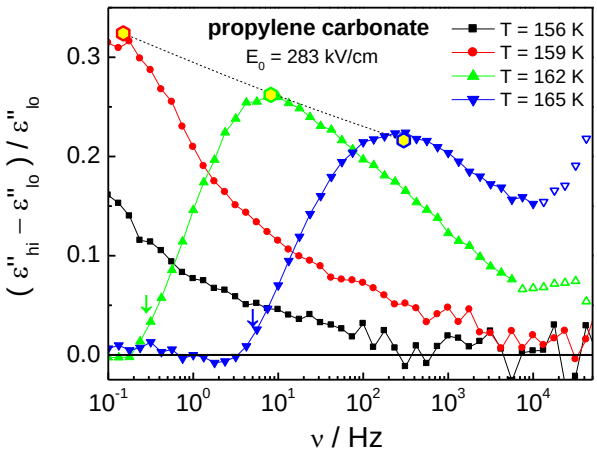

Fig. 4.3: Field induced relative changes in dielectric loss for Propylene carbonate at different temperatures. Each curve represents the observed change for a high field value of 283 kV/cm compared with the low field value of 14 kV/cm. Arrows indicate the

position of the loss peak frequency at the specified temperature. Open symbols indicate the situation where temperature is raised via excessive energy absorption. Hexagons positioned at the peak maximum of the NDE effect trace the apparent activation energy, $d\ln\tau_{max}/d(1/T)$.

Note that these data are recorded in a standard impedance mode, i.e., moderate number of high field cycles is applied. So it is possible that the loss values obtained in this manner may not reflect the steady state situation. For that reason, time resolution has been added to the above approach in order to facilitate extracting the 'instantaneous' contribution to the NDE as well as the long time limit at which ε''_{hi} has reached a steady state value. The results are shown in Fig. 4.4, in terms of the 'horizontal' difference, which is derived from the 'vertical' difference via Eq. (4.4). The temperatures and their corresponding τ_{max} values are given in the graph.

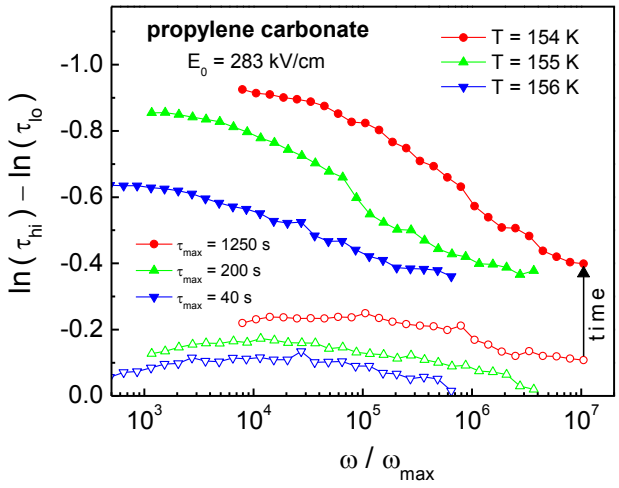

Fig. 4.4: Nonlinear dielectric effect shown in terms of "horizontal difference" for three different temperatures as indicated in the legends with their corresponding τ_{max} values. Open symbols represent the 'instantaneous' effect observed within few periods after switching on the high field (283 kV/cm), while solid symbols represent the steady state effects.

Clearly, Fig. 4.4 demonstrates that the steady state value of NDE does not approach zero for $\omega \leq 10^7 \omega_{max}$. Analogous results for MTHF and glycerol are depicted in Fig. 4.5, and the overall pattern is again that the steady state magnitude of the NDE significantly exceeds its short time value. As indicated by the arrow in Fig. 4.4, all NDE's shown in Fig. 4.4 and Fig. 4.5 are evolving in time from the level of the open symbol to that of the closed symbol.

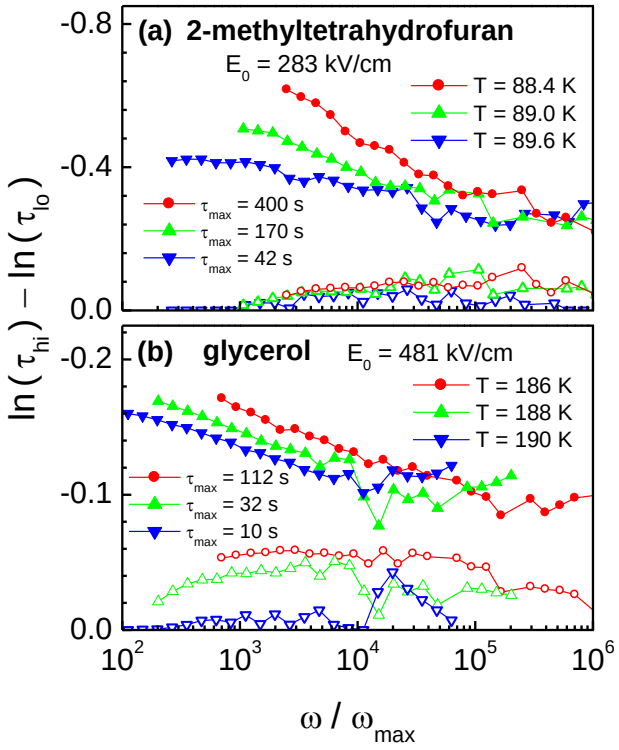

Fig. 4.5: Nonlinear dielectric effect shown in terms of "horizontal difference" for different temperatures as indicated by the legends with their corresponding τ_{max} values in case of (a) 2-MTHF for a field of value 283 kV/cm (b) glycerol for a field of value 481 kV/cm. As shown in Fig. 4.4, open symbols represent the 'instantaneous' effect observed within few periods after switching on the high field, while solid symbols represent the steady state effects.

The time evolution of the NDE that is implied in the results of Fig. 4.4 and 4.5 have been measured for all open/closed symbol pairs of these two figures. Characteristic results of such time dependent measurements are depicted as symbols in Fig. 4.6A for PC and in Fig. 4.6B for MTHF and GLY. The curves are selected in such a way so that the effect of variation of the average relaxation time τ_α (via changing temperature) at a fixed test frequency ν, as well as the variation of the test frequency ν at a fixed average relaxation time τ_α can be shown. Values of the ratios ν / ν_{max}, range from about 160 to 70,000 for the six situations included in Fig. 4.6A and Fig. 4.6B.

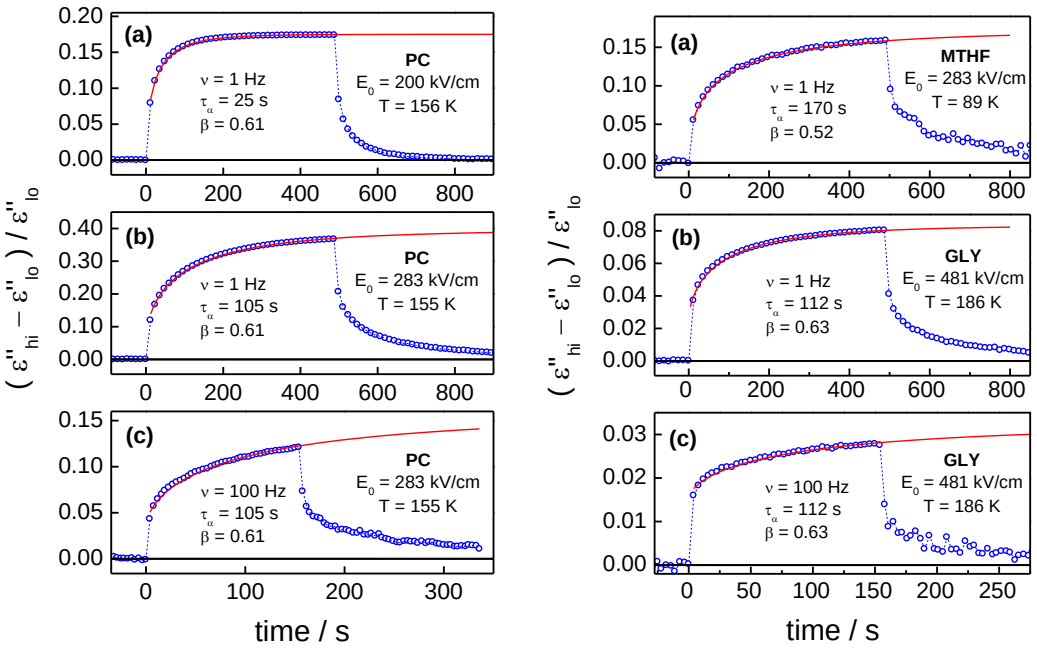

Fig. 4.6A (left): Time resolved relative change of the dielectric loss, $(\varepsilon''_{hi} - \varepsilon''_{lo})/\varepsilon''_{lo}$, in propylene carbonate for an increase of the field amplitude from E_0 = 14 kV/cm ('lo') to a significantly higher field ('hi') at t = 0. For the three panels, the high field amplitudes E_0, temperatures T, peak relaxation times τ_{max}, and test frequencies ν are as follows: (a) E_0 = 200 kV/cm, T =156 K, τ_{max} = 25 s, ν = 1 Hz; (b) E_0 = 283 kV/cm, T =155 K, τ_{max} = 105 s, ν = 1 Hz; (c) E_0 = 283 kV/cm, T =155 K, τ_{max} = 105 s, ν = 100 Hz.

Fig. 4.6B (right): Time resolved relative change of the dielectric loss, $(\varepsilon''_{hi} - \varepsilon''_{lo})/\varepsilon''_{lo}$, in 2-MTHF and glycerol for an increase of the field amplitude from E_0 = 14 kV/cm ('lo') to a significantly higher field ('hi') at t = 0. For the three panels, the material, high field amplitudes E_0, temperatures T, peak relaxation times τ_{max}, and test frequencies ν are as follows: (a) MTHF, E_0 = 283 kV/cm, T =89.0 K, τ_{max} = 170 s, ν = 1 Hz; (b) GLY, E_0 = 481 kV/cm, T =186 K, τ_{max} = 112 s, ν = 1 Hz; (c) GLY, E_0 = 481 kV/cm, T =186 K, τ_{max} = 112 s, ν = 100 Hz.

IV. Discussion

A. Non-linear effects in the excess wing

In Fig. 4.4, reductions in the magnitude of $\ln(\tau_{hi}/\tau_{lo})$ with increasing frequency range from 40 to 60%, and occur predominantly for frequencies $\omega > 10^4\omega_{max}$. Clearly, the frequency dependence of $\ln(\tau_{hi}/\tau_{lo})$ seen in Fig. 4.4 contradicts the prediction from box model, which implies frequency invariance for $\omega > 10\omega_{max}$. However, as mentioned while describing the phenomenological model in Chapter 3, the derivation of Eq. (3.6) rests on the assumption that the contributions towards Δc_p and $\Delta\varepsilon$ are proportional for a particular mode. This leads to the fact that permittivity and heat capacity enter only as the ratio $\Delta\varepsilon/\Delta c_p$ in Eq. (3.6). Near the peak, this is confirmed by comparing the profiles of $\varepsilon''(\omega)$ and $c_p''(\omega)$, which suggest proportionality of the two quantities at every frequency.[77] But corresponding data at very high frequency region is not available to claim this support. So, for the range $10^4\omega_{max}$ to $10^7\omega_{max}$ it is very possible that the ratio $\varepsilon''(\omega)/c_p''(\omega)$ has changed by about 50% relative to the smaller frequencies. Therefore, the steady state data of Fig. 4.4 are compatible with the model leading to Eq. (3.6), but with $\Delta\varepsilon/\Delta c_p$ replaced by $\varepsilon''(\omega)/c_p''(\omega)$. Accordingly, one has to be cautious while questioning the concept of

heterogeneous dynamics for frequencies $\omega >> \omega_{max}$ on the basis of the short time NDE becoming practically zero.

It is also important to note that with decreasing temperature the magnitude of the NDE grows and it scales with the apparent activation energy, $d\ln(\tau_{max})/d(1/T)$, as shown by the hexagons in Fig. 4.3 which is in accord with Eq. (3.6) also. This strong temperature dependence of the magnitude of the NDE prevents the curves in Fig. 4.4 to collapse onto a master-curve, although the frequency axis is normalized to the peak frequency.

It is interesting to note that the time scale with which the steady state level of the NDE is reached. In a previous study by Richert and Huang,[51] frequency invariant timescale for the rise in $\Delta\ln\tan\delta$ has been recognized at higher frequencies, which indicates homogeneous relaxation distribution. The threshold for this failure of the model on the frequency scale coincides with the onset of the excess wing[51] i.e., at about $10^2\omega_{max}$, but the time dependence of the configurational temperature for $\omega > 10^2\omega_{max}$ had not been investigated extensively.

In Fig. 4.6A time resolved measurements of the quantity $(\varepsilon''_{hi} - \varepsilon''_{lo})/\varepsilon''_{lo}$ are presented for propylene carbonate. Each panel is associated with a different frequency relative to the loss peak: (a) 160, (b) 660, and (c) 66000 in terms of ω/ω_{max}. Lowering the temperature from T = 156 K to 155 K and thus increasing τ_α at a constant frequency of ν = 1 Hz leads to a slower rise of the quantity $(\varepsilon''_{hi} - \varepsilon''_{lo})/\varepsilon''_{lo}$, see Fig. 4.6A (panel a and panel b). But interestingly, increasing the frequency from ν = 1 Hz to 100 Hz at a

constant temperature of T = 155 K has no effect on the time dependence of the NDE, see Fig. 4.6A (panel b and panel c). It is very clear from panel c that the NDE has not yet reached a steady state plateau even after 300 s for a frequency of ν = 100 Hz, i.e., after 30,000 periods. All these time resolved curves for $\omega > 10^2 \omega_{max}$ can be represented by the following fit function designated $\phi_x(t)$,

$$\frac{\varepsilon''_{hi} - \varepsilon''_{lo}}{\varepsilon''_{lo}} = \phi_x(t) = \phi_\infty + (\phi_s - \phi_\infty)\left(1 - \exp\left[-(t/\tau_\alpha)^\beta\right]\right), \qquad \text{Eq. (4.5)}$$

with ϕ_∞ and ϕ_s representing the 'instantaneous' (not time-resolved i.e., the rise of ε''_{hi} over ε''_{lo} that is faster than about 2 s) and the steady state level of the relative change of the loss, respectively. The values for ϕ_∞ and ϕ_s are adjustable fit parameters, while τ_α and β are the KWW parameters that describe the linear response of the α-relaxation in the time domain, $\phi(t) = \phi_0 \exp\left[-(t/\tau_\alpha)^\beta\right]$ at that temperature. Solid lines in both Fig. 4.6A and 4.6B demonstrate how well Eq. (4.5) represents the time dependence of the NDE, and the values for ϕ_∞ and ϕ_s are shown as open and solid symbols respectively in Fig. 4.4 and Fig. 4.5 also verifies that all field induced changes are completely reversible. The conclusion from these observations is that modes within the excess wing change their relaxation time constant (or, equivalently, configurational temperature) on the time scale of the overall primary structural relaxation, instead of the timescale of the mode itself as suggested by the 'box'-model. This can be considered as a drawback for the model deep in the excess wing regime.

B. Comparison with model predictions

The above analysis of the time dependent curves imply that all fast modes within the excess wing ($\tau < 10^{-2}\tau_{max}$) are equally slaved to the average structural relaxation regarding their rate at which time constants are approaching their equilibrium values. This observation can be explained by the confinement effect[102] of these fast modes by the surrounding rigid slow modes which is more abundant as reflected by the distribution of the timescales, g(τ). So modes present in the excess wings have to wait for the macroscopic softening to occur, before they can relax their fictive temperatures. This appears to contrast the basic idea of heterogeneous dynamics that fast and slow modes are mutually independent. In this regard, one must discriminate the two distinct time scales associated with each mode '*i*': On the one hand, the time constant τ_i that defines a local correlation time of some experimental variable (e.g., polarization in case of a dielectric experiment, enthalpy content in case of calorimetry), and on the other hand, the decay function $\phi_x(t)$ associated with the time τ_x required for τ_i to attain its equilibrium value after some perturbation (e.g., a change in temperature as in physical aging or calorimetric experiments, or a change in structure or configurational temperature as in the present case of an influx of energy). Actually, this latter time correlation function reflects ‘structural recovery’ instead of 'structural relaxation'. Typical experiments identifying the heterogeneous nature of dynamics are performed at a constant temperature, i.e., under quasi-equilibrium conditions. As a result, the term 'dynamical heterogeneity' typically refers to the independence of the local processes characterized by the τ_i's. The 'box'-model assumes the identity $\tau_x = \tau_i$ for each mode, which is incompatible with the present

findings. Accordingly, the concept of heterogeneous dynamics does not apply equally to the structural recovery process characterized by $\phi_x(t)$, at least not in the regime of the excess wing.

C. Relation to rate exchange and physical aging

The above mentioned high field experiment involving the influx of energy to the sample induce a equilibration process which can characterized by the function $\phi_x(t)$ as discussed above. Similar to these high field experiments, physical aging process (temperature jump below Tg),[41] and calorimetric techniques like differential scanning calorimetry (DSC) and modulated DSC (heat flow to the sample) also involve this type of equilibration process after the perturbation. These non-equilibrium processes are difficult to understand quantitatively due to the fact that relaxation times τ_i depend not only on temperature but also on structure, i.e., $\tau_i = \tau_i(T,T_f)$, where structure can be mapped onto the fictive (T_f) or configurational (T_{cfg}) temperature.[103] In all these studies enthalpy recovery is assumed to depend on a single fictive temperature which slaves the T_f's of all modes to the overall structural relaxation.[104] The experimental signature of a single fictive temperature is the common observation of time-aging time superposition (TaTS).[44] A single T_f implies that all mode specific τ_i's move towards their new equilibrium values in a concerted fashion, consistent with the present findings regarding the excess wing regime. Therefore, the slow equilibration of excess wing modes observed here is equivalent to the slow physical aging of these fast modes, for instance in response to a step in temperature to a lower value. Such a response is depicted schematically in

Fig. 4.7. The top part represents the shift of the five distinct modes to lower frequencies (higher τ_i's) in response to a small temperature down-jump as in a physical aging experiment. The fluctuation dissipation theorem states that even at a constant temperature, there should be corresponding fluctuations, as illustrated at the bottom part in Fig. 4.7. These fluctuations are known as rate exchange, and again a common exchange rate τ_x is typically assumed for all modes. Therefore, aging isotherms and the current high field experiments are considered direct measures of rate exchange effects, for which heterogeneity does not apply in the same way as for linear response isothermal relaxations.

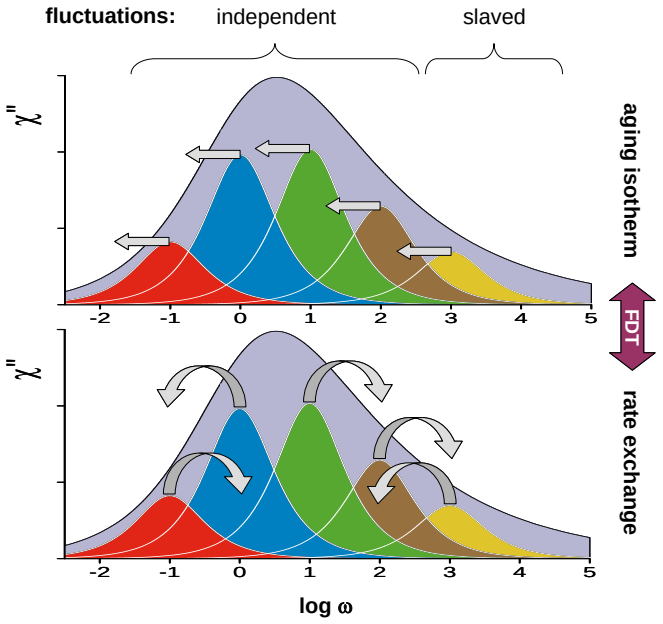

Fig. 4.7: Schematic representation of heterogeneity in terms of five distinct Debye type modes whose superposition yields a dispersive dielectric loss peak. Arrows in the top part indicate the equilibration of fictive temperatures or relaxation time constants, the process of an aging isotherm occurring in response to a temperature down-jump. Arrows in the bottom part indicate rate exchange at a constant temperature. The two scenarios are linked only qualitatively by the fluctuation dissipation theorem (FDT).

V. Summary and Conclusions

High field dielectric relaxation experiments are performed in the high frequency wing of the dielectric loss of three molecular glass-forming liquids, at field amplitude that are sufficient to drive the systems beyond the regime of linear responses. The novel feature of these measurements is the time resolution of non-linear dielectric effects that extends to about 30,000 periods of the applied field. For frequencies positioned between factors of 10^2 to 10^7 above the peak loss frequency, ω_{max}, it is found that it takes an unexpectedly long time for the system to reach steady state conditions and that is the reason for the observation of zero NDE effect by Bauer *et al*.[97] The level of the steady state non-linear effect is consistent with the 'box'-model, whereas the time scale required to reach that level is incompatible with the previous understanding of such high field effects. True structural relaxation (i.e., the time correlation function of fictive temperatures) is slaved to the macroscopically average α-relaxation in this higher frequency range, $10^2\omega_{max} < \omega < 10^7\omega_{max}$. Although the same type of experiments demonstrate heterogeneous relaxation near the peak position, mutual independence of the modes in the excess wing regime found to be absent.

4.3 Nonlinear dielectric response in JG *β*-relaxation:

I. Motivation

In the first section of this chapter, nonlinear response in excess wing regime has been studied. A definitive conclusion on their microscopic origin is not possible from these experiments. It is also not possible to make any conclusive statement on the relation of these excess wing modes with JG *β*-relaxation process. So, to gauge any kind of

connection between these two processes, nonlinear dielectric response in the JG β-relaxation modes has been studied. Before going straight into the experimental section, the universal features corresponding to JG β-relaxation needs to be mentioned. These properties[105] include i) a more sensitive dependence of the JG relaxation time on pressure and aging than other secondary relaxations ii) change in temperature dependence from Arrhenius (below Tg) to non-Arrhenius (above Tg) and finally merging with the α-relaxation at high temperature iii) a separation in frequency from the α relaxation that depends on the breadth of the α dispersion. The temperature dependence of the secondary relaxation time is usually considered to be of the Arrhenius type. However a number of recent experimental results suggest that τ_β may deviate from Arrhenius law in the equilibrium liquid state. Although the β-relaxation has been interpreted as the hindered motions within the "island of mobility"[106], ^{2}H NMR technique and solvation dynamics experiment reveal the source of the process as highly restricted orientational motion essentially involving all the molecules.[107,108,109] There are also some microscopic evidences that JG β- relaxation bears a close connection to the α-relaxation.[110,111] In toluene and polybutadiene, secondary relaxations have been found to involve angular jumps of similar magnitude above T_g.[112] Not only it is of great importance to unravel the origin of excess wing, but also as JG relaxation believed to be the precursor of primary structural relaxation, this particular study aiming at the nonlinear dielectric features of JG β-relaxation modes will be of equal importance.

As it is evident from the earlier discussions, the non-linear dielectric response for secondary relaxation processes of the Johari-Goldstein (JG) type, i.e., those β-processes

that are considered as an intrinsic feature of the dynamics of glass-forming liquids and glasses, will be of interest here. Finally, results of these experiments will be compared with the observations of NDE's in the excess wing regime in order to scrutinize the notion "the excess wing is a submerged JG β-peak".

II. Experiment

D-sorbitol has been chosen as the material for this study, as it possesses a well characterized secondary process with exceptional dielectric amplitude on an absolute scale ($\Delta\varepsilon \approx 4$) as well as relative to the primary relaxation amplitude ($\Delta\varepsilon_\beta/\Delta\varepsilon_\alpha \approx 0.1$).[113-116] The compound D-sorbitol (98%) has been purchased from Aldrich and is used as received. Sorbitol is heated to about 400 K, i.e., sufficiently above its melting point T_m = 368 K, for 10 minutes prior to cooling to T_g at a rate of ≈ 5 K/min. It is important that the process generates an optically clear liquid while avoiding caramelization. Samples are prepared in a capacitance cell in similar fashion as described earlier.

A closed cycle He refrigerator (Leybold RDK 6-320/Coolpak 6200) along with a temperature controller (Lakeshore Model 340) equipped with calibrated diode sensors are used to control temperature. High voltages are achieved using a Trek PZD- 700 high voltage amplifier boosting the generator signal of the Solarton SI-1260 gain/phase analyzer. Impedances are measured for frequencies 1 Hz to 25 kHz at a density of 8 points per decade. For the time resolved measurements, high field protocol has been kept the same as in the excess wing studies. To ensure that the system is held at isothermal conditions, sufficient waiting times are provided between two measurements. Sample temperatures are selected as follows. For experiments related to the α-peak, three

temperatures close to T_g = 268 K of D-sorbitol are chosen, T = 267, 270, and 273 K, for which a sufficient spectral separation between α- and β-process facilitates discerning their contributions. For investigating the β-relaxation process, the temperatures were kept at 195, 220, and 245 K, respectively, i.e., well below T_g so that β-process will be in the experimental frequency window. Comparing the measured loss values of the primary relaxation to literature[113,114] results on D-sorbitol indicated that the real sample thickness is 15 μm, i.e., 5 μm thicker than the nominal value determined by the spacer material. This is due to the high viscosity of the sample near the sample preparation temperature. All permittivity values reported in this thesis are corrected for the actual geometry.

III. Results

For all the sample temperatures relevant to this study, the linear regime dielectric loss spectra of D-sorbitol are depicted in Fig. 4.8.

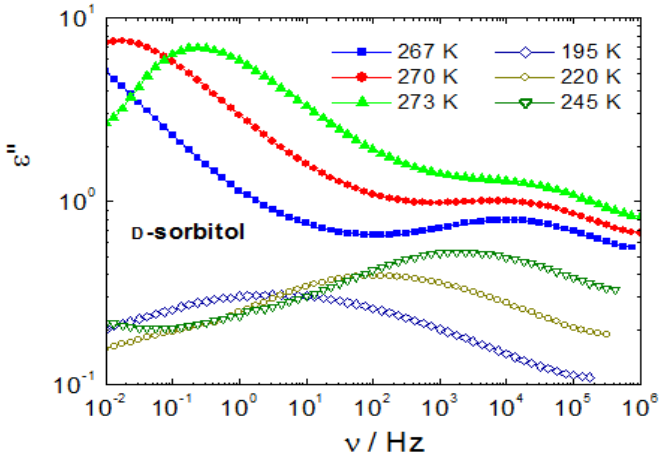

Fig. 4.8: Linear response dielectric spectra for D-sorbitol at various temperatures. The three higher temperatures (267K, 270K and 273K) are relevant for studying the α-peak, whereas three lower temperatures (195K, 220K, 245K) display only the JG β-relaxation peak in the measurement frequency window.

From the experimentally obtained curves, it can be seen that D-sorbitol has a pronounced β-peak and it is well separated from the α-process (type B) contrary to the situation for excess wings (type A). Given the present experimental frequency window of the high field measurements, the three higher temperatures have been chosen for studying the α-peak, while the three lower temperatures facilitate measuring the β-peak effects without strong interference from the primary modes. For temperatures such as the T = 267 or 270 K cases, the upper end of the frequency window used for the high field measurements reaches the onset of the β-peak. However, significant contributions from the primary structural relaxation peak at those frequencies cannot be ignored. The graphical matrix of Fig. 4.9 compiles representative examples of the time dependence of the field induced dielectric effect in terms of the relative change of the dielectric loss, $(\varepsilon''_{hi} - \varepsilon''_{lo})/\varepsilon''_{lo}$, for the three temperatures located near or above T_g and for different frequencies.

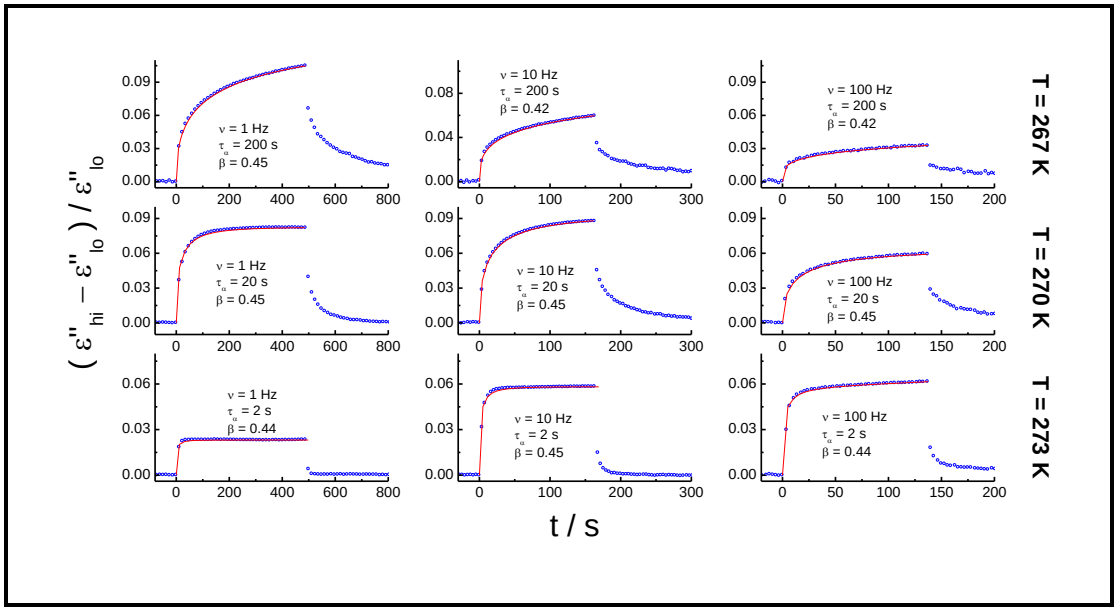

Fig. 4.9: Time dependent field induced relative change of the dielectric loss for three higher temperatures are shown for a change in field amplitude from $E_{0,lo}$ = 10 kV/cm to $E_{0,\,hi}$ = 190kV/cm. The fit lines shown in red are based on Eq. (4.5). τ_α values for these three temperatures are 200s, 20s and 2s respectively going from low to high temperature. While each row corresponds to a single temperature, each column represents measurements for a fixed frequency.

This array has a common sample temperature T for each row and a common measurement frequency ν for each column. The lines in Fig. 4.9 are fits according to Eq. (4.5). Frequency dependencies of ϕ_∞ and ϕ_s are depicted for the three liquid state temperatures in Fig. 4.10. According to the fits, the instantaneous contributions, ϕ_∞, for the temperatures T = 270 and 273 K were zero, and thus only one curve is shown for $\phi_\infty(\nu)$.

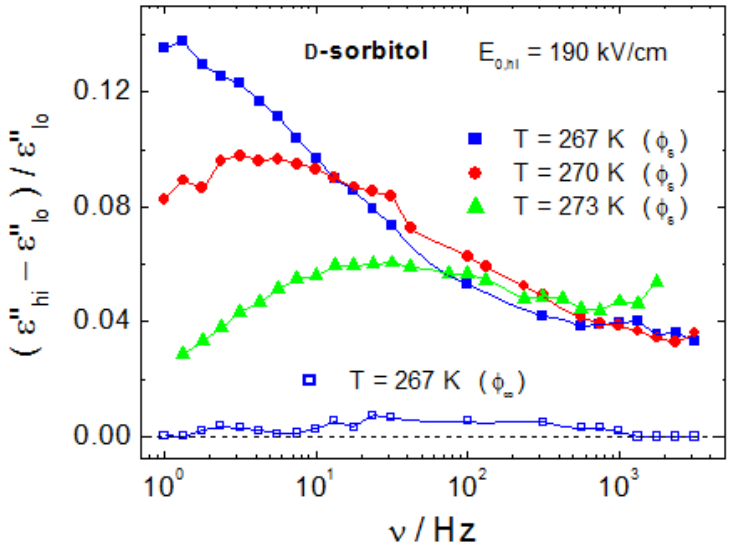

Fig. 4.10: Instantaneous and steady state values of the relative change in dielectric loss in terms of "vertical difference" for a field transition from $E_{0,lo}$ = 10 kV/cm to $E_{0,\,hi}$ = 190 kV/cm. The value of ϕ_∞ for the two high temperatures are zero and thus not shown.

Steady state non-linear effects such as those represented by the solid symbols in Fig. 4.10, $\phi_s(\nu)$, have been interpreted as a field induced modification of time constants,

rather than a change in relaxation amplitudes.[78] Therefore, it is useful to assess the so-called 'horizontal' difference curves that gauge the separation between the high field spectrum, $\varepsilon''_{hi}(\omega)$, and its low field counterpart, $\varepsilon''_{lo}(\omega)$, measured along the logarithmic frequency scale, $\ln \nu$. The results for the field induced frequency shifts, $\ln(\nu_{hi}/\nu_{lo})$, that are derived from the three $\phi_s(\nu)$ curves of Fig. 4.10, are shown in Fig. 4.11. Because the slope, $d\ln\varepsilon''/d\ln\nu$, attains values of zero at the loss minimum between primary and secondary peak, the $\ln(\nu_{hi}/\nu_{lo})$ curves for T = 267 and 270 K display poles at 100 and 1000 Hz, respectively.

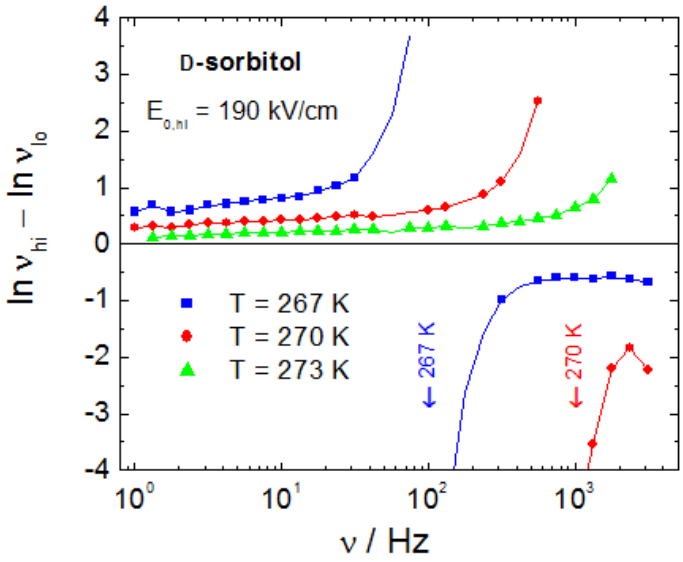

Fig. 4.11: Field induced "horizontal difference" for D-sorbitol for the three higher temperatures for a field transition from $E_{0,lo}$ = 10 kV/cm to $E_{0,\,hi}$ = 190 kV/cm. These curves are obtained by dividing the vertical differences in Fig. 4.10 by the slope according to Eq. (4.4). The value of the slope for T = 267K and 270K is found to be zero at the frequencies indicated by the arrows, leading to poles in the "horizontal difference" spectra.

Time resolved measurements analogous to those shown in Fig. 4.9 have been performed for the three lower temperatures, T = 195, 220, and 245 K, i.e., in the glassy

state where the secondary relaxation peak is within the frequency window of the high field experiments and with little interference from the primary structural relaxation signal. A selection of these results is compiled in matrix form in Fig. 4.12, which is analogous to Fig. 4.9, but with the highest frequency column showing 1 or 10 kHz results instead of a common value of 100 Hz.

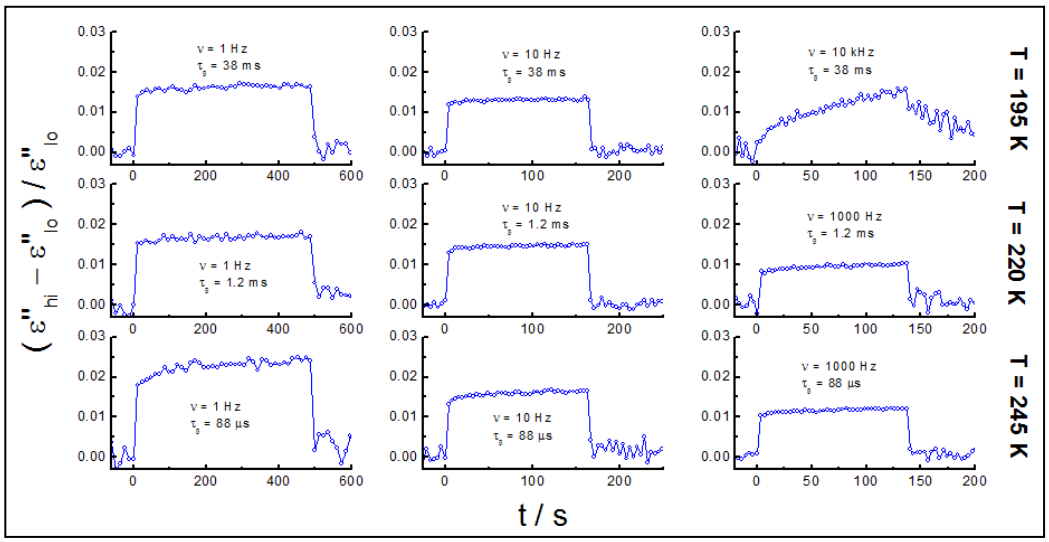

Fig. 4.12: Time dependent field induced relative change of the dielectric loss of D-sorbitol, $(\varepsilon''_{hi} - \varepsilon''_{lo})/ \varepsilon''_{lo}$, in response to the field amplitude increasing from $E_{0,lo} = E_{0,hi}/10$ to $E_{0,hi}$ = 230 kV/cm at t = 0 and then decreasing again to $E_{0,lo}$ at a later time. From top to bottom, the rows are for temperatures T = 195, 220, and 245 K. For each of the three temperatures, results for three measurement frequencies are shown, ν = 1 Hz, 10 Hz, and 1 or10 kHz. The non-linear effects amount to 1 to 2 % and are largely time invariant, with the exception of the T =195 K, ν = 10 kHz case, which is dominated by electrode heating.

In contrast to the results obtained for higher temperatures, $T > T_g$, these curves observed for $T < T_g$ show practically no time dependence and an overall smaller effect in the 1 to 2 % range. A spectrum of the field induced relative change, $\phi_s(\nu)$, of the dielectric loss at T = 220 K, derived from the long time plateau values of the (ε''_{hi} –

$\varepsilon''_{lo})/\varepsilon''_{lo}$ data of Fig. 4.12 is shown in Fig. 4.13 (panel b) along with the low field (linear response) loss spectrum (panel a) for comparison.

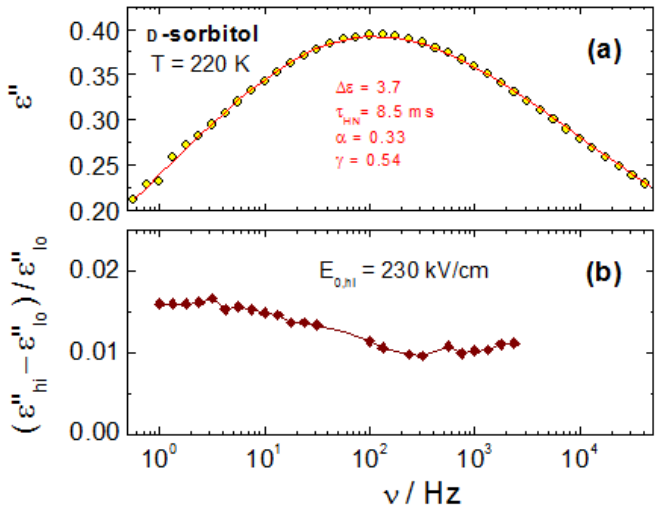

Fig. 4.13: Dielectric relaxation results for the β-process of D-sorbitol at a temperature of T = 220 K. (a) Experimental data for the low field (linear response) dielectric loss spectrum (symbols), along with an HN fit (line) based on the parameters listed in the legend. (b) The 'vertical' relative difference, $(\varepsilon''_{hi} - \varepsilon''_{lo})/ \varepsilon''_{lo}$, between loss spectra recorded at $E_{0,hi}$ = 230 kV/cm and $E_{0,lo} = E_{0,hi}/10$, as derived from the virtually time invariant curves of Fig. 4.12.

IV. Discussion

Towards higher frequencies relative to the peak loss frequency ν_{max}, i.e., in the excess wing regime with $\nu > 10^2 \nu_{max}$, the magnitude of the non-linear dielectric effect is reduced relative to the prediction of Eq. (3.6) by a factor of up to about two at $\nu = 10^7 \nu_{max}$. Moreover, it was found for several glass formers that the approach to the steady state value of ε''_{hi} occurs as slow as the average structural relaxation, even for modes as fast as $\tau = 10^{-7} \tau_{max}$.[117]

Primary Relaxation of Sorbitol: The non-linear dielectric behavior of D-sorbitol is studied at three temperatures, T = 267, 270, and 273 K, with the respective average α-process dynamics characterized by the relaxation times τ_α = 200, 20, and 2 s. In the same order, the peak frequencies of the linear response dielectric loss profiles are positioned at ν_{max} = 0.002, 0.02, and 0.2 Hz, see Fig. 4.8. Regardless of temperature T and measurement frequency ν, it is found that the field induced change as gauged by the quantity $(\varepsilon''_{hi} - \varepsilon''_{lo})/\varepsilon''_{lo}$ approaches its steady state level via Eq. (4.4), i.e. with an 'instantaneous' step of magnitude, ϕ_∞, followed by a stretched exponential rise to ϕ_s with KWW parameters τ_α and β that closely resemble the average α-relaxation in the time domain at the given temperature. The fit examples shown in Fig. 4.9 demonstrate that Eq. (4.5) captures the time dependence of the field induced relative increase of the dielectric loss with τ_α values derived from the HN fits to the α-peak and with β values that vary only slightly around the low value typical for this highly fragile (m = 127) liquid. This universally slow equilibration or structural recovery time for modes that are associated with very fast structural relaxation time scales within the high frequency wing is equivalent to the behavior observed with the same type of experiment for PC, GLY, and MTHF.

The magnitudes, ϕ_s, of the relative enhancements of the loss are compiled in Fig. 4.10, which spans a range of 6.5 to 1.5×10^6 regarding the ratio ν/ν_{max}. At the field of $E_{0,hi}$ = 190 kV/cm, levels of ϕ_s between 4 and 12 % are found, with the tendency to decrease monotonically with frequency in the range of $\nu > 10^2 \nu_{max}$. Again, these observations are

reminiscent of the high frequency non-linear dielectric effects seen with other molecular glass formers. Expressing the field effects of Fig. 4.10 in terms of the 'horizontal' difference, $\ln \nu_{hi} - \ln \nu_{lo}$, as defined in Eq. (4.1), a picture emerges in Fig. 4.11 that differs qualitatively from what has been observed previously for molecular glass formers. Here, the values of $\ln \nu_{hi} - \ln \nu_{lo}$ increase along the frequency axis, prior to displaying a pole followed by negative values at even higher frequencies, see Fig. 4.11. The pole originates from the division by the slope $d\ln\varepsilon''/d\ln\nu$ in Eq. (4.4), which becomes zero at the loss minimum between the α- and β-peak. As the materials studied previously in a similar fashion (PC, GLY, MTHF) do not exhibit a distinct β-peak, such poles and changes in sign as in Fig. 4.11 have not been observed before.

The comparatively slow approach to equilibrium observed for D-sorbitol even for frequencies that are $10^6 \times \nu_{max}$ or higher is analogous to the behavior seen for other molecular glass formers, PC, GLY, and MTHF. This slow process is the equivalent of structural recovery,[117] i.e., the approach of time constants towards their equilibrium value as discussed for the excess wing behavior.

Secondary Relaxation of Sorbitol: The distinct secondary relaxation of D-sorbitol can be observed clearly above and below T_g in Fig. 4.8. This β-relaxation in D-sorbitol has been established as JG-type and has been shown to reflect dynamic heterogeneity,[101] and a correlation between primary and secondary relaxation times has been found.[118]

Several examples of time resolved experiments across the β-peak range are shown in Fig. 4.12, where in each case the temperature is well below T_g and primary relaxation

times are strongly separated from the β time scales. An important feature of these results obtained with 230 kV/cm are that a non-linear effect of order 1.5 % in terms of $(\varepsilon''_{hi} - \varepsilon''_{lo})/\varepsilon''_{lo}$ is observed across the β-process spectrum. This level corresponds to about 1.0 % for a field of 190 kV/cm (as used for the α-process experiments), according to the field squared dependence of the overall NDE effect. Moreover, within the present experimental ranges, this field induced change is almost independent of temperature, frequency, and time. This invariance regarding T, ν, and t is strikingly different from the corresponding results observed for the α-process, see Fig. 4.9.

The lack of any considerable time dependence in Fig. 4.12 of the $\phi_X(t)$ signals as defined in Eq. (4.5) can be explained as follows. At the relevant temperatures, T = 195, 220, and 245 K, the time scale of the primary structural relaxation, τ_α, is much longer than the time ($\leq$ 500 s) over which the high field loss has been monitored. Consequently, a possible increase of $\phi_X(t)$ that traces the average structural relaxation would have remained inaccessible by this experiment. In other words, instantaneous and steady state amplitudes of the field effect are virtually the same in the glassy state with $T << T_g$. If the $\approx$ 1.5 % change had been established on the time scale of the β-process, that rise would remain unresolved given the present time resolution of about 2s. The slight rise seen for the T = 245 K and ν = 1 Hz case may be due to residual overlap with the α-peak. The linear increase for the T = 195 K and ν = 10 kHz situation can be ascribed to sample heating as a result of excessive power.

We now ask whether the field effect on the permittivity of the β-process can also be rationalized in terms of a shift of relaxation time constants, a picture that explains much of the non-linear features associated with the primary loss peak.[50] This questions is answered by the result shown in Fig. 4.13b, which shows a uniform effect of around + 1.25 % field induced gain of the loss, regardless of the slope of the β-peak spectrum. By contrast, a shift of secondary modes towards higher frequencies (at constant amplitudes) would result in a reduction of ε'' for $\nu < \nu_{\beta,max}$, an enhancement of ε'' for $\nu > \nu_{\beta,max}$, and a field invariant loss for $\nu \approx \nu_{\beta,max}$, where $\nu_{\beta,max}$ is the loss peak position of the secondary process. We conclude that the field induced change of the β-process is dominated by modifications of the amplitudes rather than time constants, whereas these roles are reversed for the non-linear features observed for the α-relaxation. A field induced reduction of time constants τ_β of the secondary relaxation process is not excluded, but appears to be a minor contribution. In the common picture of the JG-process reflecting librational motion with a longer-lived cage that confines reorientation to a certain cone angle,[107]the present field effect would correspond to a widening of that cone angle (thus increasing $\Delta\varepsilon_\beta$) with less effect on the time constant associated with that motion. The amplitude change in the β-regime is a response to fields where the energy involved is much smaller than the thermal energy ($\mu E << k_B T$). Qualitatively, this implies thermally induced fluctuations of the β-amplitude in the absence of an external field (analogous to the fluctuation-dissipation theorem for linear response). Similarly, a distribution of $\Delta\varepsilon_\beta$ values derived via MD simulations for individual molecules has been discussed by

Fragiadakis and Roland for a glass consisting of asymmetric diatomic molecules displaying a JG type secondary process.[119] In that study, local values of $\Delta\varepsilon_\beta$ and τ_β did not display a significant correlation.

This field induced increase of the β-peak amplitudes by about 1 % can be expressed in terms of a higher fictive temperature for the E_0 = 230 kV/cm case relative to the linear response limit. According to a previous study of the β-relaxation of D-sorbitol, its amplitude $\Delta\varepsilon_\beta$ varies approximately as $d\ln\Delta\varepsilon_\beta/dT$ = 0.03 K^{-1} in the glassy state.[114] Therefore, an increase in T_{cfg} of ≈ 0.35 K would explain the 1 % effect. The steady state expression $\Delta T_{cfg} = \varepsilon_0 E_0^2 \Delta\varepsilon/(2\rho\Delta C_p)$ that is derived from the balance of the influx of energy ($\propto \varepsilon'' E^2$) and relaxation to the thermal bath, and it has been demonstrated to compare favorably with experimental data for the α-process, including the case of D-sorbitol.[76] Applying this approach to the secondary peak case of Fig. 4.13b requires using $\Delta\varepsilon_\beta$ = 3.7 for the relaxation strength and E_0 = 230 kV/cm for the field amplitude. The glass-to-liquid heat capacity step associated with the α-process of D-sorbtiol is $\rho\Delta C_{p,\alpha}$ = 1.65 J K^{-1} cm^{-3}.[27] If this value were used to determine ΔT_{cfg}, the predicted field effect would be negligible compared to what is actually observed. However, because $\rho\Delta C_p$ enters in the denominator, a much smaller β-relaxation heat capacity step of order $\Delta C_{p,\beta}$ = 1.5%×$\Delta C_{p,\alpha}$ would be able to explain the field induced amplitude effect on the basis of an increased configurational (or fictive) temperature. While calorimetric data for a quantitative test of this notion is not available, heat capacity steps of secondary process are known to be much smaller than those associated with the α-relaxation.[120]

Excess Wing Behavior: The excess wing in a dielectric spectrum appears as the high frequency contribution to $\varepsilon''(\omega)$, with $\omega >> \omega_{max}$, that is in excess of the extrapolated power law that describes the high frequency side of the loss profile closer to the peak. In practice, the excess wing loss is considered to be the additional high frequency signal that is not captured by the typical fit functions with limiting power law behavior, such as the HN function and its special cases. It is being discussed frequently whether the excess wing is an unresolved JG β-relaxation or some independent feature of liquid dynamics. Supercooled liquids with lower fragility index, say $m < 70$, will tend to have a small JG type secondary process that has little spectral separation from the α-peak, which then might appear as excess wing rather than a distinct peak.[107]

The three liquids, PC, GLY, and MTHF, that have been analyzed in terms of their $\phi_X(t)$ behavior, see Eq. (4.5), all possess excess wings in their liquid states ($T > T_g$), but no obvious β-process loss maxima. The connection to the present case of D-sorbitol is founded in the observation that PC, GLY, and MTHF all display instantaneous contributions (ϕ_∞) to $(\varepsilon''_{hi} - \varepsilon''_{lo})/\varepsilon''_{lo}$ for frequencies exceeding 10^2 to 10^3 times ν_{max}, whereas ϕ_∞ is practically zero for frequencies closer to the loss peak position. A clear example for the onset of ϕ_∞ coinciding with the onset of the excess wing at $200\times\nu_{max}$ for PC at T = 156.5 K is provided in Fig. 4.14, with the level of ϕ_∞ also reaching values around 2 % at $E_{0,hi}$ = 200 kV/cm. In the case of D-sorbitol, no considerable instantaneous field induced changes has been observed across the high frequency wing of the α-process. An apparent exception is the 0.5 % effect for the T = 267 K curve in Fig. 4.10,

but the loss for frequencies ν > 30 Hz contains significant contributions from the β-process. Thus in the present experiments it is only the secondary process that displays these quasi 'instantaneous' rises of the loss at high fields. The coincidence of a quickly developed non-linear effect with loss contributions from either excess wing or JG type secondary relaxations suggests that both dynamics share a common origin.

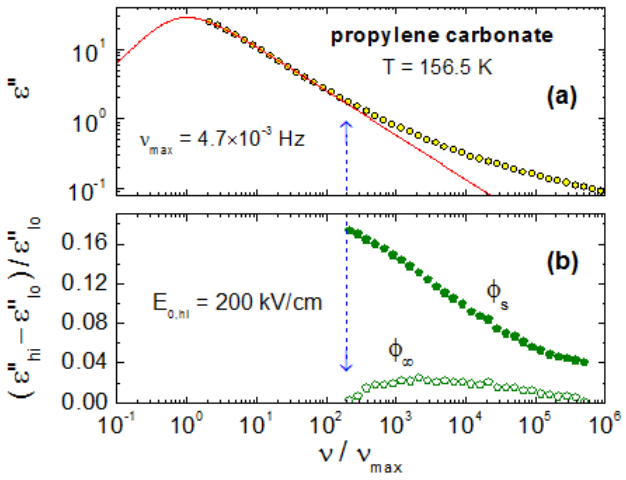

Fig. 4.14: Dielectric relaxation results for the α-process of propylene carbonate at a temperature of T = 156.5 K. (a) Experimental data for the low field (linear response) dielectric loss spectrum (symbols), along with an HN fit (line) that is extrapolated to show the loss peak. (b) The 'vertical' relative difference, $(\varepsilon''_{hi} - \varepsilon''_{lo})/\varepsilon''_{lo}$, between loss spectra recorded at $E_{0,hi}$ = 200 kV/cm and $E_{0,lo} = E_{0,hi}/10$, as derived from time resolved curves from Fig. 4.6a, analogous to those in Fig. 4.9. Open symbols represent quasi-instantaneous levels, ϕ_∞, while solid symbols are for steady state values, ϕ_s.

In this context, we note that the α-process of D-sorbitol displays time-temperature superposition (TTS) for a large range of structural relaxation times: from 10^2 to 10^{-6} s.[121] Obeying TTS simplicity requires that temperature predominantly affects the average time constant of the relaxation process, without modifying the profile of the frequency dependent susceptibility. TTS extending over a number of decades in terms of the peak

loss frequency is more commonly observed for the more fragile cases, where the JG β-process is well separated from the α-peak.[122] Liquids exhibiting excess wings are notorious to violate TTS when τ_α changes several orders of magnitude, and the explanation based on the identity of excess wing and JG-process is that primary and secondary peaks are subject to different activation behaviors, which prohibits the occurrence of TTS if the secondary peak is submerged below the primary signal. A graph of β_{KWW} versus $\log \nu_{max}$ for 14 different liquids as provided by Wang *et al.*[121] supports this idea that TTS is a consequence of the excess wing/JG β-process not interfering with the primary loss profile.

V. Summary and Conclusion

The non-linear dielectric responses of the JG-type secondary process of D-sorbitol have been explored. Field induced increase of the dielectric loss in the β-peak regime of order 1 - 2 % at fields of around 200 kV/cm has been observed. These non-linear dielectric effects are compared with those of the primary relaxation process and with those associated with the excess wing of other glass forming liquids. The effects of high fields at frequencies near the α-peak can be described by modes being accelerated, i.e., subject to a field induced reduction of their time constants. By contrast, high fields enhance the amplitudes of both the JG-type β-relaxation and the excess wing (Fig. 4.15).

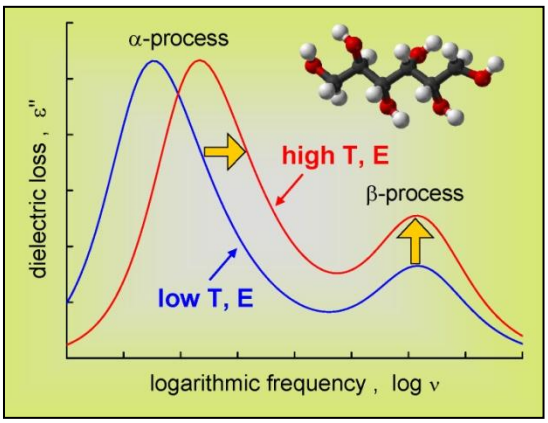

Fig. 4.15: A schematic difference of the high amplitude ac field effect on the α-relaxation and the excess wing/β-relaxation is depicted. While the effect of applying a high field near the α-process, reduce the relaxation time of the mode being investigated in terms of average τ_α; in case of excess wing regime/β-relaxation, main effect of applying high field is the modification of their amplitude in quasi-instantaneous fashion.

Similarly, in equilibrium, temperature affects τ_α much more than $\Delta\varepsilon_\alpha$ for the primary process, whereas both τ_β and $\Delta\varepsilon_\beta$ change in comparable ways with T for the secondary relaxation. Therefore, the high-field effects for both relaxation modes can be described by field induced increases in the fictive temperature. The two distinct effects also differ in their time scale for reaching steady state conditions. Modifying the time constants of the α-process requires the average primary structural relaxation time, even for contributions to frequencies that exceed the peak value, ν_{max}, by more than a factor of 10^6. Increases of the amplitudes of secondary process or excess wing modes are quasi-instantaneous compared with the α-relaxation time.

The similarity of the non-linear dielectric behavior of the JG secondary process with that of the excess wing modes supports the notion that both dynamic features share a common microscopic origin, differing only in the spectral separation from the primary

peak. This is underlined by the qualitative difference of these field effects from the non-linear response of the entire loss spectrum associated with the α-process.

Chapter 5

Nonlinear dielectric effect in high bias fields

5.1 Effect of High Bias field on structural relaxation timescale:

(An entropic approach)

I. Motivation

In this chapter I will describe the effect of applying high dc-field (>100kV/cm) to the glass forming liquids in their supercooled liquid or plastic crystalline state. This work is motivated by a recent paper from Johari.[123] The steady state change in total entropy due to isothermal polarization induced by the dc-field can be obtained from the Maxwell relation,[124]

$$\left(\frac{\partial S}{\partial E}\right)_T = \left(\frac{\partial P}{\partial T}\right)_E = \varepsilon_0 \left(\frac{\partial \varepsilon_S}{\partial T} E\right)_E$$

Integration with respect to field yields the steady state change in total entropy, $\Delta_E S$, as a result of applying a field of magnitude E. As shown by Fröhlich,[125] the amount of entropy change of a dielectric material at constant volume with the application of an external DC field can be expressed by the following equation:

$$\Delta_E S = \upsilon \frac{\varepsilon_0}{2} \left(\frac{\partial \varepsilon_S}{\partial T}\right) E^2 \qquad \text{Eq. (5.1)}$$

where υ is the molar volume and ε_0 is the permittivity of vacuum. The direction of the change in entropy will be governed by the sign of rate of change on dielectric constant with temperature, $\left(\frac{\partial \varepsilon_S}{\partial T}\right)$, whereas the overall magnitude of the change in entropy varies quadratically with the externally applied field.

As mentioned earlier in Chapter 1, the super-Arrhenius behavior of the relaxation time constants/viscosity of glass-forming liquids in their supercooled state has been thought to be due to the growing cooperativity among the molecules (Adam-Gibbs approach[29]). In this approach, increasing the timescale for the motions of the molecules while lowering the temperature is related to the exhaustion of configurational entropy.

$$log_{10}(\tau_\alpha/s) = A + \frac{C}{TS_{cfg}(T)} \qquad \text{Eq. (5.2)}$$

Johari[123] combined the above mentioned approaches and proposed that the field induced change in entropy can eventually be translated to affect the relaxation time constants at isothermal condition. Although Adam and Gibbs relates the relaxation time constants to the configurational part of the entropy, in Fröhlich's formalism the amount of change in entropy should be regarded as total entropy change.

Combining Eq. (5.1) and Eq. (5.2), for small changes one can write,

$$\Delta_E ln\tau_\alpha = -\ln(10)\frac{C}{TS^2_{cfg}(T)}\upsilon\frac{\varepsilon_0}{2}\left(\frac{\partial\varepsilon_S}{\partial T}\right)E^2 \qquad \text{Eq. (5.3)}$$

For most of the liquids, $\left(\frac{\partial\varepsilon_S}{\partial T}\right)$ is found to be negative (Type I liquids as designated by Johari[123]) as expected from the Boltzmann equation. For these liquids, the above equation predicts an increase in τ_α with the application of field. Using this approach, Johari estimated that τ_α could increase by more than a factor of 10 for a field of 500 kV/cm, using $\partial\varepsilon_S/\partial T = -2.0\ K^{-1}$, T = 200 K, a molar volume υ = 100 mL/mol, and typical values for C and S_{cfg}. Although a field of 500 kV/cm can be applied realistically to viscous liquids near their T_g, considerably smaller fields would still be expected to result in a measurable field induced change of the relaxation time, τ_α. In this chapter, measurements

will be reported for various glass-forming liquids with varying fragility values and the observed nonlinear effects will be compared quantitatively with the predicted values from above approach. All of the liquids presented in this chapter will be of type I category. As evident from the Eq. (5.3), to predict the amount of change in timescale, one has to find the value of S_{cfg} at the investigated temperature. But it is not possible to extract only the configurational part of the entropy from calorimetry measurements.[30] In reality to test the Adam-Gibbs equation, researchers used excess entropy which is obtained by taking the difference between liquid and crystal entropy ($S_{excess} = S_{liquid} - S_{crystal}$). Many literature results indicate the proportionality between these two quantities. In this chapter for the calculation purpose, excess entropy numbers will be used instead of configurational entropy as from calorimetry measurements only excess entropy values can be obtained. Measurements of excess entropy indicate that the decrease in excess entropy with temperature most often follows the following relation:

$$S_{exc}(T) = S_{\infty}(1 - {}^{T_K}/_{T}) \qquad \text{Eq. (5.4)}$$

where $S_{exc}(T)$ will vanish at the Kauzmann temperature (T_K) and S_{∞} indicates the high temperature limit of excess entropy. Empirically, it has also been found that this Kauzmann temperature T_K is close to the Vogel temperature T_0 (usually within 2K difference), suggesting a close connection between the thermodynamics and kinetics of supercooled liquids.[40]

Another trivial effect one can expect when applying a large bias field is the dielectric saturation as mean orientation, $\langle\cos\theta\rangle$, will saturate at unity. For non-

interacting dipoles the mean value of the dipole moment can be obtained from the balance between the interaction energy (W) of the dipoles with the external field, E (W = -μ·E) and the thermal energy, k_BT. μ represents the permanent dipole vector averaged over all orientations and k_B is the Boltzmann's constant. So the mean dipole moment can be expressed as:

$$\langle \mu \rangle = \frac{\int \mu exp\left(\frac{\mu \cdot E}{k_B T}\right) d\Omega}{\int exp\left(\frac{\mu \cdot E}{k_B T}\right) d\Omega} \qquad \text{Eq. (5.5)}$$

where Ω represents the solid angle. As only the dipole moment component which is in the direction of the field contribute to the polarization, interaction energy can be written as W = -μE*cosθ*, where θ is the angle between the dipole moment vector and the electric field direction. Eq. (5.5) can be simplified in terms of <*cosθ*> as:

$$\langle cos\theta \rangle = \frac{\int_0^{\pi} cos\theta \; exp\left(\frac{\mu E cos\theta}{k_B T}\right) \frac{1}{2} sin\theta d\theta}{\int_0^{\pi} exp\left(\frac{\mu E cos\theta}{k_B T}\right) \frac{1}{2} sin\theta d\theta} \qquad \text{Eq. (5.6)}$$

Substituting $x = \frac{\mu E cos\theta}{k_B T}$ and $a = \frac{\mu E}{k_B T}$ in Eq. (5.6), one will obtain the expression for average mean orientation, <*cosθ*>which is expressed by Langevin function.

$$\langle \cos\theta \rangle = \frac{1}{a} \frac{\int_{-a}^{a} e^x x dx}{\int_{-a}^{a} e^x dx} == \frac{1}{a} \frac{[xe^x - e^x]_{-a}^{+a}}{[e^x]_{-a}^{+a}} = \frac{e^a + e^{-a}}{e^a - e^{-a}} - \frac{1}{a} = \cot anha - \frac{1}{a} = L(a)$$

So, $$\langle cos\theta \rangle = cotanh\left(\frac{\mu E}{k_B T}\right) - \left(\frac{\mu E}{k_B T}\right)^{-1} = L\left(\frac{\mu E}{k_B T}\right) \qquad \text{Eq. (5.7)}$$

At small field strength, i.e. when μE << k_BT, <cosθ> = $\frac{\mu E}{3k_B T}$. But at higher field strength as <*cosθ*> will try to saturate to 1, the deviation from linearity occurs as shown in the

following figure (Fig. 5.1). As overall polarization will be dependent on <*cosθ*>, the rate of polarization with field decreases i.e. $\chi = (\partial P/\partial E)$ will decrease. The orientational saturation or Langevin saturation is measured as the difference between χ values, at fields close to zero and at any high fields, which will be a negative number.

$$\text{Orientational saturation} = (\chi_E - \chi_{E\to 0}) < 0$$

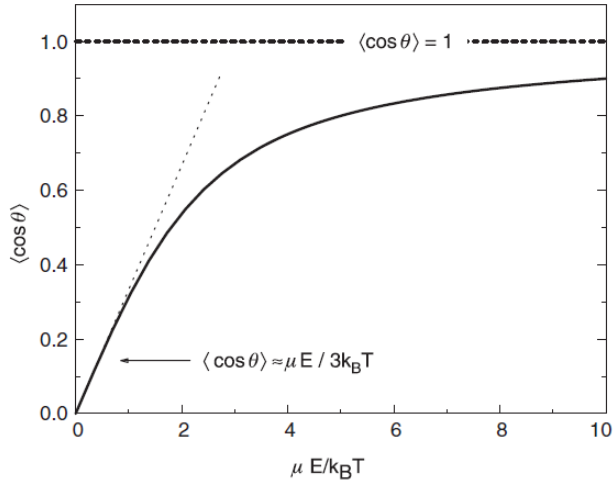

Fig. 5.1: Dependence of the Langevin function vs (μE/k_BT) (solid line) along with the linear approximation (dashed line).[picture taken from Ref. 126]

So overall what we expect to see is the combination of the two effects mentioned above: reduction in entropy which slows down the dynamics and dielectric saturation which will reduce the relaxation strength of the material.

II. Experiment

The materials employed for this study are glycerol (99.5+%, spectrophotometric grade,Sigma-Aldrich) and cyclo-octanol (97%, Alfa-Aesar), 2-methyltetrahydrofuran (99+%, anhydrous, Sigma-Aldrich) Propylene glycol (99.5%, Sigma-Aldrich), Propylene carbonate (99.7%, Sigma-Aldrich), Phenyl salicylate (99%, Sigma-Aldrich), Polyvinyl

acetate (Avg. Mw =12800, Sigma-Aldrich), N-methyl-ε-caprolactam (99% Sigma-Aldrich) and they are used as received.

For each sample prepared for a high field experiment, the linear regime permittivity is recorded using a peak field of around E_0 = 1 kV/cm or less, with no bias field (E_B = 0). The aim of the linear response measurement is to verify the properties of the sample, but also to determine the real sample thickness via the apparent value of the relaxation amplitude $\Delta\varepsilon = (\varepsilon_s - \varepsilon_\infty)$. For few materials, a separate low field measurement with Invar steel/sapphire cell (invariant with temperature and has a fixed electrode separation) has been performed. Thicknesses of the samples are determined based on the reliable published literature data or from comparing against the observed spectra from Invar cell measurements. For all measurements, i.e., both low and high field cases, the instrumentation is calibrated using low loss ($\tan\delta < 10^{-4}$) capacitors of known capacitance, using an Andeen-Hagerling AH-2700 ultra-precision capacitance bridge.

In general, the capacitor cell consists of two polished stainless steel disks (17 and 20 mm ∅), separated by a Teflon ring of 10 μm thickness that leaves an inner area of 14 mm diameter for the sample. For KDE measurements, glass beads (10-30μm) are used as spacer material instead of Teflon as dielectric breakdown strength of Teflon at high temperatures is not very high. The cell is mounted onto the cold stage of an evacuated closed-cycle He-refrigerator cryostat Leybold RDK 6-320, driven by a Leybold Coolpak-6200 compressor. The temperature of the cell is stabilized to within several mK using a Lakeshore Model 340 temperature controller equipped with DT-470-CU sensor diodes. For Cyclo-octanol, the sample is prepared between two brass electrodes, 30 and 20 mm

diameter, with Teflon strips defining a spacing of 25 μm. Using a Novocontrol Quatro temperature controller, the sample capacitor is cooled in a *l*-N_2 cryostat at a rate of around -15 K/min to near the glass transition. For PVAc and KDE, constant flow of N_2 gas is provided to control the temperature.

For observing the high field effects in a time-resolved fashion, the procedure as described in chapter 3 is followed. The waveform consists of an integer number of periods of a voltage signal, $V(t) = V_0 \sin(\omega t)$, with a bias voltage of magnitude V_B superposed for some intermediate periods. A typical sequence consists of 64 periods; 16 periods without bias, 32 periods with positive or negative high bias field, followed by another 16 periods without bias field. A voltage ratio of $V_B/V_0 = 4$ is used. The waveform is repeated once every second, with the voltage being zero for times much longer than the duration of the waveform signal. The signal frequencies used in this method span the range of 100 Hz $\leq \nu \leq$ 8 kHz. Voltage and current (using an R = 300, 1000, or 3000 Ω shunt) are recorded with a digitizing oscilloscope (Nicolet Sigma 100) with 10^6 points along the time axis and 12 or 14 bit vertical resolution. All results are averages over 3000 waveform repetitions. Integer factors n different from unity are used to evaluate the higher harmonics at $n\omega$, but averaged over a full period $2\pi/\omega$ of the fundamental frequency to achieve best spectral separation. For cases with $n > 1$, only the amplitudes (moduli) are evaluated and labeled as $V_{n\omega}$ and $I_{n\omega}$ in order to indicate the Fourier component by n.

III. Results

A. Glycerol:

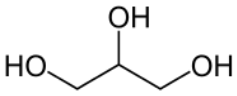

i. Effects of high dc-bias fields

Linear response spectra for glycerol at T= 216.8K is depicted in Fig. 5.2, which shows both real and imaginary part of the permittivity. The actual thickness values are generally somewhat larger (11 - 12μm) than the nominal 10μm, and the fields are reduced accordingly. The data in Fig. 5.2 and also all subsequently shown results are corrected for the actual electrode separation, and also for the additional parallel capacitance originating from the surface of the Teflon ring that is covered by electrodes.

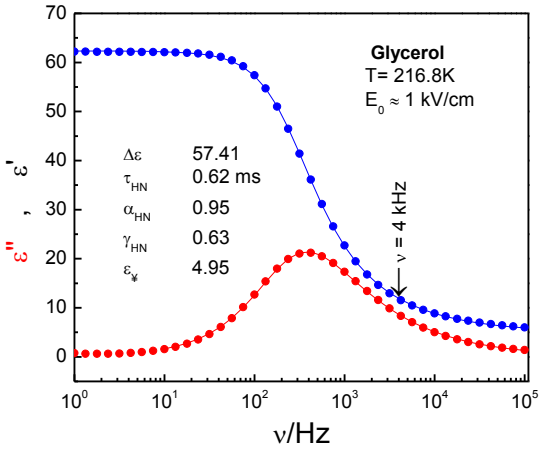

Fig. 5.2: Linear response dielectric spectrum of glycerol at T = 216.8K in terms of both storage (ε′) and loss (ε″) components is depicted. The solid lines are the corresponding HN-fit, with the values mentioned within the graph. The arrow indicates a frequency ν = 4 kHz, where time resolved measurements are performed.

In the present range of interest, the spectra are well characterized by the Havriliak-Negami (HN) dielectric function, with $\alpha_{HN} = 0.95$, $\gamma_{HN} = 0.63$, $\tau_{HN} = 0.62$ ms, $\Delta\varepsilon = 57.4$, and $\varepsilon_\infty = 4.95$ for $T = 216.8$K. In Fig. 5.2, this fit is represented as solid lines. Based upon an approximate translation between HN and KWW parameters,[74] the above mentioned HN parameters would match a KWW type decay with $\beta_{kww} = 0.65$, $\tau_{kww} = 0.34$ ms.

According to the relation between susceptibility $\varepsilon(\omega)$ and response function $d\varepsilon(t)/dt$, as shown in Eq. (2.4), this KWW decay characterizes $d\varepsilon(t)/dt$, with $\varepsilon(t)$ being understood as the retardation function describing the time dependent polarization arising from a field step of magnitude E_0 (Fig. 2.1), excluding the instantaneous contribution related to ε_∞. At constant field conditions, $d\varepsilon(t)/dt$ is proportional to current, so that $I_0(t)$ is expected to decay as $\exp[-(t/0.34\text{ms})^{0.65}]$ if the response were in the linear regime. An example of the current decay that occurs in response to the bias field step of $E_B = \pm 200$ kV/cm is shown in Fig. 5.3, for glycerol at $T = 216.8$ K. Both positive and negative bias response traces are subject to separate Fourier analyses. All four current decay traces in Fig. 5.3 follow a common time dependence, a KWW type decay, $I(t) \propto \exp[-(t/\tau)^{\beta}]$, with $\tau_{KWW} = 0.29$ ms and $\beta_{KWW} = 0.65$,i.e., a response that is somewhat accelerated compared with the linear response expectation.

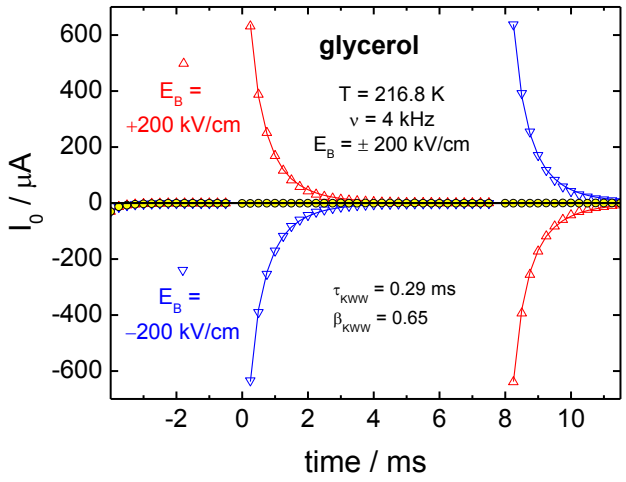

Fig. 5.3: Average current, $I_0(t)$, in response to the bias step field step of E_B = +200 kV/cm (triangles up) and E_B = −200 kV/cm (triangles down), with the bias being applied in the time range $0 \leq t \leq 8$ ms. Values for I_0 are obtained by averaging the I (t) signal over each period, thereby suppressing all higher Fourier components ($I_{n\omega}$, $n \geq 1$) that originate from the E_0 = 56 kV/cm field at ν = 4 kHz. The yellow circles near zero are for the average of the positive and negative bias traces, demonstrating how well this averaging is capable of suppressing the current response I_0. Lines are KWW decays with common parameters τ_{KWW} = 0.29 ms and β_{KWW} = 0.65.

Apart from non-linear effects due to the high field of $E_B = \pm 200$ kV/cm, these curves represent standard time domain response functions. Because this signal impacts the amplitude and phase of the current at the fundamental frequency, the average of the two bias polarities is used for assessing the harmonic signal components. Fig. 5.3 demonstrates that the $I_0(t)$ signals are highly symmetric with respect to bias field polarity, ensuring that the average of the signals with opposite bias polarity eliminates the step response contribution entirely. This average is depicted as open circles in Fig. 5.3, demonstrating that the current step response can be suppressed by a factor of about 100 via this averaging technique.

Fig. 5.4 and Fig. 5.5 respectively depict the time dependent storage and loss contributions to 'permittivity', obtained from the same data used for Fig. 5.3, but now analyzed at the fundamental frequency, ν = 4 kHz, and cast into e' and e'' representations, see Eq.(2.10).

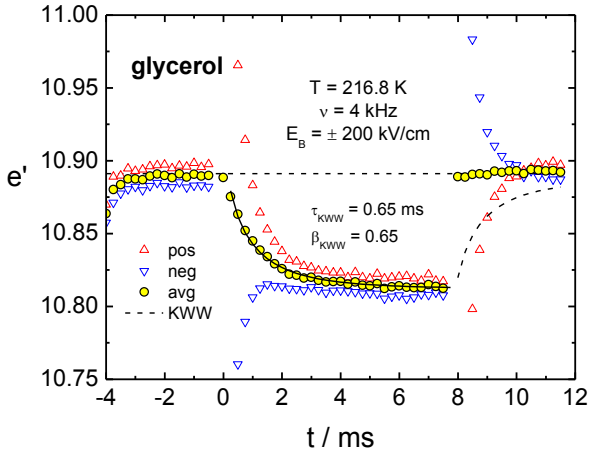

Fig. 5.4: Average signal of the dielectric storage component, e′(t), in response to the bias step field step of E_B = +200 kV/cm (triangles up) and E_B = −200 kV/cm (triangles down) at ν = 4 kHz, with the bias being applied in the time range $0 \leq t \leq 8$ ms. Circles represent the results from the average of the two signals with E_B = +200 kV/cm and E_B = −200 kV/cm, where the step response to the bias step is cancelled. The solid line is a KWW fit to the observed time dependence of e′ with τ_{KWW} = 0.65 ms and β_{KWW} = 0.65, the dashed curve indicates the recovery back to the linear response value (dashed horizontal line) if it occurred with the same KWW function.

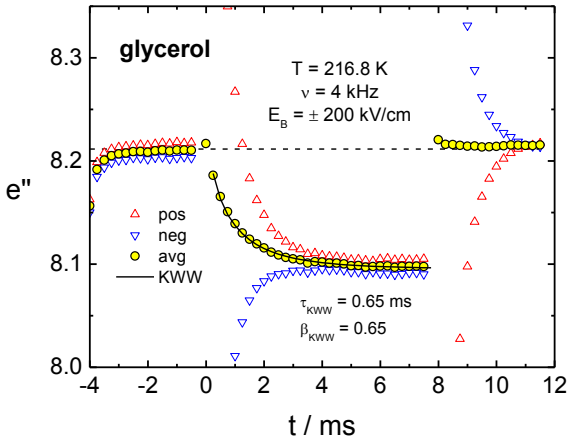

Fig. 5.5: Average signal of the dielectric loss component, e″(t), in response to the bias step field step of E_B = +200 kV/cm (triangles up) and E_B = −200 kV/cm (triangles down) at ν = 4 kHz, with the bias being applied in the time range 0 ≤ t ≤ 8 ms. Circles represent the results from the average of the two signals with E_B = +200 kV/cm and E_B = −200 kV/cm, where the step response to the bias step is cancelled. The solid line is a KWW fit to the observed time dependence of e″ with τ_{KWW} = 0.65 ms and β_{KWW} = 0.65.

In both figures, triangles represent the results from the separate bias polarities, while the open circles are for the average, where the impact of the step response on e' and e'' is eliminated. The first few periods in the time range –4 ms ≤ t ≤ –3 ms reveal the equilibration of polarization from zero field (at t < –4 ms) to the relatively small harmonic field. The amplitude E_0 of the harmonic field, $E(t) = E_0\sin(\omega t)$, is insufficient for creating any significant non-linear effects in the absence of a bias field (Δlne″ < 0.3 %). Accordingly, the levels of the quantities denoted e' in Fig. 5.4 and e'' in Fig. 5.5 for the times with no bias (–3 ms < t < 0 and t > 8 ms) agree with the low field limit values ε′ and ε″ of Fig. 5.2 at the same frequency. When the high bias field is applied within the time window 0 ≤ t ≤ 8 ms, both e' and e'' change gradually to a new level. For both cases,

e' and *e*", the steady state level in the presence of a bias field is approached by a KWW type decay with parameters τ_{KWW} = 0.65 ms and β_{KWW} = 0.65, i.e., about twice the current response time. This time constant does not change with the measurement frequency ν, but it does track τ_α when the sample temperature is altered. As a result, this time dependence could be governed by the structural recovery time of the sample.[117] The appearance of these curves changes only for frequencies $\nu << \nu_{max}$, where τ_α is short compared with a single period and the changes near $t = 0$ also appears to be very fast (due to insufficient time resolution).

The curves of Fig. 5.4 and Fig. 5.5 are representative examples of many similar measurements conducted at different frequencies ν and temperatures *T*. For each result, the steady state levels with and without bias field are recorded, and compiled graphically in Fig. 5.6 for ε' and in Fig. 5.7 for ε''. For both figures, the frequency axes are normalized to the peak loss frequency, ν_{max}, which generates master curves for the relative differences of high and low field level of the relaxing part of permittivity, $(e'_{hi} - \varepsilon'_{lo})/(\varepsilon'_{lo} - \varepsilon_\infty)$ and $(e''_{hi} - \varepsilon''_{lo})/\varepsilon''_{lo}$, respectively. In the real part case, the infinite frequency dielectric constant is subtracted because electronic polarizability is practically field invariant.

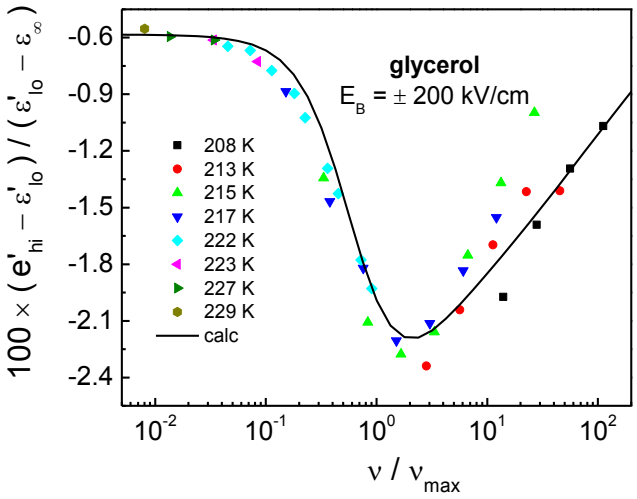

Fig. 5.6: Steady state values of the field induced relative changes of the dielectric storage component, $(e'_{hi} - \varepsilon'_{lo}) / (\varepsilon'_{lo} - \varepsilon_\infty)$, for glycerol versus reduced frequency, ν/ν_{max}. The subscripts "hi" and "lo" refer to bias electric fields of $E_B = \pm 225$ kV/cm and $E_B = 0$, respectively. Experimental results (symbols) are derived from different temperatures as indicated, but for a common bias field of $E_B = 225$ kV/cm. The line is based on the HN fit of Fig. 5.2, but with $\Delta\varepsilon$ reduced by 0.6% and τ_{HN} increased by 2.7% for the e'_{hi} case.

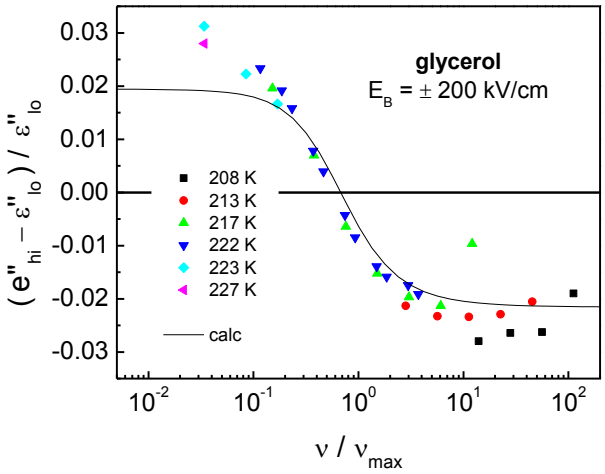

Fig. 5.7: Steady state values of the field induced relative changes of the dielectric loss component, $(e''_{hi} - \varepsilon''_{lo})/\varepsilon''_{lo}$, for glycerol versus reduced frequency, ν/ν_{max}. The subscripts "hi" and "lo" refer to bias electric fields of $E_B = \pm 225$ kV/cm and $E_B = 0$, respectively. Experimental results (symbols) are derived from different temperatures as

indicated, but for a common bias field of E_B = 225 kV/cm. The line is based on the HN fit of Fig. 5.2, but with $\Delta\varepsilon$ reduced by 0.6% and τ_{HN} increased by 2.7% for the e''_{hi} case.

In both cases, the solid line captures the essence of the field induced change, and the curves are calculated as follows. The low field permittivity (ε'_{lo}, ε''_{lo}) is assumed to be described by the HN fit shown in Fig. 5.2. The high dc-field counterparts (e'_{hi}, e''_{hi}) are calculated using the same HN parameters, except with $\Delta\varepsilon$ being reduced by 0.6% and with τ_{HN} being increased by 2.7%. The reduction of the relaxation amplitude is meant to reflect dielectric saturation. For this calculation, the saturation resulting from a dc-field has been approximated by a frequency invariant quantity.

Now, we turn our attention to the higher harmonic current signals. The effect of a high bias field on the higher harmonics of the current response is depicted in Fig. 5.8, again derived from the same $V(t)$, $I(t)$ signals that lead to the results shown in Fig. 5.3, Fig. 5.4 and Fig. 5.5. Observing saturation in a dc-bias field (see low frequency plateau at –0.6% in Fig. 5.6) suggests that the orientational isotropy is broken. It is therefore expected that a second harmonic signal appears, and that is observed as $I_{2\omega}/I_{\omega}$ in Fig 5.8. Values are represented as the modulus ratios, $I_{2\omega}/I_{\omega}$ and $I_{3\omega}/I_{\omega}$, with the average over positive and negative bias being performed for $I_{2\omega}$ after the Fourier analysis to avoid cancellation of the even Fourier terms. For both the second and third harmonic, a considerable increase is observed for times at which the bias field is present, $t > 0$. The value of $I_{3\omega}/I_{\omega}$ appears to jump to a higher level of 6.4×10^{-4}, without any visible time dependence. The increase of $I_{2\omega}/I_{\omega}$ to the plateau at 1.4×10^{-3} may take up to 2 ms, but the approach is obscured by the step response of I_0 (as can be seen in Fig. 5.3).

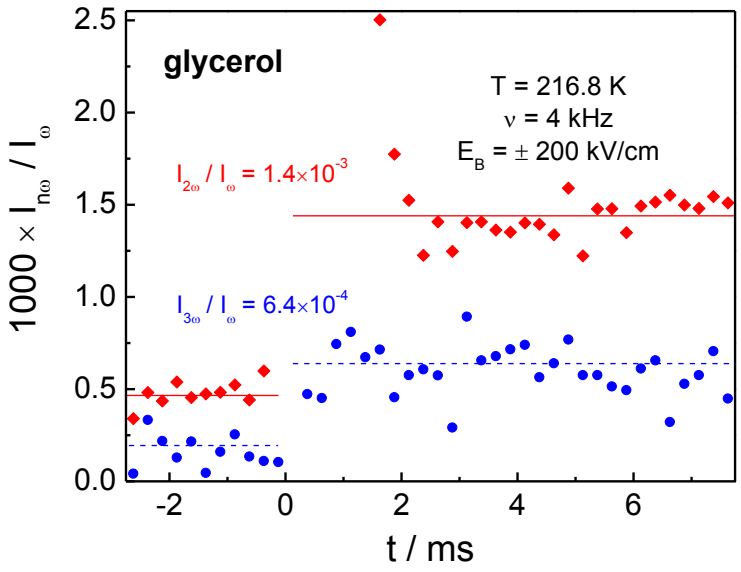

Fig. 5.8: Amplitude of second ($I_{2\omega}/I_{\omega}$) and third ($I_{3\omega}/I_{\omega}$) Fourier components of the current for glycerol at T = 216.8 K, each one normalized to the amplitude of the fundamental frequency current, I_{ω}. Values are derived from a time resolved measurement using a ν = 4 kHz sine wave with amplitude E_0 = 50 kV/cm and bias fields of E_B = ± 200 kV/cm applied in the time range $0 \leq t \leq 8$ ms. For the $I_{2\omega}$ case, each bias polarity signal is subject to separate Fourier analysis, and the average of the resulting outputs is taken. For the $I_{3\omega}$ case, the average of the signals for each bias polarity is subject to Fourier analysis, thereby eliminating all even harmonics.

The magnitudes of the field dependent effects observed in this study all scale with E_B^2. A demonstration of that feature is provided in Fig. 5.9, obtained with the bias mode of the SI-1260 gain/phase analyzer. The graph shows spectra of the field induced relative change of ε′ for fields of 150, 180, and 220 kV/cm (solid symbols), whereas open symbols in Fig. 5.9 collapse to a single master curve when normalized to the field of 200kV/cm by virtue of scaling by E_B^2.

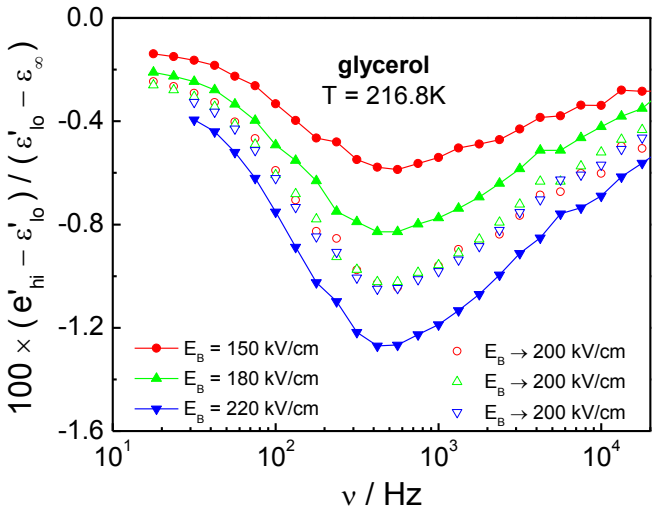

Fig. 5.9: Field induced relative changes of the dielectric storage component, $(e'_{hi} - \varepsilon'_{lo})/(\varepsilon'_{lo} - \varepsilon_\infty)$, for glycerol at T = 216.8 K versus frequency, ν. Different sets of solid symbols are for different bias fields of E_B = 150, 180, and 220 kV/cm, as indicated. Open symbols represent the same measurements (symbol style preserved), but after multiplying by E_{ref}^2/E_B^2, with E_{ref} = 200 kV/cm, indicating that the effects scale with E_B^2.

From all the measurements and data shown above, the most interesting and dominant field induced change is the increase of the relaxation time τ_α, i.e., a slowing down of the dynamics that shifts the entire loss peak to a lower peak frequency while retaining its shape which has been predicted by Johari[123]. According to low field data on glycerol, the temperature dependence of τ_α near T = 216.8 K is characterized by $d\ln\tau_\alpha/dT$ = – 0.30 K^{-1}, so that the value $\Delta_E \ln\tau_\alpha$ = +2.7% is equivalent to a net change of the fictive temperature of 0.027/(– 0.30 K^{-1}) = –90 mK at E_B = 200 kV/cm (or –22 mK at E_B = 100 kV/cm = 10^5 V/cm). The same effect can be represented by a glass transition temperature shift of ΔT_g = +90 mK. In agreement with the present results, a recent study by L'Hôte *et*

al.[127] also identified that the relaxation times in glycerol increase with E^2 as a result of applying a dc bias field. According to the report by L'Hôte *et al.*[127] , the observed change in glass transition temperature ΔT_g = +6 mK at E_B = 40 kV/cm for glycerol, equivalent to ΔT_g = +150 mK at E_B = 200 kV/cm provided that the quadratic field dependence holds over that range.

ii. Prediction from Entropy interpretation

As mentioned in the Introduction section, Johari predicted an electro-viscous effect for polar liquids by combining the field induced change of configurational entropy, Eq. (5.3), with the Adam-Gibbs relation, Eq. (5.2).[29] The net dependence of dynamics on a DC field is given by Eq. (5.3), which was assumed to hold equally for a relaxation time (τ_α) and for viscosity (η). In order to obtain a quantitative result for glycerol on the basis of Eq. (5.3), values for $\partial\varepsilon_s/\partial T$, υ, $S_{cfg}(T)$, and C are required. The sensitivity of the dielectric constant to temperature is derived from data obtained from the Invar cell measurement and recently published by Matyushov and Richert, resulting in $\partial\varepsilon_s/\partial T = -0.414$ K^{-1}.[128] The molar volume is taken to be υ = 71.95 mLmol^{-1}.[129] The configurational entropy and Adam-Gibbs parameters (A, C) are determined from calorimetry data originating from Gibson *et al.*,[130] digitized from a graph published by Takeda and collaborators,[131] and dielectric relaxation data by Stickel.[132] An Adam-Gibbs type graph, i.e., $\log\tau_\alpha$ versus $1/(TS_{exc})$, produced a linear relation in the viscous regime with the parameters A = –11.57, C = 67.4 kJ mol^{-1}, see Eq. (5.2). At the temperature of interest, the entropy was found to be $S_{exc}(T = 216.8\ K) = 37.3$ J K^{-1} mol^{-1}. For the field

used in this work, E_B = 200 kV/cm, the field induced entropy change is $\Delta_E S_{cfg}$ = –0.052 J K^{-1} mol^{-1}, which predicts $\Delta_E \ln\tau_\alpha$ = 2.71% on the basis of Eq. (5.3). The experimental value of $\Delta_E \ln\tau_\alpha$ = 2.2% is 81% of the above prediction of $\Delta_E \ln\tau_\alpha$ = 2.71%. The relative errors of the experimental and predicted values for $\Delta_E \ln\tau_\alpha$ are estimated to be 10% and 8%, respectively. To predict the observed nonlinear dielectric effect quantitatively one must compare the results for a fixed temperature as both the configurational entropy and activation energy changes with temperature. For that reason, here I will compare the steady state NDE observed during time resolved measurement at ν = 4 kHz (Fig. 5.5) of the glycerol sample held at T= 216.8K. The Δlne″ value for the steady state situation is found to be = -1.34%. So the change in timescale $\Delta_E \ln\tau_\alpha$, which can be obtained by the slope correction (slope = $-\alpha\gamma$ = -0.6 above the peak according to HN fit) as shown in the Chapter 4, is calculated to be 2.24%. The observed value in change in τ_α is almost 83% of the predicted value of 2.71% at this temperature. For a different temperature (214.2K), the observed change is found to be 80% of the predicted one. This moderate discrepancy may be due to the fact that the experimental data for the entropy of glycerol is actually the excess entropy $S_{exc}(T)$, which is generally greater than $S_{cfg}(T)$. For glycerol, a recent estimate for the ratio found $f_{S,T} = S_{cfg}(T)/S_{exc}(T) \approx 0.8$.[76] As Adam-Gibbs relates only the configurational part of entropy to the relaxation timescale, the calculation should be done in terms of change in configurational entropy. Therefore, we use $d\log\tau/dS_{exc} = -C_{AG}/(TS_{exc}^2)$, and then transition to configurational values by the term $f_{S,T}$, which should be equal to $f_C = C_{p,cfg}/C_{p,exc}$,[133] and both $f_{S,T}$ and f_C are assumed to be temperature invariant.

The overall change in time constant, τ_α, with field induced (configurational) entropy, $\Delta_E S$, Eq. (5.3) then reads,

$$\Delta_E ln\tau_\alpha = -\ln(10)\frac{C_{AG}}{TS^2_{exc}(T)}\frac{1}{f_{S,T}}\Delta_E S \qquad \text{Eq. (5.8)}$$

So the actual predicted effect based on only configurational entropy change is for 216.8K would be $\Delta_E ln\tau_\alpha$ =2.71/0.8= 3.39% and the observed changes is approximately 65% of the predicted effect. It is important to realize that an electric field may change entropy and thus relaxation time scales in much the same way as possible by small changes in temperature or pressure. However, a structural difference remains: in the presence of an electric field, a dipolar liquid becomes anisotropic, while changing entropy by temperature or hydrostatic pressure alone preserves the isotropic nature of the liquid. Johari[123] indicated the changes in $\Delta_E S$ to be completely configurational in nature, but there is no obvious justification for this claim. As it is mentioned before, that high DC field may disturb the isotropic nature of the liquid; the configurational fraction of the entropy may not be the same for both the isotropic and anisotropic samples. So here, we introduce a new factor designated as $f_{S,E}$, which describe the effect on configurational fraction of entropy in a high bias field induced sample. For glycerol at T= 216.8K this number turns out to be around 0.65. So as a result Eq. (5.8) eventually modifies to the following form:

$$\Delta_E ln\tau_\alpha = -\ln(10)\frac{C_{AG}}{TS^2_{exc}(T)}\frac{1}{f_{S,T}} \times f_{S,E}\Delta_E S \qquad \text{Eq. (5.9)}$$

iii. Relation to other models

For the relation of the present effects to the theory involving the number of dynamically correlated particles, the reader is referred to the paper by L'Hôte *et al.* and reference therein.[127]A further source of altering the time constants of a polar liquid subject to field steps is a change in sample temperature by virtue of the electro-caloric effect. Analogous to cooling by adiabatic demagnetization, the field dependent polarization P implies an entropy change that obeys the relation $(\partial S/\partial E)_T = (\partial P/\partial T)_E$.[124] For glycerol, the entropy changes are orders of magnitude below what is needed to detect temperature changes under adiabatic conditions. And even if heat flow is created, the sample thickness of only 10 μm and contact to electrodes that act as practically infinite heat baths (C_p = 3.1 J/K) create near isothermal conditions.[52] Also, the effect would result in heating on applying the field and cooling on removing it, and this type of symmetry of the changes are not observed. In a general approach to the dynamics characteristic of disordered materials, Javaheri and Chamberlin used a Landau-like theory to determine the internal energy ε as a function of the order parameter L,[134] leading to $\varepsilon = L^2 k_B T_L$ with T_L = 60 K for the case of glycerol. If dipole orientation in terms of $\langle\cos\theta\rangle$ is employed as order parameter, the non-interacting dipole case yields $L = \mu E/k_B T$. With the parameters μ = 2.6 D, E = 200 kV/cm, and T = 216.8 K, a value of L = 0.057 is obtained. Interpreting the concomitant reduction of ε/k_B by 200 mK as added barrier, the effect of the field would amount to a glass transition shift of about +200 mK. This model correctly predicts

a field induced increase of relaxation times, but overestimates the findings by a factor of two.

Based upon an order parameter model for the structural relaxation of glass forming materials, Moynihan and Lesikar obtain stability criteria on the grounds of equilibrium thermodynamics.[135] In the 'Discussion of the Paper' section, two expressions for dT_g/dE are derived, and values for ΔT_g for glycerol are provided. The first assumes constant volume (before and after relaxation), leading to $\Delta T_g = \varepsilon_0 \frac{\Delta[\partial(\chi V)/\partial P]}{2V\Delta\alpha} E^2$, where χ (= ε_s – 1) is the dielectric susceptibility, P is pressure, V is volume, α is the volume thermal expansion coefficient, and E the applied static field. For glycerol at T = 218 K, this yields ΔT_g = +2 mK for a field jump from 0 to 10^5 V/cm, equivalent to ΔT_g = +8 mK for a field of E = 200 kV/cm.

If constant entropy (before and after relaxation) is assumed instead, the following relation was obtained, $\Delta T_g = \varepsilon_0 \frac{\Delta[\partial(\chi V)/\partial T]}{2\Delta C_p} E^2$, where ΔC_p is the relaxational part of the heat capacity at constant pressure. This case gives ΔT_g = +40 mK for a field jump from 0 to 10^5 V/cm for glycerol at T = 218 K, equivalent to ΔT_g = +160 mK for a field of E = 200 kV/cm. Both cases considered by Moynihan predict a field induced increase of structural relaxation times, but a quantitative agreement with the present observation of ΔT_g = +90 mK is not reached.

B. Cyclo-octanol:

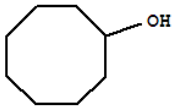

Cyclo-octanol in its plastic crystal state is measured with the bias mode of the SI-1260 gain/phase analyzer. For the plastic crystal state of cyclo-octanol, the effect of a high bias field shown in Fig. 5.10. Analogous to Fig. 5.6 for glycerol, the field induced relative change of permittivity in case of cyclo-octanol is shown as $(e'_{hi} - \varepsilon'_{lo})/(\varepsilon'_{lo} - \varepsilon_\infty)$ versus frequency ν in Fig. 5.10.

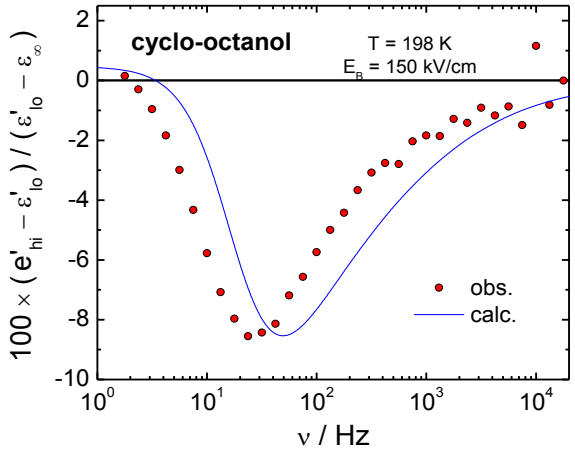

Fig. 5.10: Quasi steady state values of the field induced relative changes of the dielectric storage component, $(e'_{hi} - \varepsilon'_{lo})/(\varepsilon'_{lo} - \varepsilon_\infty)$, for the plastic crystal state of cyclo-octanol at T = 195K versus frequency, ν. Experimental results (symbols) represent the average of the results from positive and negative bias for a field of $E_B = \pm 150$ kV/cm. The line is based on a HN fit to the linear response curve, but with $\Delta\varepsilon$ enhanced by 0.5% and τ_{HN} increased by 13.5% for the e'_{hi} case.

The value of ε' is changed as much as –8.5% at a bias field of E_B = 150 kV/cm, which represents a 10 fold increase over the –2% effect observed at E_B = 200 kV/cm for

glycerol, although no indication of saturation is found in this case. The solid line in Fig. 5.10 is a calculation based on an HN fit for the low field permittivity (ε'_{lo}, ε''_{lo}), whereas the high dc-field counterparts (e'_{hi}, e''_{hi}) are calculated using the same HN parameters, but with $\Delta\varepsilon$ being increased by 0.5% and with τ_{HN} being increased by 13.5%. The two loss spectra corresponding to the E_B = 150 kV/cm and E_B = 0 case for cyclo-octanol at T = 198 K can be seen in Fig. 5.11, which reveals that the high bias field shifts the loss peak to lower frequencies while widening the loss profile. For comparison, a low field loss curve taken at T = 196 K is included in this graph. The low field HN parameters for the T = 198 K case are α_{HN} = 1.0, γ_{HN} = 0.70, τ_{HN} = 7.8 ms, $\Delta\varepsilon$ = 46.9, and ε_∞ = 5.2. The fit is consistent with previous dielectric results reported by Brand *et al.* for the same system.[136]

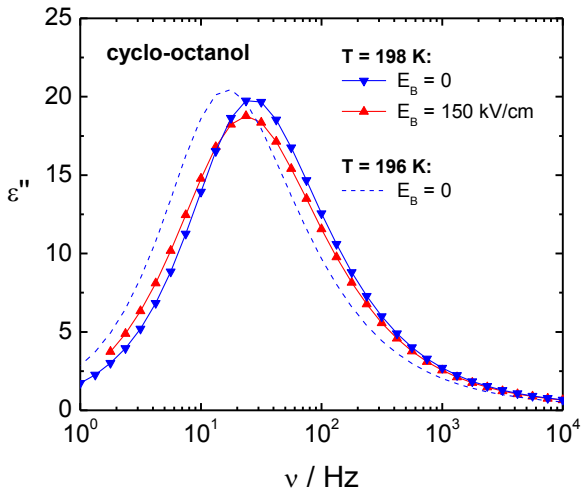

Fig. 5.11: Dielectric loss spectra of the plastic crystal state of cyclo-octanol. Triangles pointing up and down are for T = 198 K with E_B = 150 kV/cm and E_B = 0, respectively. For comparison, the dashed line represents the loss for a lower temperature and zero bias, T = 196 K and E_B = 0.

Based on the activation behavior of cyclo-octanol ($d\ln\tau_\alpha/dT$ = –0.23 K^{-1}), this amounts to a field induced fictive temperature change of –0.58 K. That the line in Fig. 5.10 is shifted along the frequency axis compared with the data is the result of a difference in the loss profiles for the high and low field spectra, see Fig. 5.11. For the plastic crystal cyclo-octanol, we obtain a higher value for the field induced reduction of the configurational entropy, even for the lower field used with cyclo-octanol. A slope of $\partial\varepsilon_s/\partial T$ = –0.75 K^{-1} is determined from the present data, and together with υ = 139 mL mol^{-1} and E_B = 150 kV/cm we obtain $\Delta_E S_{exc}$ = –0.104 J K^{-1} mol^{-1}. Analogous to the glycerol case, we digitized existing data for the dielectric relaxation time from Brand *et al.*[136] and for entropy from Yamamuro *et al.*[137] in order to generate an Adam-Gibbs plot. The range of the literature data did include the current temperature of interest (T = 198 K), but $\log\tau_\alpha$ versus $1/(TS_{exc})$ failed to display a linear dependence. The conclusion is that the Adam-Gibbs relation fails to capture the dynamics of this plastic crystal. A forced linear fit to the data in the vicinity of T = 198 K yields the Adam-Gibbs parameters A = –7.4, C = 18.1 kJ mol^{-1}. Together with S_{exc} (T = 198 K) = 17.8 J K^{-1} mol^{-1}, a value of $\Delta_E\ln\tau_\alpha$ = 6.9% is determined for the field induced slowing down of the dynamics. Given the moderate field, this is an effect of considerable magnitude, but only about half of the observed effect.

C. N-methyl-ε-caprolactam (NMEC):

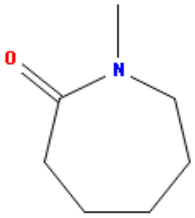

Low field measurement for a range of temperatures near glass transition temperature is performed within Invar cell in the liquid N_2 setup. The measurement data for both the real and imaginary part of permittivity is shown in Fig. 5.12a and Fig. 5.12b. From the real part data set, the slope $\frac{\partial \varepsilon_S}{\partial T}$ is determined to be -0.49K^{-1}. Low field measurement of the NMEC sample within the high field sample cell with 10μm Teflon spacer is shown in Fig. 5.13. Compared against the Invar cell measurement data it is determined that the sample thickness is actually 9.8μm and the structural relaxation timescale corresponds to the sample temperature at 187.5K. Both the red solid lines in Fig. 5.13 represents a fit based on the HN parameters listed below: $\Delta\varepsilon$ = 53.14, ε_∞ = 4.35, $\log\tau_{HN}$ = -3.06, α_{HN} = 0.96, γ_{HN} = 0.65. Based on the HN fit parameters mentioned above the KWW parameters are found to be τ_{KWW} = 0.5 ms and β_{KWW} = 0.66 respectively.

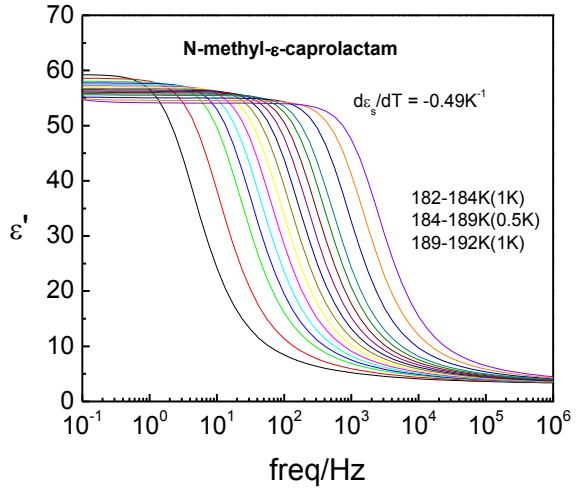

Fig. 5.12a: Real part of the permittivity data from linear response measurement for NMEC in an Invar cell setup for the temperature range 182-192K. Data was recorded for 1K temperature step in the temperature interval 182-184K and 189-192K. In between temperature was increased by 0.5K step.

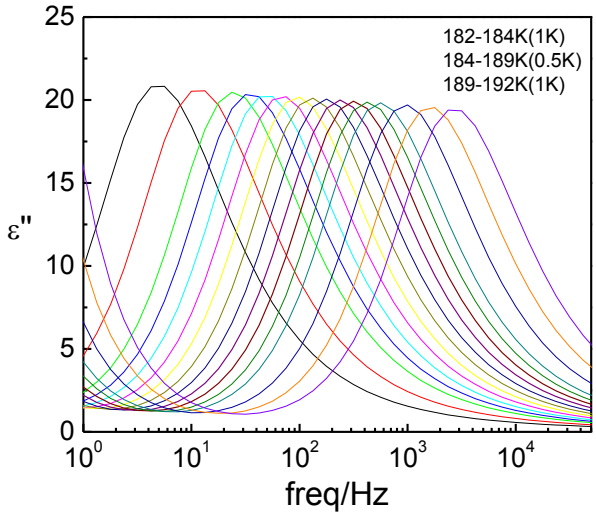

Fig. 5.12b: Imaginary part of the permittivity data from linear response measurement for NMEC in an Invar cell setup for the temperature range 182-192K. Data was recorded for 1K temperature step in the temperature interval 182-184K and 189-192K. In between temperature was increased by 0.5K step.

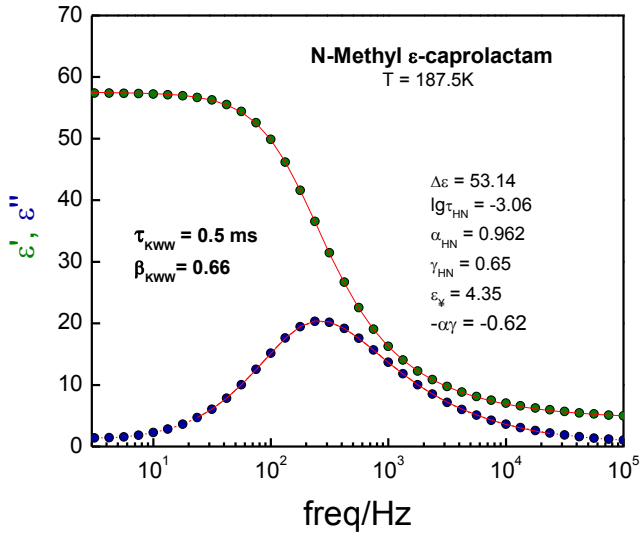

Fig. 5.13: Linear response dielectric spectrum of NMEC at T = 187.5K in terms of both storage (ε′) and loss (ε″) components is depicted. The solid lines are the corresponding HN-fit, with the values mentioned within the graph. The KWW parameters corresponding to the low field measurement are as follows: τ_{KWW} = 0.5 s, β_{KWW} =0.66.

High field measurements at different temperatures are performed at a field of 128kV/cm and the relative change in terms of the dielectric loss is shown in Fig. 5.14. The frequency axis in that figure is normalized to the peak frequencies for different temperatures. A fit to the experimental data points is performed by increasing the low field τ value by 2.8% and the Δε is being reduced by 0.67% compared to the low field HN parameters of T = 187.5K. A time resolved high field experiment for NMEC at 187.5K for ν = 4 kHz is shown in Fig. 5.15. From the graph it can be seen that for E_B = ±179 kV/cm, the experimental change in Δlne″ including saturation is -3.41%. The KWW type time dependence of the time resolved relative change in dielectric loss again closely follows the structural relaxation timescale. As no adiabatic calorimetry data are currently

available for NMEC, it is not possible to compare the experimental values with the Adam-Gibbs prediction.

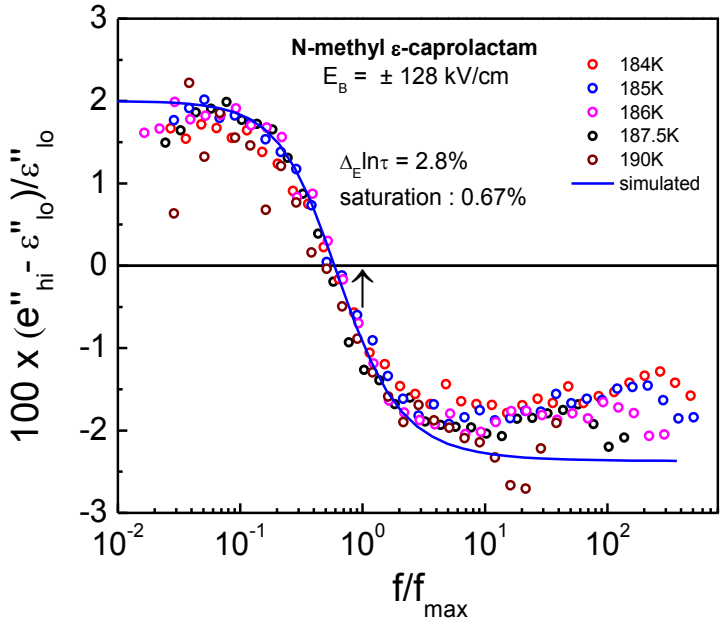

Fig. 5.14: Steady state values of the field induced relative changes of the dielectric loss component, $(\epsilon''_{hi} - \varepsilon''_{lo})/\varepsilon''_{lo}$, for NMEC vs. reduced frequency, ν/ν_{max}. The subscripts "hi" and "lo" refer to bias electric fields of $E_B = \pm 128$ kV/cm and $E_B = 0$, respectively. Experimental results (symbols) are derived from different temperatures as indicated, but for a common bias field of $E_B = 128$ kV/cm. The line is based on the HN fit of Fig. 5.13, but with $\Delta\varepsilon$ reduced by 0.67% and τ_{HN} increased by 2.8% for the ϵ''_{hi} case.

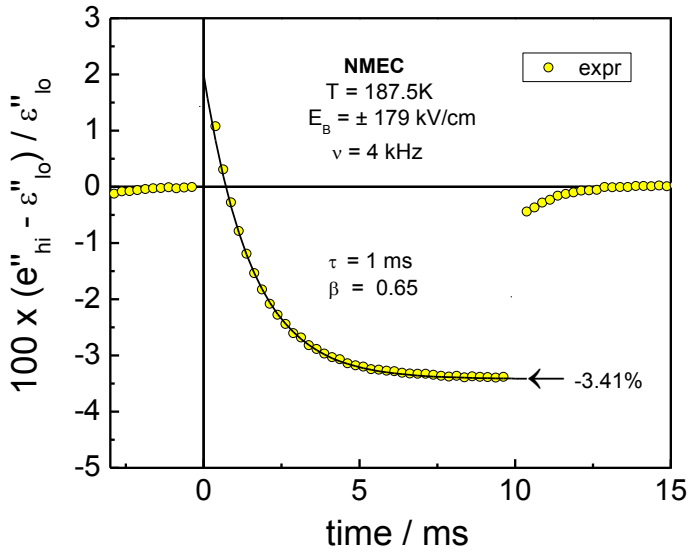

Fig. 5.15: Time resolved field induced relative change of the dielectric loss component, $(e''_{hi} - \varepsilon''_{lo})/\varepsilon''_{lo}$, for NMEC in response to the bias field step of $E_B = \pm 179$ kV/cm at $\nu = 4$ kHz, with the bias being applied in the time range $0 \leq t \leq 10$ ms. Circles represent the results from the average of the two signals with $E_B = +179$ kV/cm and $E_B = -179$ kV/cm. The solid line is a KWW fit to the observed time dependence of the relative change with $\tau_{KWW} = 1$ ms and $\beta_{KWW} = 0.65$. The steady state value of the relative change is -3.41%.

D. 2-Methyltetrahydrofuran (2-MTHF):

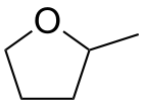

Based on the low field measurement data (Fig. 5.16), the sample thickness was determined to be 10.3μm comparing against the literature value.[138] So, the actual field applied to the sample in the time resolved measurement is $E_B = 155$ kV/cm. Time resolved measurements are performed at $\nu = 4$ kHz, which is situated almost 10 times the peak frequency ($f_{max} \approx 450$Hz). The point (olive in color) shown in the low field spectrum is the low field value of ε'' obtained from the oscilloscope measurement mentioned

above. The steady state change in oscilloscope measurement is found to be -0.98% (Fig. 5.18). Again, the time dependence of towards the steady state changes during the oscilloscope measurement is found to follow the structural relaxation timescale at that temperature (see Fig. 5.18).

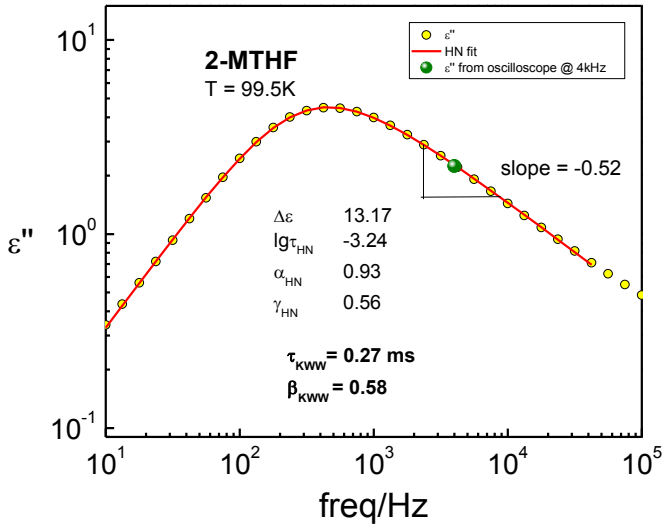

Fig. 5.16: Linear response dielectric loss (ε″) spectrum of 2-MTHF at T = 99.5K is depicted. The solid line is based on the HN-fit, with the values mentioned within the graph. The KWW parameters corresponding to the low field measurement are as follows: τ_{KWW} = 0.27 ms, β_{KWW} =0.58. The olive circle represents the low field value at T = 99.5K for ν = 4 kHz obtained from the oscilloscope measurement shown in Fig. 5.18. Slope on the high frequency side of the peak ($-\alpha_{HN}\gamma_{HN}$ = -0.52) is also indicated.

A high field measurement with SI-1260 is also performed at a slightly different temperature (T = 97.5K) for field value of 210 kV/cm as shown in the Fig. 5.17. As it can be clearly seen from the graph that the frequency spectrum of relative change in the dielectric loss value (black circles) looks very similar to what we have seen before in case of glycerol. A similar procedure is applied to fit the experimental data points and the solid red line corresponds to the fit obtained by increasing the timescale by 2.76% from

its low field counterpart with added saturation of 0.66%. The steady state change obtained from the oscilloscope measurement for a different temperature (T = 99.5K) also put together in that same graph (olive sphere) after necessary field correction.

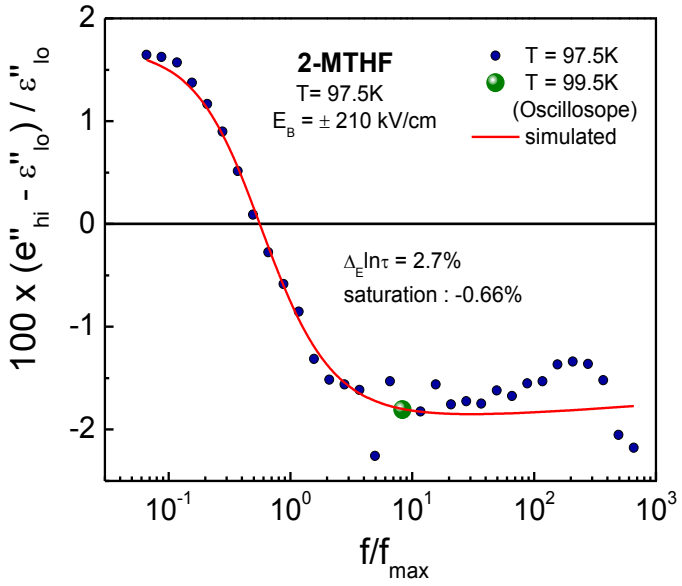

Fig. 5.17: Steady state values of the field induced relative changes (blue symbols) of the dielectric loss component, $(e''_{hi} - \varepsilon''_{lo})/\varepsilon''_{lo}$, vs. reduced frequency, f/f_{max}, for 2-MTHF at T = 97.5K. The subscripts "hi" and "lo" refer to bias electric fields of $E_B = \pm$ 210 kV/cm and $E_B = 0$, respectively. The red line is based on the HN fit, but with $\Delta\varepsilon$ reduced by 0.66% and τ_{HN} increased by 2.7% for the e''_{hi} case. The large olive sphere in the graph is based on the steady state value from the oscilloscope measurement shown in Fig. 5.18 and field corrected.

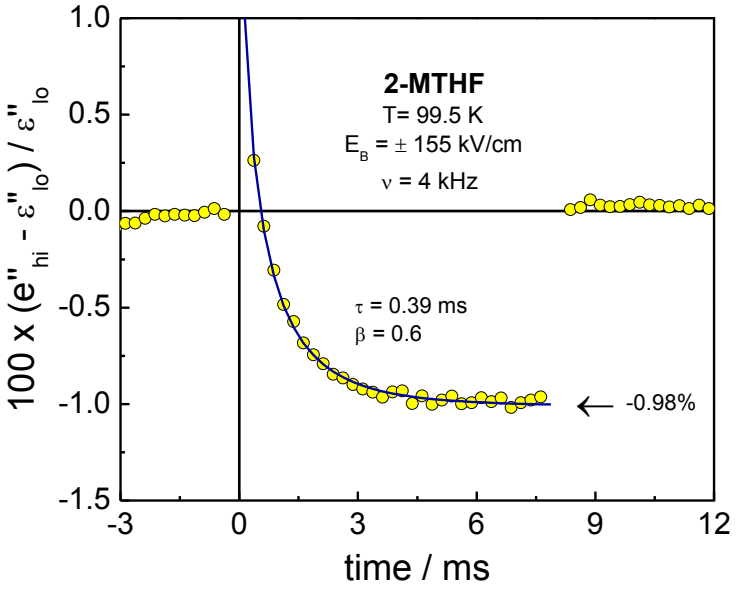

Fig. 5.18: Time resolved field induced relative change of the dielectric loss component, $(e''_{hi} - \varepsilon''_{lo})/\varepsilon''_{lo}$, for 2-MTHF in response to the bias field step of $E_B = \pm 155$ kV/cm at ν = 4 kHz, with the bias being applied in the time range $0 \leq t \leq 8$ ms. Circles represent the results from the average of the two signals with $E_B = +179$ kV/cm and $E_B = -179$ kV/cm. The solid line is a KWW fit to the observed time dependence of the relative change with $\tau_{KWW} = 0.39$ ms and $\beta_{KWW} = 0.6$. The steady state value of the relative change is -0.98%.

For the Adam-Gibbs prediction, $\partial\varepsilon_S/\partial T = -0.175K^{-1}$ at T = 99.5K is used as obtained from literature values.[138] Thermodynamic data set regarding excess entropy and the corresponding Adam-Gibbs parameter was obtained from Mizukami *et al.*[139]. The density of 2-MTHF is found to be 0.854 g ml^{-1}.[140] At T= 99.5K, excess entropy measured is equal to 29.86 J mol^{-1} K^{-1}, Adam-Gibbs parameter C_{AG} is equal 39 kJ mol^{-1}. Based on the obtained values, the predicted change in timescale is calculated to be $\Delta_E \ln\tau_\alpha$ = 1.9%. From the oscilloscope measurements, the steady state change in $\Delta\ln\varepsilon''$ at ν = 4 kHz for the field E_B =155 kV cm^{-1} is found to be -0.98%. Correcting for the relevant amount of

saturation from the overall relative change in $\Delta ln\varepsilon''$, the amount of change in timescale is calculated to be $\Delta_E ln\tau$ ($\Delta ln\varepsilon''/ -\alpha\gamma$) = 1.2% at 155 kV cm^{-1} which is actually 63% of the predicted change. Based on the fragility values of 2-MTHF, the factor $f_{S,T}$ is expected to be around 0.6.[76] So following Eq. (5.5), the field dependent entropy factor, $f_{S,E}$, is expected to be 0.38, i.e., the field induced change in configurational entropy in case of 2-MTHF is found to be 38% of the $\Delta_E S$ value.

Salol or Phenyl salicylate:

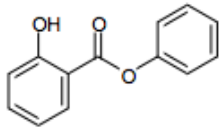

Salol

Standard linear dielectric response (both real and imaginary part) in our high field dielectric cell with 10μm Teflon spacer is shown in Fig. 5.19 (panel a) and Fig. 5.19 (panel b) for salol at T = 234K. Based on the literature values of $\Delta\varepsilon$, the thickness is found to be very close to 10μm.[141,142] Solid red lines are obtained from HN fit and the parameters are mentioned within the graph. Based on the HN fit parameters, KWW parameters are calculated to be τ_{KWW} = 2.66 ms and β_{KWW} = 0.53 respectively.

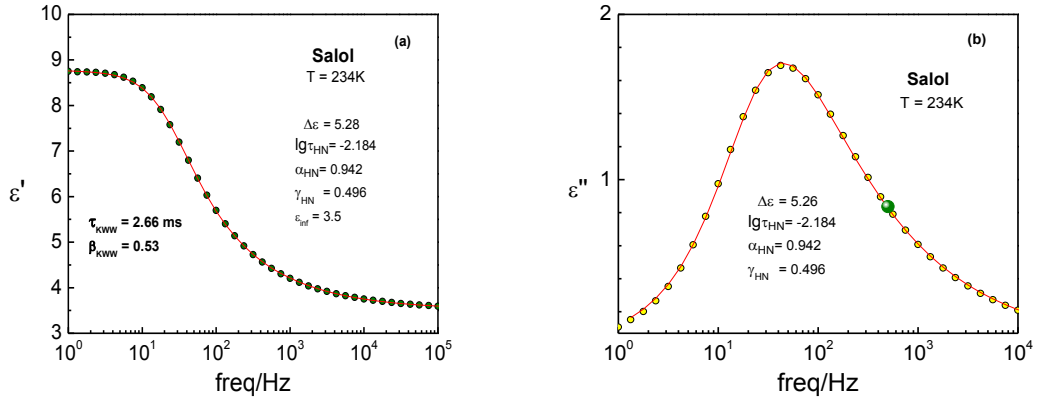

Fig. 5.19: Linear response dielectric storage (ε′) [panel (a)] and loss (ε″) [panel (b)] spectrum of Salol at T = 234 K is depicted. The solid lines are based on the HN-fit, with the values mentioned within the graph. The KWW parameters corresponding to the low field measurement are as follows: τ_{KWW} = 2.66 ms, β_{KWW} =0.53. The olive circle in panel (b) represents the low field ε'' value at T = 234K for ν = 500 Hz obtained from the oscilloscope measurement shown in Fig. 5.21.

Standard high field measurements are performed with PZD-700/SI-1260 combination for fields ranging from 250kV cm^{-1} to 480kV cm^{-1} at the same temperature (T = 234K). Fig. 5.20 shows the relative change curves in dielectric loss for the normalized field of E_B = ±450kV cm^{-1}. The blue fit curve is obtained by increasing the timescale of the low field measurement curve by 3.7% and dielectric strength (Δε) is reduced by 0.38%. The arrow indicates the peak position of the low field dielectric loss curve at that temperature. Olive and orange spheres in Fig. 5.19b and Fig. 5.20 respectively represent the dielectric loss at ν = 500Hz and the corresponding steady state value of the relative change (corrected with field) in dielectric loss at the same frequency measured via oscilloscope which is shown in Fig. 5.21. The KWW type fit curve is also shown in Fig. 5.21 which traces the time dependence of the relative change in dielectric loss towards its steady state value.

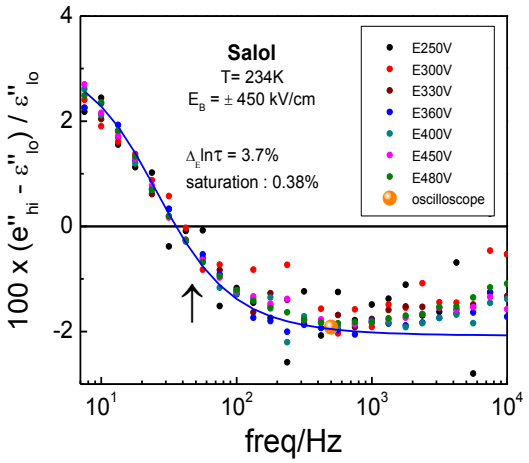

Fig. 5.20: Steady state values of the field induced relative changes (symbols) of the dielectric loss component, $(e''_{hi} - \varepsilon''_{lo})/\varepsilon''_{lo}$, vs. frequency, for Salol at T = 234K. The subscripts "hi" and "lo" refer to bias electric fields of $E_B = \pm$ 450 kV/cm and $E_B = 0$, respectively. The red line is based on the HN fit parameters from Fig. 5.19, but with $\Delta\varepsilon$ reduced by 0.38% and τ_{HN} increased by 3.7% for the e''_{hi} case. The large orange sphere in the graph is based on the steady state value from the oscilloscope measurement shown in Fig. 5.21. The solid arrow indicate the position of the peak frequency at T=234K.

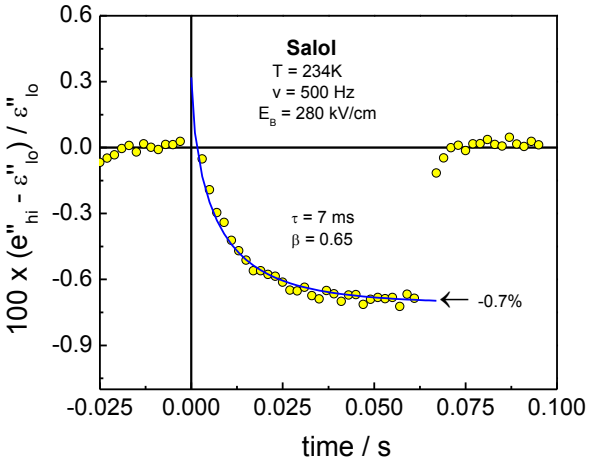

Fig. 5.21: Time resolved field induced relative change of the dielectric loss component, $(e''_{hi} - \varepsilon''_{lo})/\varepsilon''_{lo}$, for Salol in response to the bias field step of $E_B = \pm$ 280 kV/cm at ν = 500 Hz, with the bias being applied in the time range $0 \le t \le 64$ ms. Circles represent the results from the average of the two signals with E_B = +280 kV/cm and E_B = −280 kV/cm. The solid line is a KWW fit to the observed time dependence of the relative change with τ_{KWW} = 7 ms and β_{KWW} = 0.65. The steady state value of the relative change is -0.7%.

Now, we will turn our attention towards finding the Adam-Gibbs prediction of the corresponding change in structural relaxation timescale in case of salol for $E_B = \pm 280$ kV cm^{-1}. From the low field measurement it is determined that $\partial\varepsilon_S/\partial T = -0.044\ K^{-1}$. From the calorimetry and dielectric measurement S_{exc} and C_{AG} parameter values are found to be 34.61 J K^{-1} mol^{-1} at T = 234K and 113 kJ mol^{-1} respectively.[143]The Molar volume (υ) of salol is 171.38 cm^3 mol^{-1}. Based on these values, the expected change in τ_α, $\Delta_E \ln\tau_\alpha$, for the field $E_B = \pm 280$ kV cm^{-1} is calculated to be 2.43%. From the oscilloscope measurement, correcting for the corresponding saturation effect for that field, $\Delta\ln\varepsilon''$ is found to be -0.55%. Experimental change in $\Delta_E \ln\tau_\alpha$ can be obtained by dividing the slope at ν = 500 Hz, which is -0.46. So from experiment, the field induced increase in timescale, $\Delta_E \ln\tau_\alpha$ is determined to be 1.20%, which is about 50% of the predicted value obtained from Adam-Gibbs approach. Based on the fragility value of salol which is about 63, it is expected to have a value of $f_{S,T}$ around 0.6. So, from the above experiments, $f_{S,E}$ turns out to be around 0.3.

E. Propylene Glycol or Propane 1,2-diol (PG):

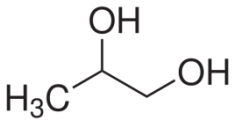

For propylene glycol, to obtain a reliable value of the dielectric constant and its temperature dependence, low field measurement is performed within the Invar cell. Fig. 5.22 (panel **a**) and Fig. 5.22 (panel **b**) represents the low field data set in the temperature range 186K-198K with 2K temperature interval in between. From the real part of the permittivity, $\partial\varepsilon_S/\partial T$ is determined, which is equal to -0.54 K^{-1}. Low field measurement of

the PG sample prepared within the high field dielectric cell with 10μm Teflon spacer is shown in Fig. 5.23 for T =190K. HN fit line and the associated parameters are also mentioned within the graph. Comparing this data with the Invar cell measurement and literature value[144], it is determined that the sample temperature is actually 190K and the sample thickness is around 10.3μm. A standard frequency sweep high field experiment with 6 average setup (3 high field, 3 low field) is performed with high voltage amplifier PZD-700 and voltage generator SI-1260 within the frequency range 1Hz – 10^5Hz for the bias field of E_B = 233kV cm^{-1}. Fig. 5.24 represents the relative change in dielectric loss (corrected for the saturation which is found to be -1.86%). The red fit line in Fig. 5.24 is obtained by increasing the τ value by 3% in comparison to the low field dielectric timescale. The olive circles in both Figure Fig. 5.23 and Fig. 5.24 represent the low field dielectric loss value and steady state relative change in dielectric loss value (after saturation correction) from the time resolved oscilloscope measurement at ν = 1.6 kHz for $E_B = \pm$ 198 kV cm^{-1} shown in Fig. 5.25. The timescale involved to develop the steady state change observed to follow the structural relaxation timescale (see solid black curve in Fig. 5.25). From the time resolved measurement, for $E_B = \pm$ 198 kV cm^{-1} the $\Delta_E \ln\tau$ value calculated to be -1.18% for PG sample at T = 190K.

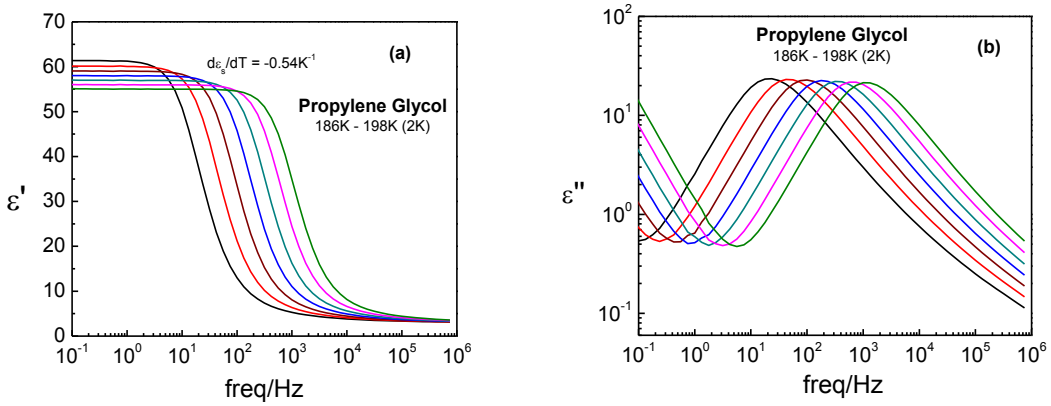

Fig. 5.22: The real (panel a) and imaginary (panel b) part of the permittivity values from linear response measurement for Propylene glycol in an Invar cell setup for the temperature range 186-198K are depicted with a temperature interval of 2K.

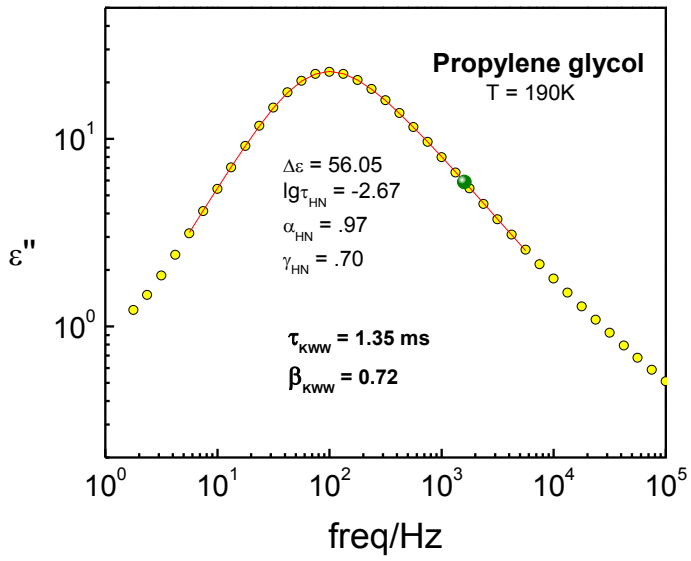

Fig. 5.23: Linear response dielectric loss (ε″) spectrum for Propylene glycol at T = 190 K is depicted. The solid lines are based on the HN-fit, with the values mentioned within the graph. The KWW parameters corresponding to the low field measurement are as follows: τ_{KWW} = 1.35 ms, β_{KWW} =0.72. The olive circle represents the low field ε″ value at T = 190K for ν = 1.6 kHz obtained from the oscilloscope measurement shown in Fig. 5.25.

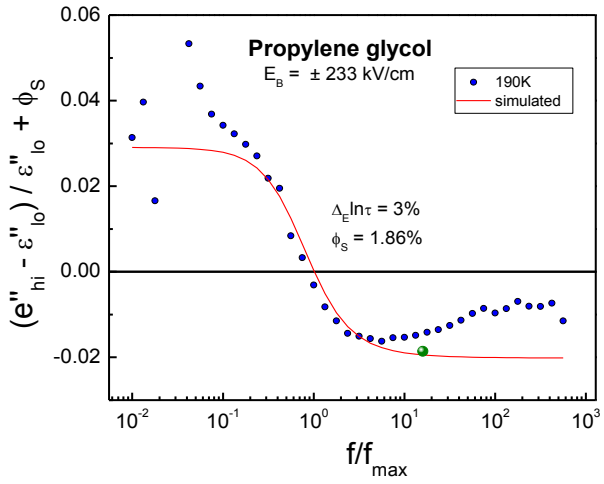

Fig. 5.24: Quasi steady state values of the field induced relative changes of the dielectric loss for Propylene glycol at T = 190 K. Symbols depict the non-linear effect, $(\varepsilon''_{hi} - \varepsilon''_{lo})/\varepsilon''_{lo}$, after correcting for the frequency invariant saturation effect, ϕ_{sat} = 1.86 %. The subscripts 'hi' and 'lo' refer to bias electric fields of E_B = 233 kV/cm and E_B = 0, respectively. The line is based on the HN fit of Fig. 5.23, with $\Delta\varepsilon$ reduced by ϕ_{sat} = 1.86 % and τ_{HN} increased by 3% for the ε''_{hi} case. Olive sphere represents the true steady state levels derived from time resolved measurement shown in Fig. 5.25.

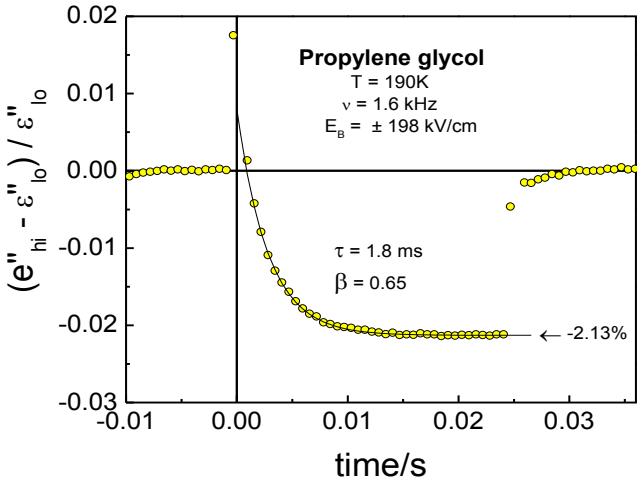

Fig. 5.25: Time resolved field induced relative change of the dielectric loss component, $(\varepsilon''_{hi} - \varepsilon''_{lo})/\varepsilon''_{lo}$, for PG in response to the bias field step of $E_B = \pm$ 198 kV/cm at ν = 1.6 kHz, with the bias being applied in the time range $0 \le t \le 25$ ms. Circles represent the results from the average of the two signals with E_B = +198 kV/cm and E_B = −198 kV/cm.

The solid line is a KWW fit to the observed time dependence of the relative change with τ_{KWW} = 1.8 ms and β_{KWW} = 0.65. The steady state value of the relative change is -2.13%.

To test for the Adam-Gibbs prediction, a reliable calorimetry data was not available. The only literature data found for the calculation of the Adam-Gibbs parameter and excess entropy is from Park et al.[145] Based on their data set, the S_{exc} at T = 190K is 17.24 J mol^{-1} K^{-1}, the slope of the $\ln\tau$ vs. $(1/TS_{exc})$ i.e., C_{AG} is found to be 35.47 kJ mol^{-1}. The obtained molar volume is 79.85 cm^3 mol^{-1} based on the measurement by Sun and Teja.[146] Depending on these numbers, $\Delta_E \ln\tau_\alpha$ at E_B = ±198 kV/cm for PG is calculated to be -10.83%. So from experiments, we are able to detect only ~ 11% of the total predicted effect. Although glycerol and propylene glycol are very similar in terms in terms of their chemical structure and properties which is also reflected in their fragility values (m = 53 for glycerol and m =52 for propylene glycol), the effect of an external field modifies their timescale very differently.

F. Cresolphthalein dimethylether (KDE or CPDE):

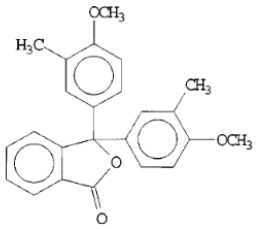

This material is obtained from H. Sillescu, Mainz, Germany where it has been synthesized and purified by distillation and recrystallization. Standard low field impedance experiments are performed for frequencies $\nu = \omega/2\pi$ from 30 mHz to 1 MHz using a system based upon a Solartron SI-1260 gain/phase analyzer and a Mestec DM-1360 transimpedance amplifier. An Invar steel/sapphire cell is used to measure the static

dielectric constant, ε_s, versus temperature. The low field loss spectra for the investigated temperature (T = 335K) along with the slope $\partial\varepsilon_s/\partial T$ is shown in the inset of Fig. 5.26.

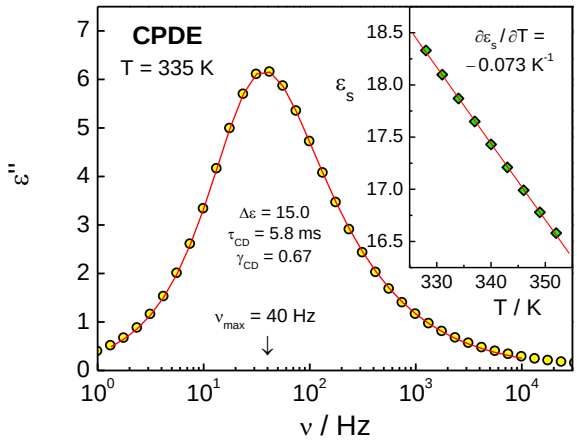

Fig. 5.26: Dielectric loss spectrum of CPDE at T = 335 K with peak frequency positioned at ν_{max} = 40 Hz. The solid line represents a Cole-Davidson fit with the parameters listed in the legend. The inset shows the temperature variation of the dielectric constant ε_s, with a slope of $\partial\varepsilon_s/\partial T = -0.073\ K^{-1}$ (solid line).

The low field spectrum matches the broadband dielectric relaxation data reported in literature.[132,147,148]These values of $\tau_{max} = 1/(2\pi\nu_{max})$ are derived from the peak frequencies, ν_{max}, of the dielectric loss spectra and for $T < 370$ K the temperature dependence of τ_{max} is well represented by the VFT relation in Eq. (1.1) with $\tau_\infty = -18.46$, $B = 1822$ K , and $T_0 = 225.6$ K. In view of the high field experiment performed at $T = 335$ K, the main result regarding the dielectric constant is that $\varepsilon_s = 17.8$ at $T = 335$ K and that the slope is $\partial\varepsilon_s/\partial T = -0.073\ K^{-1}$. The loss spectrum at $T = 335$ K is depicted in Fig. 5.26, which includes the Cole-Davidson (CD) fit, with $\Delta\varepsilon = 15.0$, $\tau_{CD} = 5.8$ ms, and $\gamma_{CD} = 0.67$.

In time domain representation, this behavior would be approximated by the KWW type stretched exponential, with τ_{KWW} = 3.6 ms and β_{KWW} = 0.72.

Using the low field result ε_s (335 K) = 17.8, the electrode separation of the high field cell is determined to be d = 16.6 μm, implying that the applied bias voltage V_B = 360V leads to field of E_B = 217 kV cm^{-1}. The effect of this high bias field on the permittivity is a reduction of the relaxation amplitude,$\Delta\varepsilon$, by ϕ_{sat} = 0.72 %, clearly observed by the field effect on the dielectric constant, $\varepsilon_s = \varepsilon'(\omega \to 0)$. The field effect on the dielectric loss is depicted in Fig. 5.27 in terms of the relative change of the loss after correcting for the saturation effect, i.e., using the quantity $(\varepsilon''_{hi} - \varepsilon''_{lo})/\varepsilon''_{lo} + \phi_{sat}$. In the inset of Fig. 5.27, which shows the spectrum of field induced shifts along the frequency axis calculated by $\Delta_E \ln(\nu) = -\dfrac{(\varepsilon''_{hi} - \varepsilon''_{lo})/\varepsilon''_{lo}}{\partial \ln \varepsilon''/\partial \ln \nu}$, indicative of an increase in relaxation time that amounts to $\Delta_E \ln \tau_{CD}$ = 0.75 %.

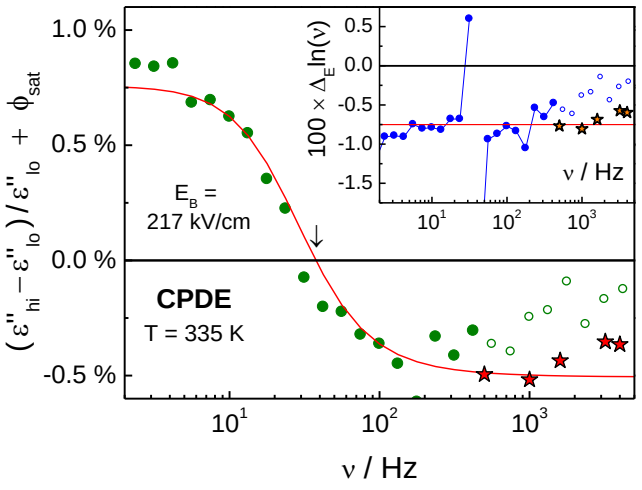

Fig. 5.27: Quasi steady state values of the field induced relative changes of the dielectric loss for CPDE at T = 335 K. Symbols depict the non-linear effect, $(\varepsilon''_{hi} - \varepsilon''_{lo})/\varepsilon''_{lo}$, after correcting for the frequency invariant saturation effect, ϕ_{sat} = 0.72 %. The subscripts 'hi' and 'lo' refer to bias electric fields of E_B = 217 kV/cm and E_B = 0, respectively. The line is based on the Cole-Davidson fit of Fig. 5.26, with $\Delta\varepsilon$ reduced by ϕ_{sat} = 0.72 % and τ_{CD} increased by 0.75 % for the ε''_{hi} case. Stars are for true steady state levels derived from time resolved measurements. The inset show the same results in terms of 'horizontal' difference, $(\ln \nu_{hi} - \ln \nu_{lo})/\ln \nu_{lo}$.

A representative example of a time resolved measurement of the change of $\varepsilon''(\omega)$ at a fixed frequency is outlined in Fig. 5.28. For this frequency of ν = 3.2 kHz, a steady state reduction of $\varepsilon''(\omega)$ by 1.07 % is observed, as indicated in Fig. 5.28. Analogous results for other frequencies are compiled as stars in Fig. 5.27.

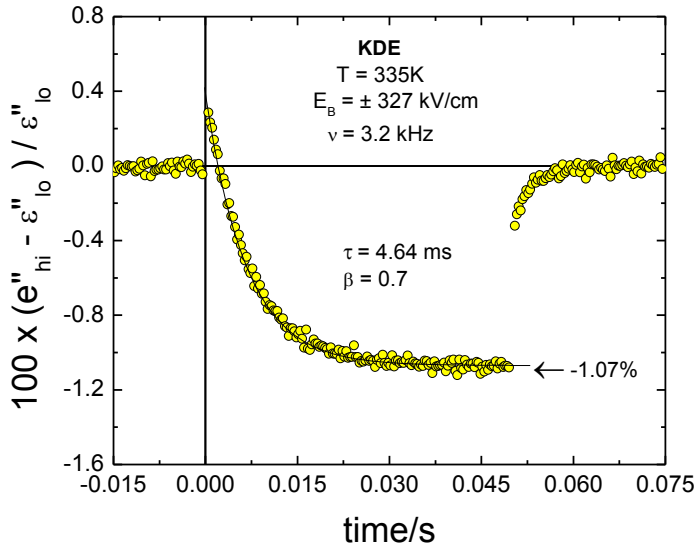

Fig. 5.28: Time resolved field induced relative change of the dielectric loss component, $(e''_{hi} - \varepsilon''_{lo})/\varepsilon''_{lo}$, for KDE in response to the bias field step of $E_B = \pm$ 327 kV/cm at ν = 3.2 kHz, with the bias being applied in the time range $0 \le t \le 50$ ms. Circles represent the results from the average of the two signals with E_B = +327 kV/cm and E_B = −327 kV/cm. The solid line is a KWW fit to the observed time dependence of the relative change with τ_{KWW} = 4.65 ms and β_{KWW} = 0.7. The steady state value of the relative change is -1.07%.

For Adam-Gibbs parameters, calorimetry data was provided by Osamu Yamamuro.[149] From this, excess entropy value is obtained with temperature (Fig. 5.29) and an Adam-Gibbs plot [log(τ_{max}) vs 1/(TS_{exc})] is created which is shown in Fig. 5.30. One interesting feature is to mention here that Vogel temperature (T_0) and Kauzmann temperature (T_K) do not coincide; instead these two are having a 30K difference, which hasn't been seen in any other glass formers investigated in this thesis.

The large $T_K - T_0$ difference mentioned above might be understood as an indication of the Adam-Gibbs model failing for this compound, but Fig. 5.30 reveals that this discrepancy develops only for $\tau_{max} > 1$ s, i.e., in the immediate vicinity of T_g. At higher temperatures, where 10^{-6} s < τ_{max} < 1 s, the dynamics follow a VFT law with $T_0 = T_K$ and log(τ_{max}) vs 1/(TS_{exc}) is practically linear, implying that the AG type Eq. (5.2) accurately predicts the dielectric relaxation time with C = 174 kJ mol^{-1} in this range. Therefore, we can quantify the impact of a change of S_{exc} on the relaxation time for time scales between 1 μs and 1 s.

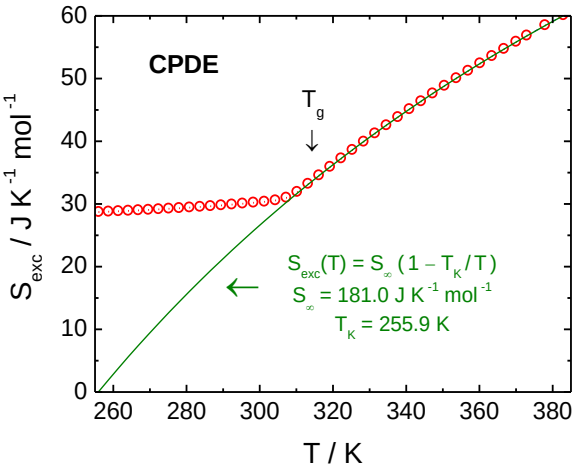

Fig. 5.29: Excess entropy, $S_{exc}(T)$, of CPDE as derived via Eq. (1.7) from the integration of the heat capacity difference, $C_{p,liquid} - C_{p,crystal}$. According to the solid line, the equilibrium excess entropy can be represented by Eq. (5.4) with S_∞ = 181.0 J K^{-1} mol^{-1} and T_K = 255.9 K. The vertical arrow marked T_g indicates the kinetic glass transition at 314.3 K, where τ_{max} = 100 s.

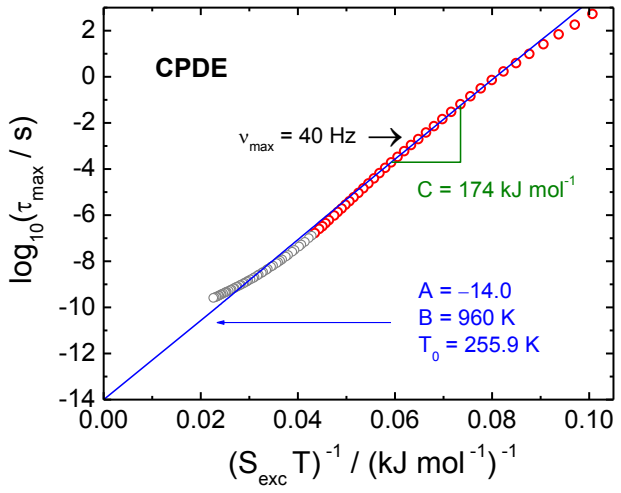

Fig. 5.30: Adam-Gibbs plot of the logarithmic peak dielectric relaxation time, $\log(\tau_{max}/s)$, versus $1/[TS_{exc}(T)]$ for CPDE. Near T = 335 K, where the loss peak frequency is ν_{max} = 40 Hz, $\tau_{max}(T)$ obeys a VFT law with A = –14.0, B = 960 K, and $T_0 = T_K$ = 255.9 K. In this regime, the dielectric relaxation times follow the Adam-Gibbs approach with A = –14.0 and $C = d\log_{10}\tau/d(1/TS_c) = S_\infty B$ = 174 kJ mol^{-1} in Eq. (5.2).

Using the parameters obtained from the experimental results, C = 174 kJ mol^{-1}, T = 335 K, $S_{exc}(T = 335\ K)$ = 42.75 J K^{-1} mol^{-1}, υ = 294 cm^3 mol^{-1}, $\partial\varepsilon_s/\partial T$ = –0.073 K^{-1}, and E_B = 217 kV cm^{-1}, the prediction derived from Eq. (5.3) is $\Delta_E\ln(\tau_{CD})$ = 2.93 %, which is a factor of 4 higher than the experimental observation. So the observed effect is approximately 25% of the overall prediction. Based on the fragility value of KDE, which is around 67, one would expect to have a f_C or $f_{S,T}$ value around 0.6. This implies that

based on the experimental facts, $f_{S,E}$ would be around 0.15, which is a very small number like in propylene glycol.

G. Propylene carbonate (PC):

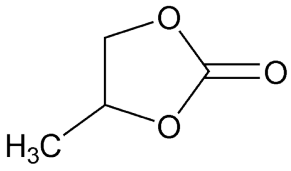

The low field measurement of the sample is performed in the Invar cell setup. The real part permittivity data for the temperature range 164K -174K with 2K step is shown in Fig. 5.31. The slope of the static dielectric permittivity with temperature is determined to be $-0.51K^{-1}$. A standard high field impedance measurement is performed for the sample prepared in the high field cell with 10um Teflon spacer in between at T = 168K for the field of value 360 kV/cm. Percentage relative changes in both real and imaginary part of the permittivity are shown in Fig. 5.32a and Fig. 5.32b. Solid lines are the fit obtained by changing the low field Δε value by -6% and increasing the relaxation time by 9%. Time resolved measurement is performed with an oscilloscope for a sample

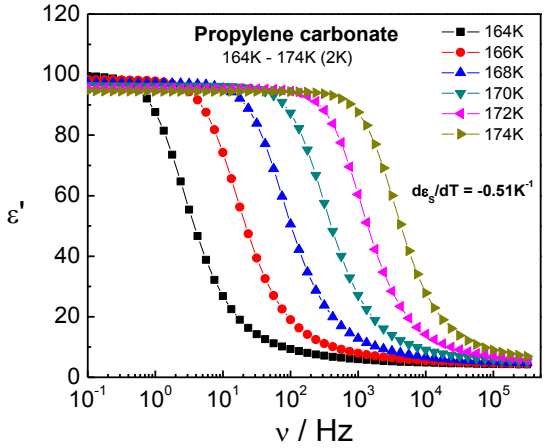

Fig. 5.31: The real part of the permittivity values from linear response measurement for Propylene carbonate in the Invar cell setup for the temperature range 164-174K are depicted with a temperature interval of 2K.

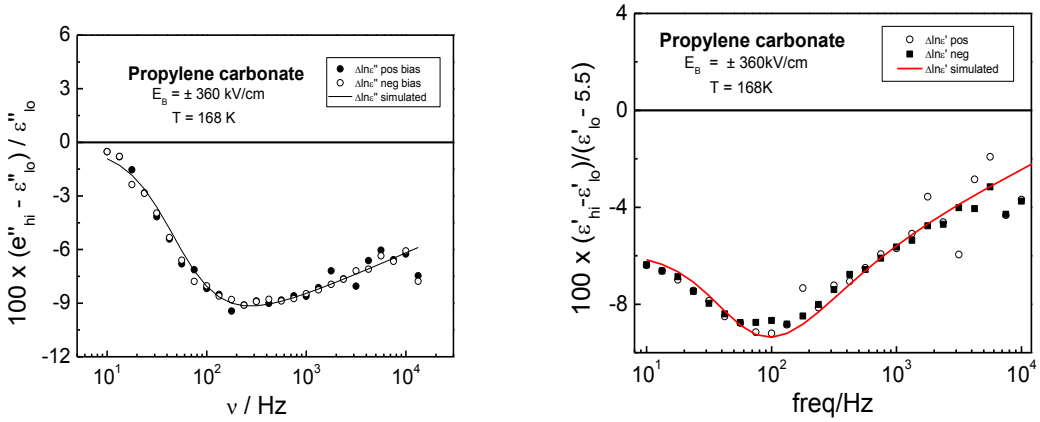

Fig. 5.32: Steady state values of the field induced relative changes of the dielectric loss (left) and storage (right) component for PC versus frequency. The subscripts "hi" and "lo" refer to bias electric fields of E_B = ± 360 kV/cm and E_B = 0, respectively. Experimental results (symbols) are derived from T = 168K as indicated, but using both +ve and -ve bias field of E_B = 360 kV/cm. Both the lines are obtained with Δε reduced by 6% and τ_{HN} increased by 9% for the e'_{hi} , e''_{hi} case. ε_∞ = 5.5 is used for the real part.

temperature T = 166.5K. Corresponding low field curve at that temperature is shown in Fig. 5.33 and the red fit line is obtained via HN fit and the parameters corresponding to the fit line is mentioned within the graph. The bold olive point in that graph is the low field ε″ value obtained during time resolved measurement. The timescale required to observe the steady state change due to the application of high field is within a factor of 2 of the original structural relaxation timescale of the sample as shown in Fig 5.34.

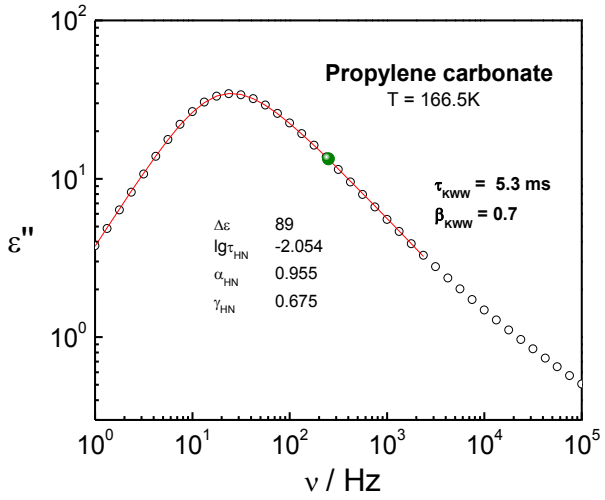

Fig. 5.33: Linear response dielectric loss (ε″) spectrum for Propylene carbonate at T = 166.5 K is depicted. The solid lines are based on the HN-fit, with the values mentioned within the graph. The KWW parameters corresponding to the low field measurement are as follows: τ_{KWW} = 5.3 ms, β_{KWW} =0.7. The olive circle represents the low field ε'' value at T = 166.5K for ν = 250 Hz obtained from the oscilloscope measurement shown in Fig. 5.34.

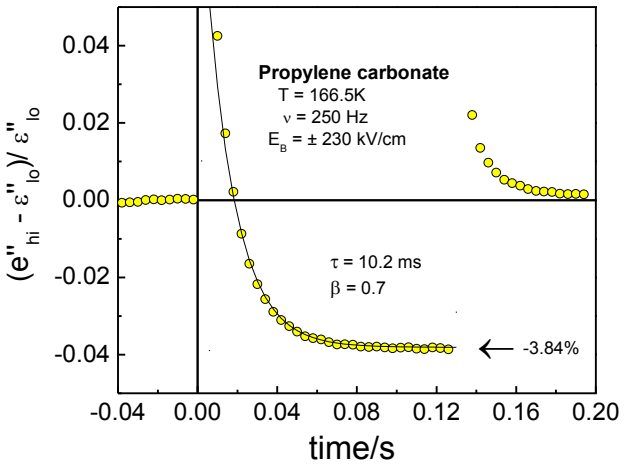

Fig. 5.34: Time resolved field induced relative change of the dielectric loss component, $(e''_{hi} - \varepsilon''_{lo})/\varepsilon''_{lo}$, for PC in response to the bias field step of $E_B = \pm$ 230 kV/cm at ν = 250 Hz, with the bias being applied in the time range $0 \leq t \leq 125$ ms. Circles represent the results from the average of the two signals with E_B = +230 kV/cm and E_B = −230 kV/cm. The solid line is a KWW fit to the observed time dependence of the relative change with τ_{KWW} = 10.2 ms and β_{KWW} = 0.7. The steady state value of the relative change is -3.84%.

Based on the amount of saturation observed, from the time resolved analysis the time scale change due to the application of field ($\Delta_E \ln\tau$) is calculated to be 2.31% at 166.5K at ν = 250 Hz.

Adam-Gibbs parameter and excess entropy data was available from Fujimori and Oguni *et al.*[120] At the investigated temperature S_{exc} was found to be 20.28 J $K^{-1}mol^{-1,}$ whereas from the Adam-Gibbs plot the slope C_{AG} is determined to be equal to 44.9 kJ mol^{-1}. Density at T =166.5K is calculated based on the relation of density with temperature found in Simeral *et al.*,[150] which turns out to be 1.35 g/cm^3. Based on these numbers, the amount of change predicted in timescale calculated to be 13.6%. So for propylene carbonate, the experimental change in timescale is approximately 17% of the expected effect.

H. Polyvinyl acetate (PVAc):

Polyvinyl acetate sample is prepared within the high field cell by first melting the sample and then cooling it down to the desired temperature. Low field spectra are obtained by standard impedance measurement procedure. Fig. 5.35 depicts the low field response curves for PVAc at T =323K. Comparing against the literature data,[79,151] the sample thickness is determined to be 11μm. Both standard and time resolved high field experiments are performed with the sample and shown in Fig. 5.36 and Fig. 5.37. The big red sphere in Fig. 5.36 represents the steady state value of the relative change in dielectric loss obtained from the time resolved measurement at ν = 500 Hz. Again the timescale with which steady state has been reached closely resemble the structural relaxation

timescale of the investigated temperature. The solid line in Fig. 5.36 is obtained by increasing the timescale by 2% and reducing the Δε value by 0.15% compared against its low field HN fit parameters as indicated within Fig 5. 35.

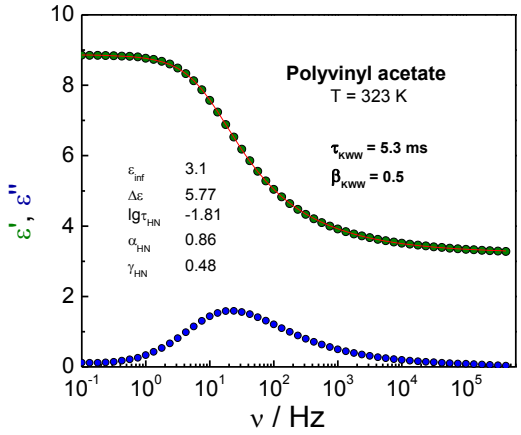

Fig. 5.35: Linear response dielectric storage (ε′) and loss (ε″) component of Polyvinyl acetate at T = 323 K are depicted. The solid lines are based on the HN-fit, with the values mentioned within the graph. The KWW parameters corresponding to the low field measurement are as follows: τ_{KWW} = 5.3 ms, β_{KWW} =0.5.

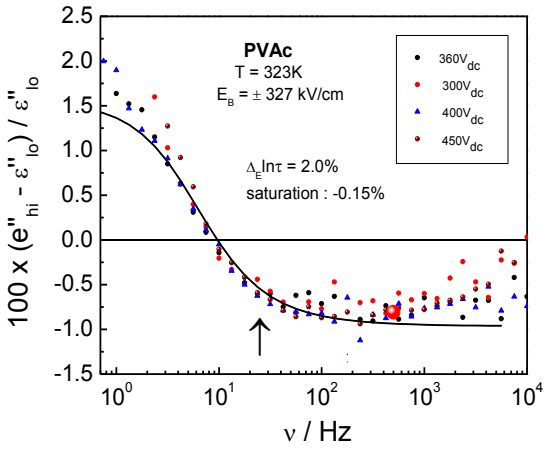

Fig. 5.36: Steady state values of the field induced relative changes (small symbols) of the dielectric loss component, $(\varepsilon''_{hi} - \varepsilon''_{lo})/\varepsilon''_{lo}$, vs. frequency for PVAc at T = 323K. The subscripts "hi" and "lo" refer to bias electric fields of E_B = ± 327 kV/cm and E_B = 0, respectively. The solid line is based on the HN fit, but with Δε reduced by 0.15% and τ_{HN}

increased by 2.0% for the e''_{hi} case. The large red sphere in the graph is based on the steady state value from the oscilloscope measurement shown in Fig. 5.37 and field corrected accordingly. The solid arrow indicates the peak position at this temperature.

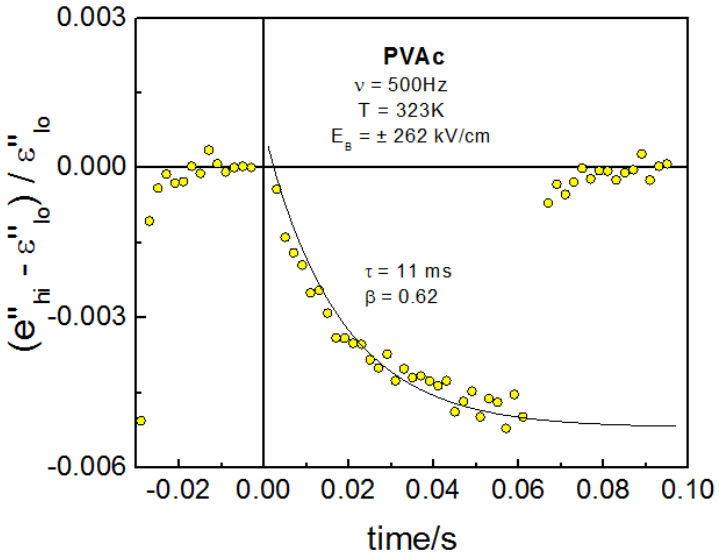

Fig. 5.37: Time resolved field induced relative change of the dielectric loss component, $(e''_{hi} - \varepsilon''_{lo})/\varepsilon''_{lo}$, for PVAc in response to the bias field step of $E_B = \pm$ 262 kV/cm at ν = 500 Hz, with the bias being applied in the time range $0 \leq t \leq 64$ ms. Circles represent the results from the average of the two signals with E_B = +262 kV/cm and E_B = −262 kV/cm. The solid line is a KWW fit to the observed time dependence of the relative change with τ_{KWW} =11 ms and β_{KWW} = 0.62. The steady state value of the relative change is -0.52%.

5.2 Rise and decay time asymmetry of the field induced NDE

I. Motivation

In the previous section, we looked into the high dc field effect on the structural relaxation timescale for various glass forming liquids varying in their fragility values. In order to understand on which timescale these changes are taking place, we employed time resolved measurements with ms time resolution. For all the materials studied in the previous section, one thing that is common is the observation of the asymmetry in terms of their rise and decay time. For example, one can clearly see from both figures (Fig. 5.4

and Fig 5.5), the steady state changes are established in a gradual fashion while bias field is on but complete reversal to the original permittivity level is achieved when the bias field is switched off (t > 8 ms), instantaneously. Based upon the symmetry relations established by Onsager,[152]one would expect the behavior indicated by the dashed KWW type rise in Fig. 5.4, but that expectation is justified only in the regime of linear responses. The asymmetry features observed in Fig. 5.4 and Fig. 5.5 are found for various frequencies, temperatures, and many other different liquids under study. Based on this observation one may think of the following picture of polarization vs. field graph (Fig. 5.38). According to this picture the deviation from the linear polarization response is only visible at high field regime, that is why when a bias field was applied, deviation from linear response value of either ε″ or ε′ is evident from Fig. 5.4 and Fig. 5.5. But when the bias field has been removed, one probe the system at low field region, where slope was unchanged and for that reason, ε″ or ε′ would remain the same in value as one will get from linear response measurement. For this case, the polarization response will have a non-zero $\chi^{(3)}$ contribution at high fields which will cause the deviation from the linear response shown by the blue line.

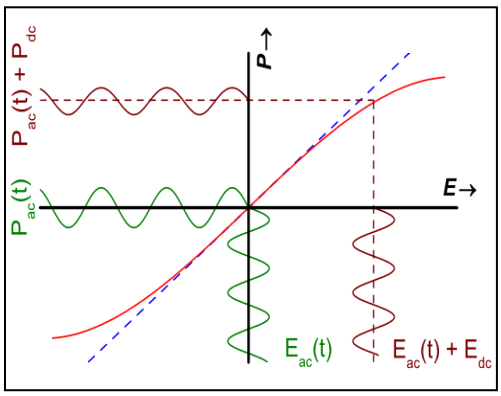

Fig. 5.38: Non-linear polarization behavior against field is represented by the red solid curve, which deviates symmetrically from the blue dashed linear line. Brown and green sinusoidal curves are for the field and polarization versus time with and without bias field, respectively. In the absence of a large dc-field, E_{dc}, the small amplitude sine, E_{ac} (t), will always probe only the original linear P(E) dependence.

One thing that has been ignored while looking at the data for previous time resolved measurements is that, energy absorption from the time dependent field (while switching the bias on or off). From the 'box model' we can correct for that energy that is being absorbed from the external field for a sample having a dispersive nature of the dynamics. In the next section we will consider the heating correction necessary to unravel the true nature of the time dependence of NDE's.

II. Model Considerations:

We consider a dielectric between planar electrodes with surface area *A* and uniform separation *d*, leading to a sample volume $V = Ad$. The initial condition is characterized by zero voltage across the capacitor, $V(t < 0) = 0$, resulting in the depolarized state of the dielectric, with polarization $P(t < 0) = 0$ and thus displacement $D(t < 0) = 0$. The dielectric has a frequency dependent permittivity, expressed here as superposition of Debye type contributions following the probability density $g(\tau_D)$ regarding its dielectric time constant,

$$\hat{\varepsilon}(\omega) = \varepsilon'(\omega) - i\varepsilon''(\omega) = \varepsilon_\infty + \Delta\varepsilon \int_0^\infty \frac{1}{1+i\omega\tau_D} g(\tau_D) d\tau_D \qquad \text{Eq. (5.10)}$$

The relaxation amplitude is defined as $\Delta\varepsilon = \varepsilon_S - \varepsilon_\infty$, with ε_s and ε_∞ being the low and high frequency limits of the permittivity, respectively. The function $g(\tau_D)$ can be determined from a Havriliak-Negami (HN) fit to permittivity. For times $0 < t < t_{off}$, the voltage is set to a value of V_B, leading to a field of magnitude $E_B = V_B/d$, whereas $E_B = 0$

at all other times. The time t_{off} is sufficiently long so that steady state is reached prior to the end of the high field time segment. The field transitions are considered to be fast compared with all retardation times of the dielectric, but slow enough to ensure reversibility of the processes involved. The temperature of the dielectric is uniform and held constant at T_0 by thermal contact to a large heat bath.

A. Effects of field switching

Due to the inevitable presence of dc-conductivity in polar liquids, experiments involving bias field require that the time duration of the field application be limited, so that switching on/off effects have to be considered. The work involved in generating steady state polarization following $t = 0$ is the sum of U_∞ and $\Delta U(t)$, respectively associated with the instantaneous (ε_∞) and slow ($\Delta\varepsilon$) contributions to permittivity. For the former contribution, displacement follows the field without lag, $D_\infty = \varepsilon_0\varepsilon_\infty E_B$ and

$$U_\infty = \upsilon \int_0^{D_\infty} E' dD' = \varepsilon_0\varepsilon_\infty \upsilon \int_0^{D_\infty} E' dE' = \frac{1}{2}\varepsilon_0\varepsilon_\infty \upsilon E_B^2 \qquad \text{Eq. (5.11)}$$

For the latter contribution that involves slower degrees of freedom, the displacement follows the field in a retarded fashion, $D(t) - D_\infty = \varepsilon_0[\varepsilon(t) - \varepsilon_\infty]E_B$, where ε(t) is given by

$$\varepsilon(t) = \varepsilon_\infty + \Delta\varepsilon \int_0^\infty (1 - e^{-\frac{t}{\tau_D}}) g(\tau_D) d\tau_D \qquad \text{Eq. (5.12)}$$

i.e., $-d(\varepsilon(t) - \varepsilon_\infty)/dt$ and $\hat{\varepsilon}(\omega) - \varepsilon_\infty$ are related by the Fourier-Laplace transform. The result for $\Delta U(t)$ is given by[125]

$$\Delta U(t) = \upsilon \int_{D_\infty}^{D(t)} E' dD'(t) = \varepsilon_0 \upsilon E_B^2 \int_{0^+}^t \frac{d\varepsilon(t')}{dt'} dt' = \upsilon E_B \int_{0^+}^t j(t') dt' \qquad \text{Eq. (5.13)}$$

In the steady state limit, we obtain $\Delta U(t \to \infty) = \Delta U\text{s} = V_\text{B}\Delta Q = \Delta C V_B^2$, where ΔQ is the total charge transferred to the capacitance $\Delta C = \varepsilon_0 \Delta\varepsilon A/d$. Since no work in excess of U_∞ is regained when the field is removed, the entire amount of ΔU_s is transferred irreversibly from the field to the sample. Following the previous success of applying these ideas to the effects of high ac fields,[50,62,76] we assume heterogeneous dynamics in the sense that the overall dispersive polarization response is the superposition of independent domains or modes. Each mode has its individual retardation time constant τ_D, and the volume fraction of modes with time constants in the range between τ_D and $\tau_\text{D} + d\tau_\text{D}$ is $g(\tau_\text{D})d\tau_\text{D}$, see Eq. (5.10) and Eq. (5.12). As a result of domain specific τ_D values, different modes absorb different amounts of energy from the field. For modes with $\tau_\text{D} \pm d\tau_\text{D}/2$, the rate of energy increase following each field step (i.e., at $t = 0$ and $t = t_\text{off}$) is given by the 'power' term $p(t)$, determined analogous to a previous approach,[153]

$$p(t) = \varepsilon_0 \upsilon E_B^2 \Delta\varepsilon \frac{1}{\tau_D} \exp\left(-\frac{2t}{\tau_D}\right) g(\tau_D) d\tau_D \qquad \text{Eq. (5.14)}$$

The total energy absorbed is obtained by integration over all τ_D and over time, which amounts to $\varepsilon_0 \upsilon E_B^2 \Delta\varepsilon$, half of which is transferred at each of the two field transitions (at $t = 0$ and $t = t_\text{off}$). Domains are also considered independent regarding their effective temperature, T_eff, that is determined on the basis of the energy absorbed by that mode, $p(t)dt$, and its heat capacity, $\Delta C_\text{cfg} g(\tau_\text{D})d\tau_\text{D}$, where ΔC_cfg is the configurational contribution to the glass-to-liquid heat capacity step of the sample at constant pressure. Since calorimetry will yield excess heat capacities, a correction according to $\Delta C_\text{cfg} = f_\text{C}\Delta C_\text{exc}$ is applied,[133] provided that f_C is known and temperature invariant. For each

domain, the equation governing the balance of effective temperature has a gain term involving $p(t)$, and a loss term originating from the relaxation of the excess effective temperature to the real temperature at a rate given by the inverse enthalpy relaxation time (τ_T) of that domain,

$$\frac{dT_{eff}(t)}{dt} = \frac{p(t)}{\Delta C_{cfg} g(\tau_D) d\tau_D} - \frac{T_{eff}(t) - T_0}{\tau_T} \qquad \text{Eq. (5.15)}$$

For isothermal conditions (constant T_0), the solution to Eq. (5.15) with $p(t)$ from Eq. (5.14) is

$$\Delta_E T_{eff}(t) = T_{eff}(t) - T_0 = \frac{\varepsilon_o \upsilon \Delta\varepsilon E_B^2}{\Delta C_{cfg}} \left(\frac{\tau_T}{\tau_D - 2\tau_T}\right) \left[e^{-\frac{2t}{\tau_D}} - e^{-\frac{t}{\tau_T}}\right] \qquad \text{Eq. (5.16)}$$

The time constants associated with dielectric and enthalpy dynamics would be considered identical for many simple molecular liquids, i.e., $\tau_T = \tau_D$.[154] The impact of this field induced change in effective temperature, $\Delta_E T_{eff}$, is mainly that of altering the relaxation time constant, τ_D, while the effect on the relaxation amplitude is relatively small. Therefore, small changes of T_{eff} modify the permittivity via

$$\Delta_E ln\tau_D = \frac{dln\tau}{dT} \Delta_E T_{eff}(t) \qquad \text{Eq. (5.17)}$$

where the slope, $d\ln\tau/dT$, is taken from the overall activation behavior of the dielectric retardation times. The assumption that the energy absorbed by a mode has the same effect as an equivalent temperature increase but remains localized in that domain for the time τ_T is clearly non-trivial. However, this phenomenological model (a 'box' model analogue for field steps) has been demonstrated to yield quantitative agreement with the effect of energy absorbed from time-dependent fields of high amplitudes.[52,57] For the case of

dispersive (non-Debye) dynamics, a final integration over all τ_D according to Eq. (5.12) is required.

B. Effects of a bias field

The consequences of a steady state polarization on the dynamics are determined following the idea of Johari,[123] proposing that slower dynamics result from the field induced reduction in entropy if the Adam-Gibbs[29]relation is employed for connecting configurational entropy with relaxation time or viscosity. For including a time dependence, it has to be realized that $\Delta_E S$ depends quadratically on field, while polarization *P* is approximately linear in the field, even at relatively high electric fields. A consequence of $\Delta_E S \propto P^2$ is that the time dependence of $\Delta_E S$ should reflect that of the dielectric retardation squared. This yields for each domain,

$$\Delta_E S(t) = \frac{E_B^2 M \varepsilon_0}{2\rho} \frac{\partial \varepsilon_s}{\partial T} R^2(t), \qquad \text{Eq. (5.18a)}$$

$$R^2(t) = \begin{cases} (1 - e^{-t/\tau_D})^2, \ 0 \le t \le t_{off} \\ (e^{-(t-t_{off})/\tau_D})^2, \ t \ge t_{off} \end{cases} \qquad \text{Eq. (5.18b)}$$

where *M* is the molar mass and ρ is the density. The top and bottom exponential terms in Eq. (5.18b) are associated with applying (t = 0) and removing ($t = t_{off}$) the field, E_B, respectively. Fig. 5.39 demonstrates an important feature of the quadratic dependence on polarization:

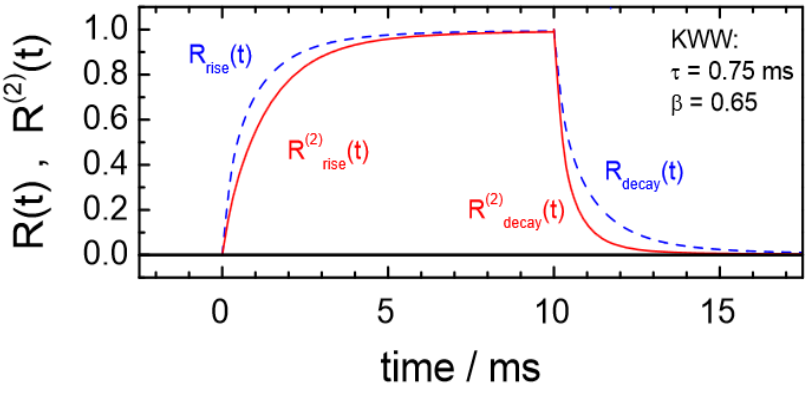

Fig. 5.39: Comparison of symmetric rise and decay behavior, R_{rise} (t)=1−φ(t) and R_{decay} (t) = φ(t−t_{off}) with φ(t) = exp[− (t/τ_D)$^{\beta}$], and their squared coun-terparts,R^2(t) , obtained by applying the power of two separately to each Debye contribution: for the stretched exponential or Kohlrausch-Williams-Watts (KWW) case with τ = 0.75ms and β= 0.65.

If $R(t)$ as defined in Eq. (5.18b) represents the normalized time dependent contribution to polarization, then $R_{rise}(t)$ =1 - exp(-t/τ_D) and $R_{decay}(t)$ = exp(-(t-t_{off})/τ_D) display symmetric rise and decay behavior, as shown as dashed lines in Fig. 5.39. By contrast, the rise of $R^{(2)}(t)$ is always slower that its decay counterpart, see solid lines in Fig. 5.39.

For the case of dispersive (non-Debye) dynamics, the resulting changes of τ_D with time can be entered into Eq. (5.12) to assess the effect of the time dependent field on the overall ε′(ω) and ε″(ω). Note that both field induced time constant modifications, $\Delta_E \ln\tau_D$ from Eq. (5.3) and from Eq. (5.17), will impact permittivity and that they generally have opposite signs.

III. Results and Discussion

A. Glycerol

The effect of the field induced entropy change on dynamics which is captured by the original data (yellow dots) appear inconsistent with the expectation of a more symmetric and gradual time dependence of the field effect, since the observed NDE rises slowly and decays back almost instantaneously when the field is removed. The remedy to this situation is the recognition that switching the field on or off transfer energy from the field to the sample, as detailed in the previous section. Analogous to heating, this effect counteracts that of the entropy reduction by leading to temporarily smaller time constants, resulting in the positive transients in terms of $(e''_{hi} - \varepsilon''_{lo})/\varepsilon''_{lo}$ at a frequency $\nu > \nu_{max}$, which are determined using Eq. (5.16) and shown in Fig. 5.40 as open squares (blue). The parameters are: $\Delta\varepsilon = 56.7$, $\tau_{HN} = 0.61$ ms, $\alpha_{HN} = 0.95$, $\gamma_{HN} = 0.63$, $\tau_T = \tau_D$, $E_B = 200$ kV/cm, $\partial ln\tau/\partial T$ = -0.298 K^{-1}, $\Delta C_{exc} = 1.245$ J K^{-1} cm^{-3},[24] and $f_C = 0.8$, which is consistent with the results for glycerol based upon high ac field measurements.[76] Subtracting these from the observed values (circles) leads to the 'heating' corrected (red) diamonds in Fig. 5.40, which now represent the impact of the presence of a high bias field but without the transient effects of switching the bias on or off. The steady state amplitude of the remaining NDE is unchanged and amounts to -1.38% regarding $(e''_{hi} - \varepsilon''_{lo})/\varepsilon''_{lo}$.

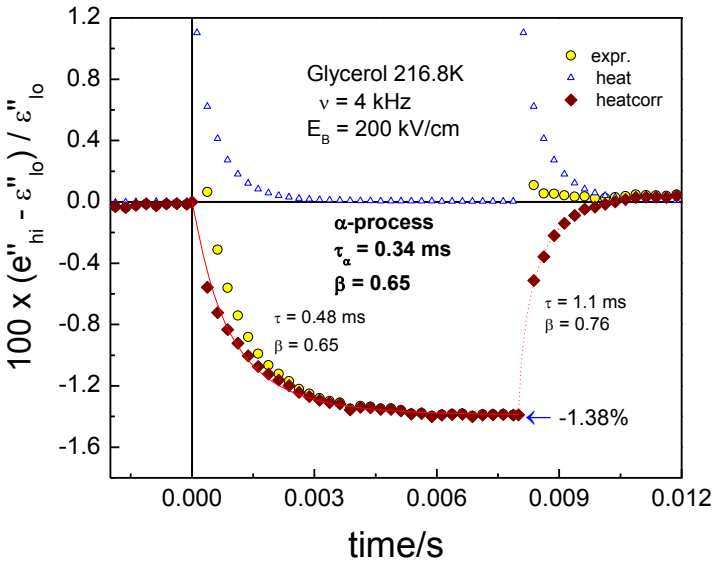

Fig. 5.40: Field induced relative change of the "dielectric loss" component, e″(t), probed at ν = 4 kHz for glycerol at a temperature of T = 216.8 K. The bias field E_B is applied in the time range $0 \leq t \leq 8$ms. Circles (yellow) are the results from the average of the two signals with $E_B = +200$ kV/cm and $E_B = -200$ kV/cm, where the direct response to the bias step is cancelled. The diamonds (red) represent the experimental data after subtracting the heating effect shown as squares (blue). The solid and dashed curves are respective fits to the rise and decay of the NDE with the parameters indicated.

Supported by the analysis discussed above, the time-resolved NDE results obtained after correcting for the switching effects are now understood to reflect the consequences of the field induced entropy reduction, $\Delta_E S$. The diamonds in Fig. 5.40 reveal transitions between the zero field and high field levels that are now gradual in time, but still not symmetric, i.e., the rise of the NDE following $t = 0$ is still slower that the decay initiated at t = 8ms. This complex time dependence is well approximated by the quadratic exponentials in Eq. (5.18b) that originate from the quadratic dependence of the NDE on field and thus on polarization. Both rise and decay of the NDE are respectively approximated by the solid and dashed line, which are based on Eq. (5.18b). It is evident

that the rise curve is obtained using the same $g(\tau_D)$ that represents the dielectric retardation in the linear response regime (β_{KWW} = 0.65 in terms of a stretched exponential representation), but with time constants that are a factor of 1.4 larger (τ_{KWW} = 0.48ms) than the linear response value of τ_α = 0.34ms. It needs to be mentioned here that the quadratic polarization is still not able to capture the decay pattern with the same value and distribution of the timescale as of rise curve. To this end we employ a more complex field pattern which is outlined in Fig. 5.41a. Here, the field transitions between three levels, zero, $E_B/\sqrt{2}$, and E_B, and the resulting levels of the NDE are -0.61% and about twice that value, -1.32%, as expected from the quadratic field dependence, see Fig. 5.41b. As the transitions from -0.61% to -1.32% and back result from field changes of only 59 kV/cm (compared with 141 kV/cm when starting from zero), the heating effect associated with those transitions are only 17% of those involving the 0 to -0.61% levels (see blue triangles), while leading to the same NDE magnitude. For these curve segments, 'heating' is practically negligible and the uncorrected data (yellow dots) display transitions that are gradual in time. Also, the rise and decay curves associated with the -0.61% and -1.32% levels in Fig. 5.41b are more symmetric that those between the levels 0 and -0.61%.

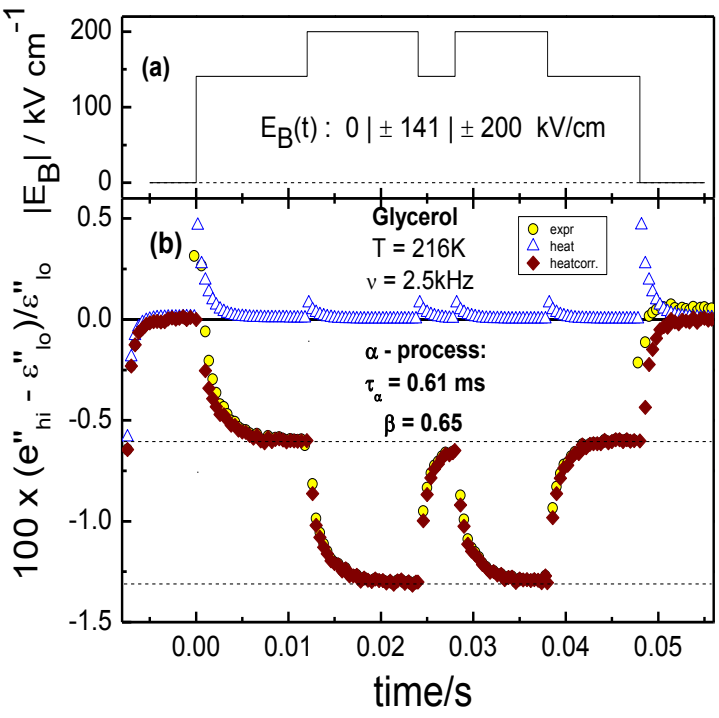

Fig. 5.41: (a) The bias field pattern, $E_B(t)$, used to measure the data in this plot. (b) Field induced relative change of the "dielectric loss" component, e″(t), probed at ν = 2.5 kHz for glycerol at a temperature of T=216K. Circles (yellow) represent the results from the average of the two signals with positive and negative $E_B(t)$ pattern, where the direct response to the bias step is cancelled. The diamonds (red) represent the experimental data after subtracting the heating effect shown as squares (blue).

The solid and dashed lines in Fig. 5.42 (showing only the heat corrected data points only), demonstrate that all these features are captured by $\Delta_E S \propto P^2$ feature demonstrated in Eq. (5.18b). Again using the linear response $g(\tau_D)$ but with time constants which are very much similar to low field timescale, all six curves can be well fitted with quadratic polarization dependence.

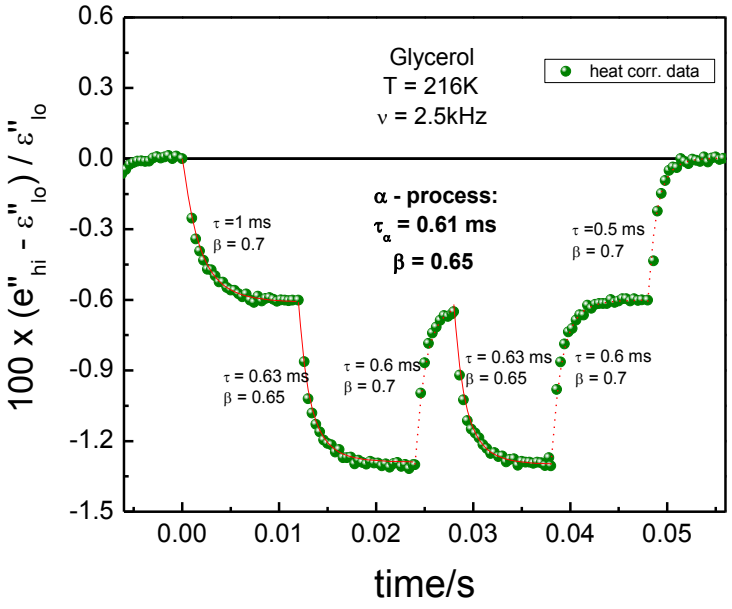

Fig. 5.42: 'Heat corrected' data points (symbols) of the field induced relative change of the "dielectric loss" for glycerol at T = 216K probed at ν = 2.5 kHz. Solid and dashed curves are respective fits to the rise and decay of the NDE according to the Eq. (5.18b) with their respective KWW parameters indicated. For the four transitions between -0.61% and -1.32%, the KWW parameters describing the square fits closely resemble the linear response τ and β values.

B. NMEC:

A Similar approach has been taken for NMEC. Fig. 5.43 depicts the unmodified data (yellow circles), heating curves (blue triangles) and heat corrected curves (diamonds) for measurement performed at frequency ν = 4 kHz for a sample at T = 187.5K upon application of a bias field of 184 kV cm^{-1}. As mentioned in the legend section, f_C or f_S value of 0.72 is used for the heating correction. At this temperature structural relaxation timescale τ_α and the stretching exponential have the value 0.5 ms and 0.65 respectively. Similar to glycerol case, in this sample the rise time closely follows the structural

timescale along with the distribution function for the quadratic polarization fit curve, but the decay curve show a significant deviation from the linear response values. Following the same protocol as in glycerol, we employ similar complex field pattern steps and the result is depicted in Fig. 5.44. In case of N-methyl-ε-caprolactam, the agreement with the $\Delta_E S \propto P^2$ notion is better than glycerol as evident from the τ and β values for all the six curves.

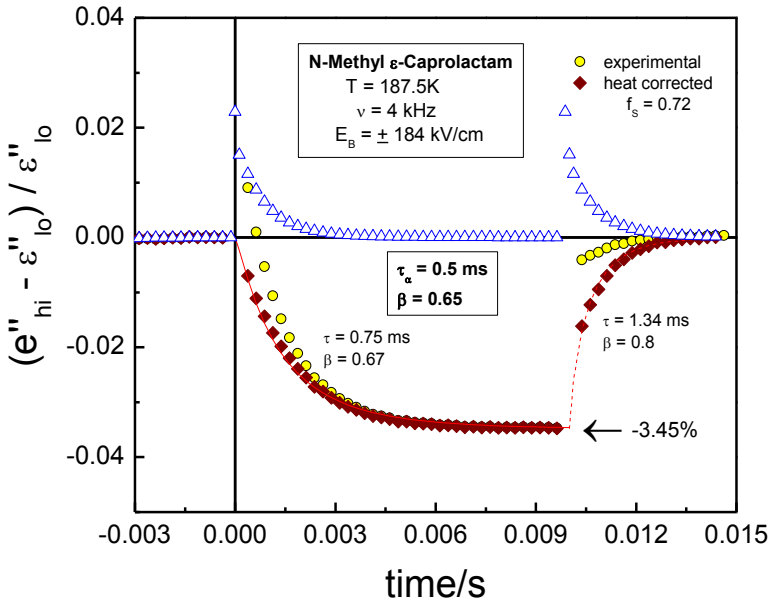

Fig. 5.43: Field induced relative change of the "dielectric loss" component, e″(t), probed at ν = 4 kHz for NMEC at a temperature of T = 187.5 K. The bias field E_B is applied in the time range $0 \leq t \leq 10$ms. Circles (yellow) are the results from the average of the two signals with E_B = +184 kV/cm and E_B = −184 kV/cm, where the direct response to the bias step is cancelled. The diamonds (red) represent the experimental data after subtracting the heating effect shown as upward triangles (blue). The solid and dashed curves are respective fits to the rise and decay of the NDE with the parameters indicated.

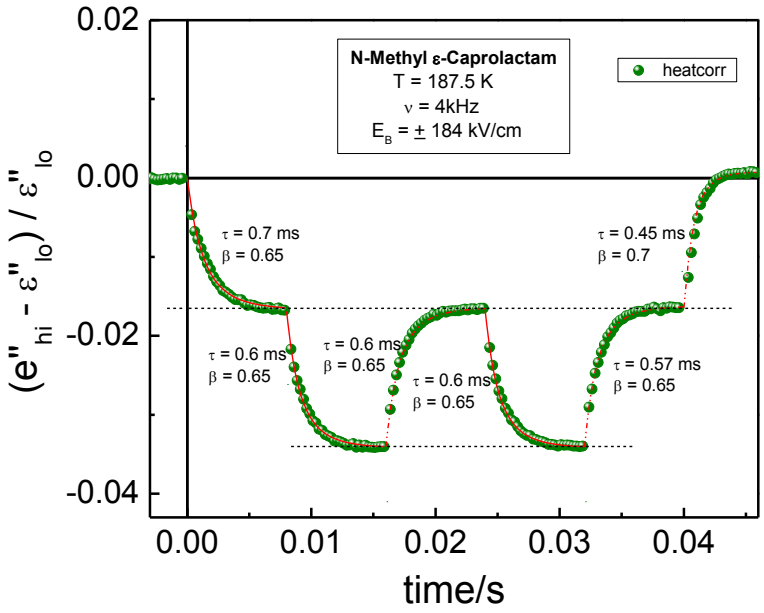

Fig. 5.44: Heat corrected data points (symbols) of the field induced relative change of the "dielectric loss" for NMEC at T = 187.5K probed at ν = 4 kHz. Solid and dashed curves are respective fits to the rise and decay of the NDE according to the Eq. (5.18b) with their respective KWW parameters indicated. For all the six transitions, the KWW parameters describing the square fits closely resemble the linear response τ and β values.

The original time-resolved entropy effect measurement (circles in Fig. 5.5 prior to accounting for the 'heating' effects) for glycerol suggested that the NDE disappears abruptly when the high dc bias field is removed. Such an abrupt return to the linear response behavior would be compatible with the scenario sketched in Fig. 5.38, where the $P(E)$ curve near zero field never changes. By contrast, after unveiling the true gradual nature of the transition of the entropy effect with time (diamonds in Fig. 5.40 and Fig. 5.43, after accounting for the 'heating' effects) clearly invalidates Fig. 5.38 for the present NDE. Instead, it has to be assumed that the high field modifies the $P(E)$ curve also at $E \approx 0$, as depicted in Fig. 5.45. In other words, the main effect of the high dc field at the

fundamental frequency of the small ac field is to modify the (linear) susceptibility χ in Eq. (1.7).

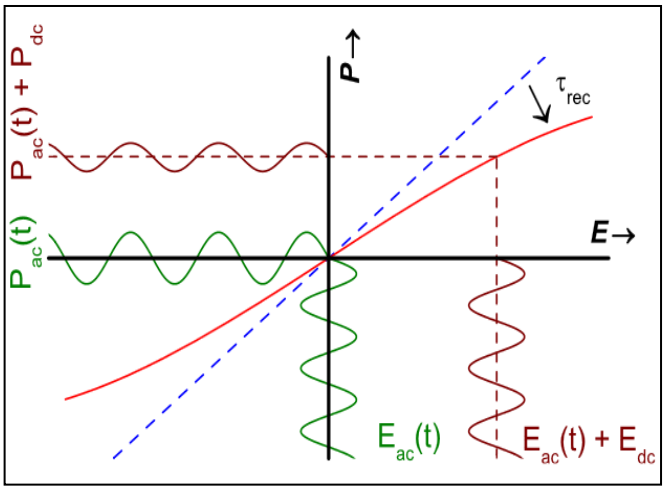

Fig. 5.45: Non-linear polarization behavior against field is represented by the red solid curve, which deviates symmetrically from the blue dashed linear line. Brown and green sinusoidal curves are for the field and polarization versus time with and without bias field, respectively. On a structural recovery time scale (τ_{rec}), the large dc-field leads to a deviation from linearity and to a change in the slope (dP/dE), even near E=0.

Since χ is altered as a result of shifting time constants via configurational entropy, the time scale involved in this process is the equivalent of a structural recovery time (τ_{rec}).[155] It should be noted that the considerable polarization not only reduces entropy but in parallel will also lead to dielectric saturation and to susceptibilities of even order, e.g., $\chi^{(2)}$.[75] All these consequences of significant polarization anisotropy are expected to follow the same time dependence observed for the present NDE.

Here I summarize the results for all the materials investigated in the thesis. For the materials, where a reliable number of the configurational heat capacity (f_C or $f_{S,T}$) is not available, we deduce this number from appropriate heat correction of the time dependent relative change of the dielectric loss curves. Most of the numbers of $f_{S,T}$ is in agreement

with the previously published data.[76] $f_{S,E}$ values are calculated based on the Eq. (5.6).

Table 5.1: List of the materials investigated (with their respective temperatures in Kelvin) in this thesis along with their fragility values (m). Bias fields (E_{dc}) are mentioned in kV/cm. Both $\Delta_E \ln\tau$ values (from experiment and AG-prediction) are listed. $f_{S,T}$, $f_{S,E}$ indicate the configuration fractions of the total entropy in case of temperature and field induced change respectively. Percentage of the observed effect is the ratio of the experimental and predicted $\Delta_E \ln\tau$ values.

Materials	Field E_{dc}	Fragility (m)	% $\Delta_E \ln\tau$ (exper.)	% $\Delta_E \ln\tau$ (predicted)	$f_{S,T}$	$f_{S,E}$	% of observed effect
Glycerol (216.8K)	200	53	1.72	2.7	0.8	0.50	63
PG (190K)	198	52	1.18	10.83	0.9	0.10	11
Salol (234K)	280	63	1.20	2.43	0.62	0.31	50
2-MTHF (97.5K)	155	65	1.2	1.9	0.6	0.38	63
KDE (335K)	217	67	0.75	2.93	0.6	0.15	25
NMEC (187.5K)	128	85	2.8	?	0.72	?	?
PVAc (323K)	327	95	2	?	?	?	?
PC (166K)	230	104	2.31	13.6	0.4	0.07	17

As evident from Table I, there is no correlation of $f_{S,E}$ values against fragility parameters. We also calculated ($\Delta_E \ln\tau / \Delta_E S$) value and found no correlation with apparent activation energy parameter, $d\ln\tau/d(1/T)$.

C. Relation to electro-optical Kerr effect

The electro-optical Kerr effect (EKE) describes the birefringence, Δn, induced by a static electric field by virtue of the anisotropy created in the case of dipolar liquids. The effect is quadratic in the electric field, $\Delta n = B \lambda E^2$, where B is the Kerr constant, λ the optical

wavelength, and E the electric field.[156] Time-resolved experiments have been documented with the rise and decay behavior of the birefringence for viscous liquids, including glycerol.[156] Due to the fact that birefringence and the present NDE are both signatures of field induced anisotropy, the two experiments are very similar, but with the EKE typically measured at much smaller fields compared with the NDE of this work. A survey of studies that compare dielectric retardation (τ_D) with EKE rise (τ_{rise}) and decay (τ_{decay}) times reveals that τ_{rise} is usually larger than τ_{decay}, and that the EKE time constants are near the dielectric times τ_D, with a matching temperature dependence.[156-158] For the case of glycerol, linear fits to $\Delta n(t)$ resulted in $\tau_{rise} \approx 1.5\tau_{decay}$ and $\tau_D \approx 0.5\tau_{decay}$,[156] while the same analysis applied to the data (diamonds) in Fig. 5.40 would give $\tau_{rise} \approx 2\ \tau_{decay}$ and $\tau_D \approx 0.7\tau_{decay}$. No attempt has been made to explain the asymmetry of experimental EKE rise and decay transients in terms of the quadratic field dependence as implied in Eq. (5.18b). It would be interesting to explore to what extent the quadratic field dependence is capable of rationalizing this difference in rise and decay time constants observed in EKE measurements.

IV. Summary and conclusion

The dynamics of several glass-forming materials subject to a high bias field, mostly in their supercooled liquid states and for cyclo-octanol in its plastic crystal state have been measured. All these measurements display a field induced increase of the dielectric relaxation time, for example, in case of glycerol equivalent to glass transition shifts of +74 mK at 225 kV/cm for glycerol and +0.58 K at 150 kV/cm for cyclo-octanol respectively. Time-evolution of the non-linear dielectric effects (NDE's) have also been

measured along with their steady state values. These field induced changes are monitored by evaluating the dielectric 'loss' versus time, $e''(t)$, with a resolution of one period of the small signal test frequency. The impact of the polarization responses to the large field steps that occurs when switching the bias field on and off is eliminated by averaging over two measurements, one with positive and one with negative bias of identical amplitudes. Almost in all of these liquids that have been studied here, it is observed that a dc field leads to dielectric saturation leading to anisotropy within the sample. The rise time for the field induced effect is found to be higher than the collapse time which is almost instantaneous when the bias field is removed. This observation is very much consistent for all the liquids studied. Transient effects analogous to local 'heating' are accounted for subsequent to applying and removing the dc field using the concept of 'box' model. This might be a likely source of e'' being slightly above the baseline for a few periods following a change in the bias field, see Fig. 5.5. The observation that the quantities e' and e'' approach steady state levels near the end of the high bias field interval excludes effects of continuous heating due to excessive dc-conductivity. After correcting for the resulting temporary reductions of time constants due to heating, the true time dependent feature of polarization anisotropy in the non-linear regime has been observed due to the increase in the retardation time constants. This observation is analogous to what had been observed repeatedly for the rise/decay behavior of the electro-optical Kerr effect in similar systems. Since the magnitude of this NDE is quadratic in field, its time dependence should follow that of the polarization squared, i.e., $(1 - e^{-(t/\tau)^{\wedge}\beta})^2$ and $(e^{-(t/\tau)^{\wedge}\beta})^2$ for the rise and decay transients respectively. It is demonstrated that this quadratic field

dependence explains these asymmetric rise/decay patterns. Similar effects have been recorded for the three mono-hydroxy alcohols, where the rise and decay of the NDE is linked to the time scale of the prominent Debye type dielectric process.[159] Based on the evidence compiled in this chapter, it is safe to conclude that the reduction in configurational entropy is a dominant factor in the non-linear dielectric behavior of polar liquids subject to high dc fields. Both the time dependence and the steady state level of the NDE can be rationalized on the basis of the change in entropy. The gradual decay of the NDE after removing the bias field is observed via a low field sinusoidal excitation, which implies that the modifications are described by a field and time dependence of the (linear) 'susceptibility', $\chi(E,t)$, rather than requiring higher order terms such as $\chi^{(3)}$ (see Fig. 5.45).

We had set out to study the electro-viscous behavior of molecular liquids based on the field induced change of entropy, which in turn is translated into a change of the relaxation time via the Adam-Gibbs relation, an idea put forward by Johari.[123] But for all the liquids under investigation, the present results appear to validate the idea that entropy do not control dynamics in a way quantitatively consistent with the Adam-Gibbs model. Also the present results suggest that this Adam-Gibbs relation has failed to account for an electric field variation of S_{cfg} at isothermal condition although $1/S_{cfg}(T)$ is established to be a reliable parameter for governing the temperature dependence of the activation barrier.[6,36,160] For glycerol, the observed steady state change of the structural relaxation time ($\Delta_E \ln\tau_\alpha = 1.7\%$) is found to be only 60% effective in its impact on the dynamics via

the Adam-Gibbs relation, which predicts $\Delta_E \ln\tau_\alpha = 2.7\%$. For other materials, this impact is found to be much less (see for example KDE, PC or PG in Table 5.1).

However this entropy effect is likely at the origin of low frequency features that have been detected in non-linear dielectric measurements using high amplitude ac fields (without bias). The effect shows as an increase of the loss at frequencies below that of the dielectric loss peak, and is bound to disappear near and above the loss peak frequency. Indication of such features can be found for 2E1B,[57] for 5M3H,[59] and more clearly for plastic crystals.[81,161]

As described before, one must realize that although an electric field may change entropy and thus relaxation time scales, it is not as effective as generating the same amount of entropy change via temperature or pressure. This may be due to the following reason: in the presence of an electric field, a dipolar liquid becomes anisotropic as evident from the current response at 2ω, while changing entropy by temperature or hydrostatic pressure alone preserves the isotropic nature of the liquid. Two other nonlinear effects which turn out to be also present during the application of the high bias field are dielectric saturation and local heating. Firstly, dielectric saturation is a general phenomenon, because the average dipole orientation has an upper bound of $\langle\cos\theta\rangle = 1$ and only for small fields the linear approximation, $\langle\cos\theta\rangle = \mu E/(3k_B T)$, holds for non-interacting dipoles. Secondly, if the sample is associated with dielectric loss, a certain amount of power p will be transferred irreversibly from any time dependent field to the sample, with Joule's law quantifying the extent of the effect for a harmonic field via $p = \varepsilon_0 E^2 \varepsilon''(\omega)\omega / 2$. Albeit

with different results, both effects, saturation and heating, will in principle occur for ac-fields and for rectangular dc-like field steps as used in this study.

Finally, we compare the high dc bias field experiments with non-linear dielectric relaxation techniques using ac-fields of high amplitudes. For observing deviations from the linear $P \propto E$ behavior, small amplitude oscillations about a high bias level is more effective, because the entire field variation occurs in the non-linear response regime. By contrast, much of the response to an oscillating large amplitude field at zero bias pertains to the linear regime, often with only the extreme values of the entire field signal reaching into the non-linear regime. In apparent contradiction to this notion, high ac-field dielectric measurement without bias have detected changes in the dielectric loss exceeding 40%,[97]whereas the effects derived from high dc fields are found to be much smaller.[75]

It is important to note that the non-linear dielectric features due to high ac fields have also been related to the number of dynamically correlated particles or non-trivial length scales in supercooled liquids.[162,163]However none of these theories have taken field induced entropy effects into consideration explicitly. A recent study aims at deriving the nonlinear features in viscous liquids due to the entropy effect, without invoking a length scale and observed the ‘hump’ feature in third harmonic susceptibility spectrum.[164]

Bibliography

[1] P.W. Anderson, Science **267**, 1615 (1995).

[2] S. Torquato, Nature **405**, 521 (2000).

[3] T. Hecksher, Ph.D. thesis, Roskilde University (2011).

[4] H. Vogel, Phys. Z. **22**, 645 (1921); G.S. Fulcher, J. Am. Ceram. Soc. **8**, 339 (1925); G. Tammann, W. Hesse, Z. Anorg. Allgem. Chem. **156**, 245 (1926).

[5] C.A. Angell, Science **267**, 1924 (1995).

[6] R. Richert and C.A. Angell, J. Chem. Phys. **108**, 9016 (1998).

[7] K.L. Ngai, J. Non-Cryst. Solids **275**, 7 (2000).

[8] R. Kohlrausch, Ann. Phys. **167**, 179 (1854); G. Williams and D.C. Watts, Trans. Faraday Soc. **66**, 80 (1970).

[9] M.D. Ediger, Annu. Rev. Phys. Chem. **51**, 99 (2000).

[10] R. Richert, J. Phys.: Condens. Matter **14**, R703 (2002).

[11] L.J. Kaufman, Annu. Rev. Phys. Chem. **64**, 177 (2013).

[12] K. Schmidt-Rohr and H.W. Spiess, Phys. Rev. Lett. **66**, 3020 (1991).

[13] B. Schiener, R. Böhmer, A. Loidl, and R.V. Chamberlin, Science **274**, 752 (1996).

[14] R. Richert, J. Phys. Chem. B **101**, 6323 (1997).

[15] M.T. Cicerone and M.D. Ediger, J. Chem. Phys. **103**, 5684 (1995).

[16] D. Bingemann, R.M. Allen, and S.W. Olesen, J. Chem. Phys. **134**, 024513 (2011).

[17] M.T. Cicerone, F.R. Blackburn, and M.D. Ediger, Macromolecules **28**, 8224 (1995).

[18] T. Köddermann, R. Ludwig, and D. Paschek, ChemPhysChem **9**, 1851 (2008).

[19] M.K. Mapes, S.F. Swallen, and M.D. Ediger, J. Phys. Chem. B **110**, 507 (2006).

[20] R. Böhmer, K.L. Ngai, C.A. Angell, and D.J. Plazek, J. Chem. Phys. **99**, 4201 (1993).

[21] M.D. Ediger and P. Harrowell, J. Chem. Phys. **137**, 080901 (2012).

[22] V. Lubchenko and P.G. Wolynes, Annu. Rev. Phys. Chem. **58**, 235 (2007).

[23] G.P. Johari, J. Chem. Phys. **116**, 2043 (2002).

[24] W. Kauzmann, Chem. Rev. **43**, 219 (1948).

[25] P.G. Debenedetti and F.H. Stillinger, Nature **410**, 259 (2001).

[26] L.M. Martinez and C.A. Angell, Nature **410**, 663 (2001).

[27] L.M. Wang, C.A. Angell, and R. Richert, J. Chem. Phys. **125**, 074505 (2006).

[28] C. Alba, L.E. Busse, D.J. List, and C.A. Angell, J. Chem. Phys. **92**, 617 (1990).

[29] G. Adam and J.H. Gibbs, J. Chem. Phys. **43**, 139 (1965).

[30] S. Corezzi, L. Comez, and D. Fioretto, Eur. Phys. J. E **14**, 143 (2004).

[31] G.P. Johari, J. Chem. Phys. **112**, 7518 (2000).

[32] M. Goldstein, J. Chem. Phys. **64**, 4767 (1976).

[33] D. Prevosto, M. Lucchesi, S. Capaccioli, R. Casalini, and P. Rolla, Phys. Rev. B **67**, 174202 (2003).

[34] D. Prevosto, S. Capaccioli, M. Lucchesi, D. Leporini, and P. Rolla, J. Phys.: Condens. Matter **16**, 6597 (2004).

[35] C.A. Angell and S. Borick, J. Non-Cryst. Solids **393**, 307 (2002).

[36] S. Takahara, O. Yamamuro, and T. Matsuo, J. Phys. Chem. **99**, 9589 (1995).

[37] O. Yamamuro, I. Tsukushi, A. Lindqvist, S. Takahara, M. Ishikawa, and T. Matsuo, J. Phys. Chem. B **102**, 1605 (1998).

[38] U. Tracht, M. Wilhelm, A. Heuer, H. Feng, K. Schmidt-Rohr, and H. Spiess, Phys. Rev. Lett. **81**, 2727 (1998).

[39] J.C. Dyre, T. Hechsher, and K. Niss, J. Non-Cryst. Solids **355**, 624 (2009).

[40] C.A. Angell, J. Res. Natl. Inst. Stand. Technol. **102**, 171 (1997).

[41] A.J. Kovacs, J. Polym. Sci. **30**, 131 (1958).

[42] L.C.E. Struick, *Physical aging in amorphous polymers and other materials* (Amsterdam, Elsevier, 1978).

[43] J.M.G. Cowie and R. Ferguson, Macromol. **22**, 2307 (1989).

[44] P. Lunkenheimer, R. Wehn, U. Schneider, and A. Loidl, Phys. Rev. Lett. **95**, 055702 (2005).

[45] D. Cangialosi, M. Wübbenhorst, J. Groenewold, E. Mendes, H. Schut, A. Van Veen, and S.J. Picken, Phys. Rev. B **70**, 224213 (2004).

[46] A.Q. Tool, J. Am. Ceram. Soc. **29**, 240 (1946).

[47] C.T. Moynihan, P.B. Macedo, C.J. Montrose, C.J. Montrose, P.K. Gupta, M.A. DeBolt, J.F. Dill, B.E. Dom, P.W. Drake, A.J. Easteal, P.B. Elterman, R.P. Moeller, H. Sasabe, and J.A. Wilder, Ann. N. Y. Acad. Sci. **279**, 15 (1976).

[48] R. Richert, J. Non-Cryst. Solids **172-174**, 209 (1994).

[49] J.-P. Bouchaud and G. Biroli, Phys. Rev. B **72**, 064204 (2005).

[50] R. Richert and S. Weinstein, Phys. Rev. Lett. **97**, 095703 (2006).

[51] W. Huang and R. Richert, J. Phys. Chem. B, **112** 9909 (2008).

[52] A. Khalife, U. Pathak, and R. Richert, Eur. Phys. J. B **83**, 429 (2011).

[53] B. Schiener, R.V. Chamberlin, G. Diezemann, and R. Böhmer, J. Chem. Phys. **107**, 7746 (1997).

[54] S. Weinstein and R. Richert, Phys. Rev. B **75**, 064302 (2007).

[55] S. Weinstein and R. Richert, J. Phys.: Condens. Matter **19**, 205128 (2007).

[56] W. Huang and R. Richert, J. Chem. Phys. **131**, 184501 (2009).

[57] W. Huang and R. Richert, J. Chem. Phys. **130**, 194509 (2009).

[58] A. Chelkowski, J. Chem. Phys. **28**, 1249 (1958).

[59] L.P. Singh and R. Richert, Phys. Rev. Lett. **109**, 167802 (2012).

[60] A. Piekara and A. Chelkowski, J. Chem. Phys. **25**, 794 (1956).

[61] G.B. Dudley, R. Richert, and A.E. Stiegman, Chem. Sci. **6**, 2144 (2015).

[62] T. Bauer, P. Lunkenheimer, and A. Loidl, Phys. Rev. Lett. **111**, 225702 (2013).

[63] W. Huang and R. Richert, Eur. Phys. J. B **66**, 217 (2008).

[64] S.A. Reinsberg, A. Heuer, B. Doliwa, H. Zimmermann, and H.W. Spiess, J. Non-Cryst. Solids, **307-310**, 208 (2002).

[65] X.H. Qiu and M.D. Ediger, J. Phys. Chem. B **107**, 459 (2003).

[66] S.A. Reinsberg, X.H. Qiu, M. Wilhelm, H.W. Spiess, and M.D. Ediger, J. Chem. Phys. **114**, 7299 (2001).

[67] K. Paeng, H. Park, D.T. Hoang, and L.J. Kaufman, Proc. Natl. Acad. Sci. USA **112**, 4952 (2015).

[68] R. Böhmer, G. Hinze, G. Diezemann, B. Geil, and H. Sillescu, Europhys. Lett. **36**, 55 (1996).

[69] H. Wendt and R. Richert, Phys. Rev. E **61**, 1722 (2000).

[70] E.V. Russell and N.E. Israeloff, Nature **408**, 695 (2000).

[71] R. Richert, Proc. Natl. Acad. Sci. USA **112**, 4841 (2015).

[72] K.S. Cole and R.H. Cole, J. Chem. Phys. **9**, 341 (1941).

[73] S. Havriliak and S. Negami, Polymer **8**, 161 (1967).

[74] F. Alvarez, A. Alegría, and J. Colmenero, Phys. Rev. B **47**, 125 (1993).

[75] S. Samanta and R. Richert, J. Chem. Phys. **142**, 044504 (2015).

[76] L.-M. Wang and R. Richert, Phys. Rev. Lett. **99**, 185701 (2007).

[77] K. Schröter and E. Donth, J. Chem. Phys. **113**, 9101 (2000).

[78] R. Richert and W. Huang, J. Non-Cryst. Solids **356**, 787 (2010).

[79] U. Pathak and R. Richert, Colloid Polym. Sci. **292**, 1905 (2014).

[80] H. Huth, L.M. Wang, C. Schick, and R. Richert, J. Chem. Phys. **126**, 104503 (2007).

[81] B. Riechers, K. Samwer, and R. Richert, J. Chem. Phys. **142**, 154504 (2015).

[82] M. Winterlich, G. Diezemann, H. Zimmermann, and R. Böhmer, Phys. Rev. Lett. **91**, 235504 (2003).

[83] C.M. Roland and R. Casalini, Macromol. **40**, 3631 (2007).

[84] G.P. Johari and M. Goldstein, J. Chem. Phys. **53**, 2372 (1970).

[85] P. Hopkins, A. Fortini, A. J. Archer, and M. Schmidt, J. Chem. Phys. **133**, 224505 (2010).

[86] P. Lunkenheimer, R. Wehn, T. Riegger, and A. Loidl, J. Non-Cryst. Solids **307-310**, 336 (2002).

[87] A. Kudlik, S. Benkhof, T. Blochowicz, C. Tschirwitz, and E. Rössler, J. Mol. Struct. **479**, 201 (1999).

[88] P. Dixon, L. Wu, S.R. Nagel, B.D. Williams, and J. Carini, Phys. Rev. Lett. **65**, 1108 (1990).

[89] A. Schönhals, F. Kremer, and E. Schlosser, Phys. Rev. Lett. **67**, 999 (1991).

[90] R. Casalini, M. Paluch, and C.M. Roland, J. Therm. Anal. **69**, 947 (2002).

[91] J. Schneider, R. Brand, P. Lunkenheimer, and A. Loidl, Phys. Rev. Lett. **84,** 5560 (2000).

[92] J. Mattsson, R. Bergman, P. Jacobsson, and L. Börjesson, Phys. Rev. Lett. **90**, 075702 (2003).

[93] T. Blochowicz and E.A. Rössler, Phys. Rev. Lett. **92**, 225701 (2004).

[94] A.A. Pronin, M.V. Kondrin, A.G. Lyapin, V.V. Brazhkin, A.A. Volkov, P. Lunkenheimer, and A. Loidl, Phys. Rev. E **81**, 041503 (2010).

[95] K.L. Ngai. Dielectr. Electr. Insul. IEEE Trans. **8**, 329 (2001).

[96] S.A. Galema, Chem. Soc. Rev. **26**, 233 (1997).

[97] T. Bauer, P. Lunkenheimer, S. Kastner, and A. Loidl, Phys. Rev. Lett. **110**, 107603 (2013).

[98] K. Duvvuri and R. Richert, J. Chem. Phys. **118**, 1356 (2003).

[99] C. Brun, F. Ladieu, D. L'Hôte, M. Tarzia, G. Biroli, and J.-P. Bouchaud, Phys. Rev. B **84**, 104204 (2011).

[100] C. Crauste-Thibierge, C. Brun, F. Ladieu, D. L'Hôte, G. Biroli, and J.P. Bouchaud, J. Non-Cryst. Solids **357**, 279 (2011).

[101] H. Wagner and R. Richert, J. Non-Cryst. Solids **242**, 19 (1998).

[102] R. Richert, Eur. Phys. J. Spec. Top. **189**, 223 (2010).

[103] O.S. Narayanaswamy, J. Am. Ceram. Soc. **54**, 491 (1971).

[104] A.J. Kovacs, J.J. Aklonis, J.M. Hutchinson, and A.R. Ramos, J. Polym. Sci., Polym. Phys. **17**, 1097 (1979).

[105] D. Fragiadakis and C.M. Roland, Phys. Rev. E **88**, 042307 (2013).

[106] G.P. Johari, Ann. N. Y. Acad. Sci. **279**, 117 (1976).

[107] A. Döß, M. Paluch, H. Sillescu, and G. Hinze, Phys. Rev. Lett. **88**, 095701 (2002).

[108] H. Wagner and R. Richert, J. Non-Cryst. Solids **242**, 19 (1998).

[109] M. Vogel and E. Rössler, J. Chem. Phys. **114**, 5802 (2001).

[110] K.L. Ngai, Phys. Rev. E **57**, 7346 (1998).

[111] R. Casalini and C.M. Roland, Phys. Rev. Lett. **102**, 035701 (2009).

[112] S.A. Lusceac, C. Gainaru, M. Vogel, C. Koplin, P. Medick, and E.A. Rössler, Macromol. **38**, 5625 (2005).

[113] N.B. Olsen, J. Non-Cryst. Solids **235**, 399 (1998).

[114] H. Wagner and R. Richert, J. Phys. Chem. B **103**, 4071 (1999).

[115] G. Power, G.P. Johari, and J.K. Vij, J. Chem. Phys. **119**, 435 (2003).

[116] A. Faivre, G. Niquet, M. Maglione, J. Fornazero, J.F. Jal, and L. David, Eur. Phys. J. B **10**, 277 (1999).

[117] S. Samanta and R. Richert, J. Chem. Phys. **140**, 054503 (2014).

[118] R. Böhmer, G. Diezemann, B. Geil, G. Hinze, A. Nowaczyk, and M. Winterlich, Phys. Rev. Lett. **97**, 135701 (2006).

[119] D. Fragiadakis and C.M. Roland, Phys. Rev. E **86**, 020501 (2012).

[120] H. Fujimori and M. Oguni, J. Chem. Thermodyn. **26**, 367 (1994).

[121] L.-M. Wang and R. Richert, Phys. Rev. B **76**, 064201 (2007).

[122] N.B. Olsen, T. Christensen, and J.C. Dyre, Phys. Rev. Lett. **86**, 1271 (2001).

[123] G.P. Johari, J. Chem. Phys. **138**, 154503 (2013).

[124] J.F. Scott, Annu. Rev. Mater. Res. **41**, 229 (2011).

[125] H. Fröhlich, *Theory of Dielectrics* (Clarendon, Oxford, 1958).

[126] R. Richert, Adv. Chem. Phys. **156**, 101 (2014).

[127] D. L'Hôte, R. Tourbot, F. Ladieu, and P. Gadige, Phys. Rev. B **90**, 104202 (2014).

[128] D.V. Matyushov and R. Richert, J. Chem. Phys. **144**, 041102 (2016).

[129] I.V. Blazhnov, N.P. Malomuzh, and S.V. Lishchuk, J. Chem. Phys. **121**, 6435 (2004).

[130] G.E. Gibson and W.F. Giauque, J. Am. Chem. Soc. **45**, 93 (1923).

[131] K. Takeda, O. Yamamuro, I. Tsukushi, T. Matsuo, and H. Suga, J. Mol. Struct. **479**, 227 (1999).

[132] F. Stickel, Ph.D. thesis, Mainz University (1995).

[133] M. Goldstein, J. Chem. Phys. **123**, 244511 (2005).

[134] M.R.H. Javaheri and R. V Chamberlin, J. Chem. Phys. **125**, 154503 (2006).

[135] C.T. Moynihan and A.V. Lesikar, Ann. N. Y. Acad. Sci. **371**, 151 (1981).

[136] R. Brand, P. Lunkenheimer, and A. Loidl, Phys. Rev. B **56**, R5713 (1997).

[137] O. Yamamuro, H. Yamasaki, Y. Madokoro, I. Tsukushi, and T. Matsuo, J. Phys.: Condens. Matter **15**, 5439 (2003).

[138] C. Streck and R. Richert, Ber. Bunsenges. Phys. Chem. **98**, 619 (1994).

[139] M. Mizukami, H. Fujimori, and M. Oguni, Prog. Theor. Phys. Suppl. **126**, 79 (1997).

[140] R.-R. Tan, X. Shen, L. Hu, and F.-S. Zhang, Chinese Phys. B **21**, 086402 (2012).

[141] J. Bartoš, M. Iskrová, M. Köhler, R. Wehn, O. Šauša, P. Lunkenheimer, J. Krištiak, and A. Loidl, Eur. Phys. J. E **34**, 104 (2011).

[142] P. Dixon, Phys. Rev. B **42**, 8179 (1990).

[143] T. Hikima, M. Hanaya, and M. Oguni, Solid State Commun. **93**, 713 (1995).

[144] J. Bartoš, O. Šauša, M. Köhler, H. Švajdlenkova, P. Lunkenheimer, J. Krištiak, and A. Loidl, J. Non-Cryst. Solids **357**, 376 (2011).

[145] I.S. Park, K. Saruta, and S. Kojima, J. Phys. Soc. Japan **67**, 4131 (1998).

[146] T. Sun and A.S. Teja, J. Chem. Eng. Data **49**, 1311 (2004).

[147] M. Paluch, K.L. Ngai, and S.Hensel-Bielowka, J. Chem. Phys. **114**, 10872 (2001).

[148] R. Casalini, M. Paluch, and C.M. Roland, J. Phys.: Condens. Matter **15**, S859 (2003).

[149] S. Samanta, O. Yamamuro, and R. Richert, *Connecting Thermodynamics and Dynamics in a Supercooled Liquid: Cresolphthalein-Dimethylether* Thermochim. Acta. (2016) (submitted)

[150] L. Simeral and R.L. Amey, J. Phys. Chem. **74**, 1443 (1970).

[151] H. Wagner and R. Richert, Polymer **38**, 255 (1997).

[152] L. Onsager, Phys. Rev. **37**, 405 (1931).

[153] R. Richert, Physica A **322**, 143 (2003).

[154] R. Richert, J. Non-Cryst. Solids **357**, 726 (2011).

[155] I.M. Hodge, J. Non-Cryst. Solids **169**, 211 (1994).

[156] M.S. Beevers, D.A. Elliott, and G. Williams, J. Chem. Soc. Faraday Trans. 2 **76**, 112 (1980).

[157] J. Crossley and G. Williams, J. Chem. Soc. Faraday Trans. 2 **73**, 1906 (1977).

[158] M.S. Beevers, J. Crossley, C.D. Garrington, and G. Williams, Faraday Symp. Chem. Soc. **11**, 38 (1981).

[159] A.R. Young-Gonzales, S. Samanta, and R. Richert, J. Chem. Phys. **143**, 104504 (2015).

[160] J.H. Magill, J. Chem. Phys. **47**, 2802 (1967).

[161] M. Michl, T. Bauer, P. Lunkenheimer, and A. Loidl, Phys. Rev. Lett. **114**, 067601 (2015).

[162] C. Brun, C. Crauste-Thibierge, F. Ladieu, D. L'Hôte, J. Chem. Phys. **134**, 194507 (2011).

[163] G. Diezemann, Phys. Rev. E **85**, 051502 (2012).

[164] R. Richert, J. Chem. Phys. **144**, 114501 (2016).

APPENDIX A

COPYRIGHT PERMISSIONS

A) AIP PUBLISHING LLC LICENSE
TERMS AND CONDITIONS

Mar 25, 2016

This Agreement between Subarna Samanta ("You") and AIP Publishing LLC ("AIP Publishing LLC") consists of your license details and the terms and conditions provided by AIP Publishing LLC and Copyright Clearance Center.

License Number: 3836110568831
License date: Mar 25, 2016
Licensed Content Publisher: AIP Publishing LLC
Licensed Content Publication: Journal of Chemical Physics
Licensed Content Title : Limitations of heterogeneous models of liquid dynamics: Very slow rate exchange in the excess wing
Licensed Content Author: Subarna Samanta,Ranko Richert
Licensed Content Date: Feb 4, 2014
Licensed Content Volume Number:140
Licensed Content Issue Number:5
Type of Use: Thesis/Dissertation
Requestor type: Author (original article)
Format: Electronic
Portion: Figure/Table
Number of figures/tables: 7
Title of your thesis /dissertation: Dielectric Response of Glass-Forming Liquids in the Nonlinear
Regime
Expected completion date: May 2016
Estimated size (number of pages): 170
Requestor Location Subarna Samanta
1050 S Stanley Place
Apt 233
TEMPE, AZ 85281
United States

B) AIP PUBLISHING LLC LICENSE
TERMS AND CONDITIONS

Mar 25, 2016

This Agreement between Subarna Samanta ("You") and AIP Publishing LLC ("AIP Publishing LLC") consists of your license details and the terms and conditions provided by AIP Publishing LLC and Copyright Clearance Center.

License Number: 3836110352571
License date : Mar 25, 2016
Licensed Content Publisher : AIP Publishing LLC
Licensed Content Publication: Journal of Chemical Physics
Licensed Content Title: Limitations of heterogeneous models of liquid dynamics: Very slow rate exchange in the excess wing
Licensed Content Author: Subarna Samanta,Ranko Richert
Licensed Content Date: Feb 4, 2014
Licensed Content Volume Number: 140
Licensed Content Issue Number: 5
Type of Use: Thesis/Dissertation
Requestor type: Author (original article)
Format: Electronic
Portion: Excerpt (> 800 words)
Will you be translating? No
Title of your thesis /dissertation: Dielectric Response of Glass-Forming Liquids in the Nonlinear Regime
Expected completion date: May 2016
Estimated size (number of pages): 170
Requestor Location Subarna Samanta
1050 S Stanley Place
Apt 233
TEMPE, AZ 85281
United States

C) AIP PUBLISHING LLC LICENSE
TERMS AND CONDITIONS

Mar 25, 2016

This Agreement between Subarna Samanta ("You") and AIP Publishing LLC ("AIP Publishing LLC") consists of your license details and the terms and conditions provided by AIP Publishing LLC and Copyright Clearance Center.

License Number : 3836110725576
License date : Mar 25, 2016
Licensed Content Publisher : AIP Publishing LLC
Licensed Content Publication: Journal of Chemical Physics
Licensed Content Title Dynamics of glass-forming liquids. XVIII. : Does entropy control structural relaxation times?
Licensed Content Author: Subarna Samanta,Ranko Richert
Licensed Content Date: Jan 28, 2015
Licensed Content Volume Number: 142
Licensed Content Issue Number: 4
Type of Use: Thesis/Dissertation
Requestor type: Author (original article)
Format: Print and electronic
Portion : Excerpt (> 800 words)
Will you be translating? : No
Title of your thesis /dissertation: Dielectric Response of Glass-Forming Liquids in the Nonlinear Regime
Expected completion date: May 2016
Estimated size (number of pages): 170
Requestor Location: Subarna Samanta
1050 S Stanley Place
Apt 233
TEMPE, AZ 85281
United States

D) AIP PUBLISHING LLC LICENSE
TERMS AND CONDITIONS

Mar 25, 2016

This Agreement between Subarna Samanta ("You") and AIP Publishing LLC ("AIP Publishing LLC") consists of your license details and the terms and conditions provided by AIP Publishing LLC and Copyright Clearance Center.

License Number: 3836110847236
License date: Mar 25, 2016
Licensed Content Publisher: AIP Publishing LLC
Licensed Content Publication: Journal of Chemical Physics
Licensed Content Title Dynamics of glass-forming liquids. XVIII. : Does entropy control structural relaxation times?
Licensed Content Author: Subarna Samanta,Ranko Richert
Licensed Content Date: Jan 28, 2015
Licensed Content Volume Number: 142
Licensed Content Issue Number :4
Type of Use: Thesis/Dissertation
Requestor type: Author (original article)
Format : Print and electronic
Portion: Figure/Table
Number of figures/tables: 11
Title of your thesis / dissertation: Dielectric Response of Glass-Forming Liquids in the Nonlinear Regime
Expected completion date: May 2016
Estimated size (number of pages) : 170
Requestor Location: Subarna Samanta
1050 S Stanley Place
Apt 233
TEMPE, AZ 85281
United States

E) AIP PUBLISHING LLC LICENSE
TERMS AND CONDITIONS

Mar 25, 2016

This Agreement between Subarna Samanta ("You") and AIP Publishing LLC ("AIP Publishing LLC") consists of your license details and the terms and conditions provided by AIP Publishing LLC and Copyright Clearance Center.

License Number: 3836110983381
License date: Mar 25, 2016
Licensed Content Publisher: AIP Publishing LLC
Licensed Content Publication: Journal of Chemical Physics
Licensed Content Title: Dynamics of glass-forming liquids. XIX. Rise and decay of field induced anisotropy in the non-linear regime
Licensed Content Author: Amanda R. Young-Gonzales,Subarna Samanta,Ranko Richert
Licensed Content Date: Sep 9, 2015
Licensed Content Volume Number: 143
Licensed Content Issue Number: 10
Type of Use: Thesis/Dissertation
Requestor type: Author (original article)
Format: Print and electronic
Portion: Excerpt (> 800 words)
Will you be translating? : No
Title of your thesis / dissertation: Dielectric Response of Glass-Forming Liquids in the Nonlinear Regime
Expected completion date: May 2016
Estimated size (number of pages): 170
Requestor Location: Subarna Samanta
1050 S Stanley Place
Apt 233
TEMPE, AZ 85281
United States

F) AIP PUBLISHING LLC LICENSE
TERMS AND CONDITIONS

Mar 25, 2016

This Agreement between Subarna Samanta ("You") and AIP Publishing LLC ("AIP Publishing LLC") consists of your license details and the terms and conditions provided by AIP Publishing LLC and Copyright Clearance Center.

License Number: 3836111156286
License date: Mar 25, 2016
Licensed Content Publisher: AIP Publishing LLC
Licensed Content Publication: Journal of Chemical Physics
Licensed Content Title Dynamics of glass-forming liquids. XIX. : Rise and decay of field induced anisotropy in the non-linear regime
Licensed Content Author: Amanda R. Young-Gonzales,Subarna Samanta,Ranko Richert
Licensed Content Date: Sep 9, 2015
Licensed Content Volume Number: 143
Licensed Content Issue Number: 10
Type of Use: Thesis/Dissertation
Requestor type: Author (original article)
Format: Print and electronic
Portion: Figure/Table
Number of figures/tables: 5
Title of your thesis /dissertation: Dielectric Response of Glass-Forming Liquids in the Nonlinear Regime
Expected completion date: May 2016
Estimated size (number of pages): 170
Requestor Location: Subarna Samanta
1050 S Stanley Place
Apt 233
TEMPE, AZ 85281
United States